Università degli Studi di Cagliari

DOTTORATO DI RICERCA IN:

SCIENZE E TECNOLOGIE CHIMICHE E FARMACEUTICHE

Ciclo **XXV**

TITOLO TESI

Ion Specific Effects on Charged Interfaces

Settore/i scientifico disciplinari di afferenza:

CHIM/02

Presentata da: **Luca Medda**

Coordinatore Dottorato: **Prof. Mariano Casu**

Relatori: **Prof.ssa Maura Monduzzi, Dr. Andrea Salis**

Anno Accademico **2011 – 2012**

Make things as simple as possible, but not simpler.

Albert Einstein

To my family

Acknowledgments

Foremost, I would like to express my deep and sincere gratitude to my supervisors, Dr. Andrea Salis and Prof. Maura Monduzzi. Andrea patiently provided teaching, friendship, encouragement and advice both at academic and personal level. The support of Maura was irreplaceable to proceed through the doctorial project and to complete this thesis work.

A particular acknowledgment is dedicated to Prof. Edmond Magner and to his group for the expert and friendly environment at the Materials and Surface Science Institute (MSSI) of the University of Limerick (Ireland) during the Master and Back project.

I greatly appreciated the support received through the collaboration with Prof. Barry Ninham and Dr. Drew Parsons of Australian National University (Canberra, Australia), as well as Dr. Mathias Bostrom (University of Stockholm, Sweden) with whom I spent a great time during his staying in Cagliari as visiting scientist. Their contribution has been of great value in this study.

Thanks to my colleagues of Biocatalysis and Colloids and Interfaces Laboratory Francesca, Daniela, Brajesh, Pradip for their invaluable contribution to this PhD work, and to Maura C. and Sandrina for their friendship in the labs.

I would like also to thank: Alberto, Annarita, Claudia, Cristina, Daniela, Davide, Elisa, Erika, Maria, Martina, Matteo, Paula, Riccardo, Shaji, Smoriko for their encouragement and for all the fun we had in these years.

A special thank is due to the Department of Scienze Chimiche e Geologiche, University of Cagliari, for the opportunities offered by a very friendly and international environment.

Lastly, I would like to thank all those who supported me during the completion of the project.

SUMMARY

List of papers

Paper I: "*Measurements and Theoretical Interpretation of Points of Zero Charge/Potential of BSA Protein*" A. Salis, M. Boström, L. Medda, F. Cugia, B. Barse, D. F. Parsons, B. W. Ninham, and M. Monduzzi *Langmuir* **2011**, 27, 11597-11604

Paper II: "*Hofmeister Challenges: Ion Binding and Charge of the BSA Protein as Explicit Example*" L. Medda, B. Barse, F. Cugia, M. Boström, D. F. Parsons, B. W. Ninham M. Monduzzi and A. Salis *Langmuir* **2012**, 28, 16355-16363.

Paper III: "*Ion Specific Surface Charge Density of SBA-15 Mesoporous Silica*" A. Salis, D. F. Parsons, M. Boström, L. Medda, B. Barse, B. W. Ninham and M. Monduzzi *Langmuir* **2010**, 26(4), 2484-2490.

Paper IV: "*Specific ion effects on the electrochemical properties of cytochrome c*" L. Medda, A. Salis, E. Magner *Phys. Chem. Chem. Phys*. **2012**,14, 2875-2883.

Paper V: "*Lysozyme Adsorption and Release from Ordered Mesoporous Materials*" M. S. Bhattacharyya, P. Hiwale, M. Piras, L. Medda, D. Steri, M. Piludu, A. Salis, M. Monduzzi *J. Phys. Chem*. **2010**,114, 19928-19934.

1. *Chapter*: Charged interfaces

1.1.   The interface of the dispersed systems

The boundary surface among two different phases is defined interface. The extension of the interface depends on the area / volume ratio between the two phases considered. Usually the systems that show a high interface, constituted by a substance forming particles or droplets (dispersed phase) in a second substance where the particles are distributed (dispersion medium), are defined as dispersed systems.[1] The dispersed phase and the dispersion medium can be either solid, liquid and gaseous leading to a wide variety of systems and features (Tab 1.1).

Table 1.1 Summary of some of the descriptive names used to designate two-phase systems.

Dispersion medium	Dispersed phase	Descriptive names
Gas	Liquid	Fog, mist, aerosol
Gas	Solid	Smoke, aerosol
Liquid	Gas	Foam
Liquid	Liquid	Emulsion
Liquid	Solid	Sol, Colloidal solution, Gel, Suspension
Solid	Gas	Solid Foam
Solid	Liquid	Gel, solid emulsion
Solid	Solid	Alloy

A dispersion can be classified as a function of the particle dimensions. When the particle diameter is in the range 1-1000 nm the area / volume ratio is very high, then the particles exhibit a very large interface. In this condition the particles are defined colloids and the system is referred as '*colloidal dispersion'*. When the dimension of the particles exceeds 1000 nm, the area / volume ratio decreases and '*coarse dispersions'* (or suspensions) are obtained.

A colloidal dispersion can also be classified as a function of the affinity between the particle surface and the medium. *Lyophilic colloids* have a high affinity towards the medium and they can stand in solution indefinitely in the absence of any chemical or temperature change. *Lyophobic colloids*, instead, have a low affinity towards the medium and can separate spontaneously from the medium into two phases.[1] According to the tendency to separate in phases, the *lyophilic colloids* possess a thermodynamic stability whereas *lyophobic colloids* display a kinetic stability only. The stability of a colloidal system, however, always depends on the forces acting among the colloidal particles and can be understood only analyzing the single contributes that determine the global effects.

1.2.   The electrical double layer

A particle in contact with a polar medium may acquire a charge through two main mechanisms:[2]

  − dissociation of surface groups
  − surface adsorption of ions.

The charged interface will modify the concentration profile of the ions in the surrounding space as a function of the distance from the surface in a pattern known as "electrical double layer" (EDL). Figure 1.1 shows a graphical representation of a charged particle immersed in an electrolyte solution.
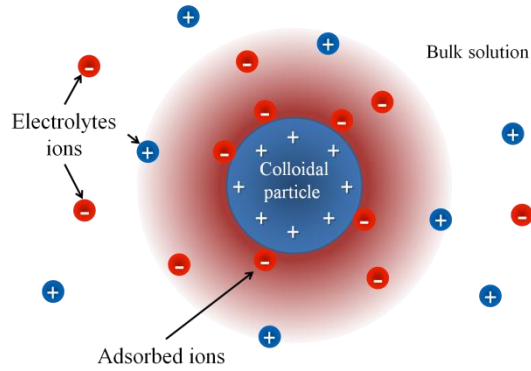
Figure 1.1 Graphical representation of a charged particle immersed in an electrolyte solution.

The charge density ρ is a physical property of the interface and can be related to the electrostatic potential ψ and to the distance from the surface via the Poisson equation:

$$\nabla^2 \psi = -\frac{\rho}{\varepsilon_0 \varepsilon_r}$$

$$(1.1)$$

Eq. 1.1 describes the charge density as a function of the spatial distance and direction, and the dielectric properties of the medium ($\varepsilon_0 \varepsilon_r$) where the particle is dispersed. The model used makes the following fundamental assumptions:[2]

− The surface is assumed to be uniformly charged;

− The ions in the diffuse part of the double layer are assumed to be point charges distributed according to the Boltzmann distribution;

− The solvent is assumed to influence the double layer only through its dielectric constant, which is assumed to have the same value throughout the diffuse part.

The charge density is a function of different parameters, such as the ion charge (z_i) and can be calculated by using the statistical approach of the Boltzmann distribution:

$$\rho = \sum_i n_i z_i e^{\left(\frac{-z_i e \psi}{k_b T}\right)}$$

(1.2)

where k_b is the Boltzmann constant, T is the temperature, n_i is the number of ions per volume unit having z_i valence, and e is the elementary charge. Combining eq. 1.1 with eq. 1.2 the Poisson-Boltzmann equation is obtained:

$$\nabla^2 \psi = \frac{1}{\varepsilon_0 \varepsilon_r} \sum_i n_i z_i e^{\left(\frac{-z_i e \psi}{k_b T}\right)}$$

(1.3)

or in spherical coordinates:

$$\frac{1}{r^2} \frac{d}{dr}\left(r^2 \frac{d\psi}{dr}\right) = \frac{1}{\varepsilon_0 \varepsilon_r} \sum_i n_i z_i e^{\left(\frac{-z_i e \psi}{k_b T}\right)}$$

(1.4)

Eq. 1.4 is a differential equation that has not an explicit general solution. It can be analytically integrated only using suitable approximations and applying opportune boundary conditions.

A simple quantitative treatment of the diffuse part of the double layer is that developed by Gouy (1910) and Chapman (1913).[2] For an infinite flat surface eq. 1.3 can be solved for one dimension (x):

$$\gamma = \gamma_0 e^{-\kappa x}$$

(1.5)

where γ is defined by the relationship:

$$\gamma = \frac{\exp(ze\psi / 2k_bT) - 1}{\exp(ze\psi / 2k_bT) + 1} \qquad (1.6)$$

Eq. 1.6 shows that γ, rather than ψ, vary exponentially with x. For high potentials γ tends to 1, while for low potentials, Eq. 1.5 coincides with the solution obtained by using the Debye-Hückel approximation treated below.[1,3]

The parameter κ in eq. 1.5, is the inverse Debye length and represents the inverse "thickness" of the double layer. The Debye length can be calculated by the equation:

$$\kappa^{-1} = \sqrt{\frac{2k_bT\varepsilon_0\varepsilon_r}{N_a e^2 1000 I}} \qquad (1.7)$$

where, e, k_b, T, ε_0, ε_r have been defined above, N_a is the Avogadro's number, and I is the ionic strength obtained by the equation:

$$I = \frac{1}{2}\sum_{i}^{n} c_i z_i^2 \qquad (1.8)$$

where c_i is the ionic concentration and z_i the ionic charge. The Debye length is inversely proportional to the square root of the ionic strength of the solution (eq. 1.7). Some typical Debye length values for a 1:1 electrolyte are reported in Table 1.2.

Another method to solve the Poisson-Boltzmann equation is to consider the thermal agitation much higher than the electrostatic interactions ($z_i e\psi \ll k_bT$) in eq. 1.3.

Table 1.2 Debye length for different values of ionic strength.

Ionic Strenght (M)	κ^{-1}(nm)
0.001	9.620
0.010	3.040
0.100	0.962

This assumption, referred as the Debye-Hückel approximation,[2] limits the validity of the solution only to values of the electrostatic potential lower than 25 mV. By using this approximation, and limiting eq. 1.3 to one dimension (x), a solution for an infinite flat surface can be obtained:

$$\psi = \psi_0 e^{-\kappa x} \tag{1.9}$$

However, the Debye-Hückel approximation cannot be used in the treatment of several colloid and surface phenomena and for some applications the solutions obtained through the Gouy-Chapman theory is preferred.

A collection of PB solutions as a function of the approximations and the geometries considered, is given in Table 1.3.

All these solutions, however, fail for small distances from the interface due to the model assumed in the Poisson-Boltzmann equation, where ions are considered as point charges. Indeed, the finite size of the ions limits the boundary of the diffuse part of the double layer, since the centre of an ion can only approach the surface not more than its hydrated radius without becoming specifically adsorbed.

Table 1.3 Collection of Poisson-Boltzmann equation solutions for different geometries and methods of elaboration.

PB Solution		Geometry	Elaboration
$$\psi = \frac{a}{x}\psi_0^{[-\kappa(x-a)]}$$	x= distance from the surface a= radius of the particle	spherical	Debye-Huckel approximation
$$\psi = \psi_0 \frac{\cosh x}{\cosh d}$$	d= distance between the plates	Two parallel plates	Debye-Huckel approximation
$$\gamma = \gamma_0 e^{-\kappa x}$$ $$\gamma = \frac{\exp(ze\psi/2k_bT)-1}{\exp(ze\psi/2k_bT)+1}$$		planar	Gouy-Chapman theory
$$\psi = \left(\frac{64\pi k_b TR\rho_\infty \gamma^2}{\kappa^2}\right)e^{-\kappa D}$$ $$\gamma = \tanh\left(\frac{e\psi_0}{4k_bT}\right)$$	ρ_∞= ionic density of the solution	Two identical spheres	Guoy-Chapman theory

A correction to this model was proposed in 1924 by O. Stern.[4] In this treatment, the first variation in electrostatic potential is due to the specific adsorption of the counter-ions on the interface. This spatial organization of electrical charges can be approximated to a parallel plate capacitor of dielectric constant ε_δ. The potential (ψ_δ) at the Stern layer (δ) is given by the equation:

$$\psi_\delta = \psi_0 - \frac{4\pi\delta\sigma_\delta}{\varepsilon_\delta}$$

(1.10)

where σ_δ is the surface charge density which can be obtained by using a Langmuir isotherm model:

$$\frac{\sigma_\delta}{\sigma_{\delta 0}} = \frac{Kn_0}{1 + Kn_0}$$

(1.11)

where the ratio $\dfrac{\sigma_\delta}{\sigma_0}$ is the fraction of surface sites occupied, n_0 is the concentration of the adsorbed ions in the solution and K is a constant that depends on the potential (ψ_δ) and the chemical energy associated with the adsorption (ϕ):[1]

$$K \approx \exp\left(\frac{ze\psi_\delta + \phi}{k_b T}\right)$$

(1.12)

In Fig. 1.2 the graphical representation of the electrical double layer is reported. The electrostatic potential (ψ) in the surroundings of the particle, is reported as a function of the distance from the particle surface (x). The space around the interface can be divided into three main regions:

– the *Stern layer*: is the closest region to the surface and is constituted by the ions having opposite charge respect to that of the interface (counter-ions) due to the electro-neutrality condition;

– the *Gouy-Chapman (diffuse) layer:* is constituted by the counter-ions and co-ions (ions with the same charge of the particle) whose concentration is a function of the distance from the interface;

– the *bulk solution*: is the part of the solution where electro-neutrality occurs.
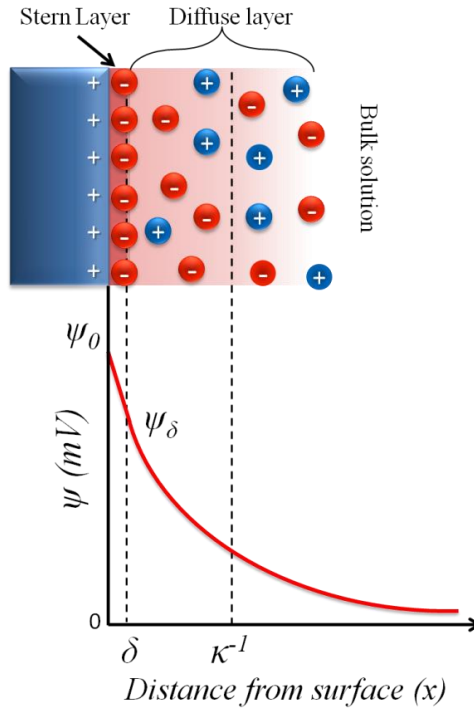
Figure 1.2 Representation of the electrostatic potential (ψ) and the ion concentration (c_i) as a function of the distance from the surface.

For an infinite planar surface, the electrostatic potential in the *Stern layer* varies linearly with the distance (x) according to eq. 1.10, while in the *diffuse layer* decreases exponentially as described by the Poisson-Boltzmann solution (eq. 1.9), and tends to zero to infinity. When two particles are close enough, so that their respective double layers overlap, they repel each other with an electrostatic force that depends on the charge of the particle (z_i) and the potential (eqs. 1.3 and 1.4). A high electrostatic potential prevents the coagulation, thus stabilizing the suspension.

The theory of the electric double layer deals with the distribution of ions and, hence, with the magnitude of the electric potentials which occurs in the surroundings of the charged surface. This is a necessary first step towards the understanding of many experimental observations concerning the electro-

kinetic phenomena and stability of charged colloidal systems.[3] However, it should be considered that electrostatic forces are not the only type of interactions to which the particles are subjected. Charged surfaces can attract each other at small separations, due to the action of van der Waals forces.

1.3.   Van der Waals forces

Van der Walls forces include all types of non electrostatic interactions and can be summarized in three main categories:[5]

   − Interaction between two permanent dipoles (Keesom);

   − Interaction between permanent dipoles and induced dipoles (Debye);

   − Interaction between instantaneous dipoles caused by fluctuations of
   the charge distribution (London).

Interaction between dipoles, whether permanent or induced, are the result of the electric field produced by one dipole acting on the second dipole. The dipoles will set up an electric field in their surroundings as a function of the distance (x). The functions to calculate the interaction energy (Φ) between pairs of isolated entities are reported in tab. 1.4.

For a pair of identical ions or molecules the three contributes (Debye, Keesom and London) can be combined to give the net van der Waals attraction (w_{att}):

$$w_{att} = \Phi_D + \Phi_K + \Phi_L = -\left(\frac{\beta}{x^6} \right)$$

(1.13)

where β is the interaction parameter and is given by:

$$\beta = 2\alpha_{0,1}\mu_1^2 + \frac{2\mu_1^4}{3k_bT} + \frac{3h\nu_1\alpha_{0,1}^2}{4}$$

(1.14)

Table 1.4 Functions for the calculation of the interaction energy between pairs of isolated ions or molecules.

Description	Interaction energy	Definition	Attributed to
Permanent dipole 1 - permanent dipole 2	$\Phi_K = -\frac{2(\mu_2^2\mu_1^2)}{2k_bTx^6}$	Free rotation of dipoles	Keesom
Permanent dipole 1 - induced dipole 2	$\Phi_D = -\frac{(\alpha_{0,1}\mu_2^2 + \alpha_{0,2}\mu_1^2)}{x^6}$	=polarizability μ= dipole moment	Debye
Induced dipole 1 -induced dipole 2	$\Phi_L = -\frac{3h\nu_1\nu_2}{2x^6(\nu_1+\nu_2)}\alpha_{0,1}\alpha_{0,2}$	= characteristic vibrational frequency of electrons	London

Van der Waals interaction between two atoms is in general weak and decays rapidly with increasing distance (inverse sixth power). However, since this interaction is ubiquitous, for larger objects the total dispersion interactions among their respective constituent atoms is indeed quite large.

Hamaker (1937) was one of the first who related the interatomic van der Waals dispersion interactions to the total van der Waals interaction among aggregates.[3] The theory makes the drastic assumption that all the atomic dispersion interactions contributing to the total energy, are pair wise additive.[5]

The interaction energy can be calculated by the general equation:

$$w_{att} = -\frac{1}{2}\left(\frac{\rho N_A}{MW}\right)^2 \beta \iint \frac{dV_1 dV_2}{x^6}$$

(1.15)

where dV_1 and dV_2 are the volume elements of the two interacting molecules, N_A is the Avogadro number, ρ is the atomic density of the particle, and MW is its molecular weight. In the case of two spherical particles of the same composition and the same radius R, the integration between D (distance of closest approach) and infinity, gives the following expression:

$$w_{att} = -\frac{AR}{12D}$$

(1.16)

where A is the Hamaker constant expressed by:

$$A = \left(\frac{\rho N_A}{MW}\right)^2 \beta$$

(1.17)

This expression is valid only when the radius of the particles is much larger than the distance between the particles. Other expressions can be derived for other geometries.[1,3]
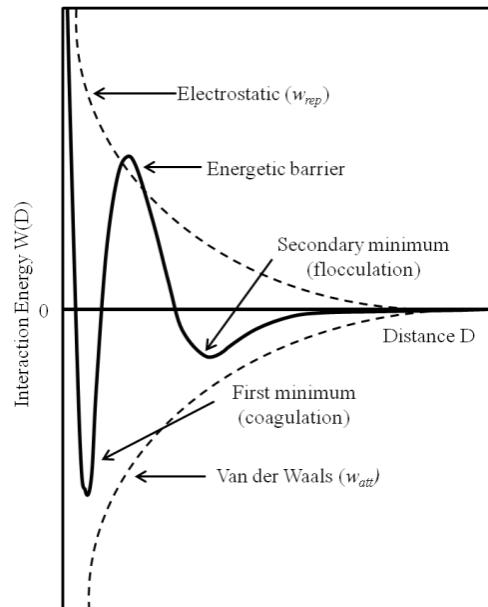
1.4. The DLVO theory

The theory of the stability of colloidal dispersions was separately elaborated – during the 40s of the past century - by D. Derjaguin and L. Landau [7] and by E. Verwey and J.T.G. Overbeek.[8] The theory is called DLVO in honor of the four scientists.[1] The DLVO theory considers colloidal stability due to the action of two opposite forces: a repulsive interaction due to the presence of the electrical double layer (w_{rep}) and an attractive interaction due to hydrogen-bond and non-electrostatic van der Waals forces (w_{att}). The total interaction energy $W(D)$ between two colloidal particles can be obtained by summing up

the two contributes. If two identical spherical particles are considered,[5] the total interaction energy is given by the equation:

$$W(D) = w_{rep} + w_{att} = \left(\frac{64\pi k_b T R \rho_\infty \gamma^2}{\kappa^2} \right) e^{-\kappa D} - \frac{AR}{12D}$$

(1.18)

where the first term is the solution of the Poisson-Boltzmann equation (Table 1.2), A is the Hamaker constant, D is the distance between the charged particles and R is the radius of the colloidal particle.

The DLVO theory considers the stability of a colloidal system due to the action of attractive and repulsive forces as the particles approach each other due to Brownian motions. This theory proposes that an energy barrier, due to the repulsive force, prevents the two approaching particles from coming into contact (Fig. 1.3). But if the particles collide with sufficient energy to overcome that barrier, the attractive force will pull them into contact, and they will adhere strongly and irreversibly together. Substantially if the energy barrier is sufficiently high, the colloidal dispersion will not coagulate and the system will stably be dispersed. On the contrary, if the repulsion is not strong enough, coagulation will eventually take place. In certain situations (e.g. at high salt concentrations), there is the possibility that flocculation phenomena may happen. This occurs in the presence of a "secondary minimum" where a much weaker, and potentially reversible, adhesion between particles takes place. These weak flocks are sufficiently stable to not be broken by the Brownian motions, but may dissociate under an externally applied force such as vigorous agitation. Figure 1.3 shows how the repulsive and the attractive energies combine to give the total DLVO interaction energy.
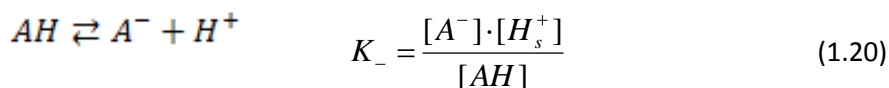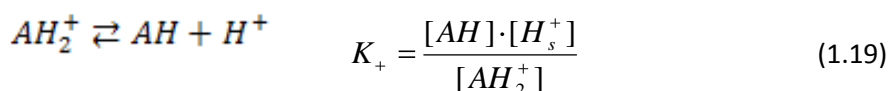
Figure 1.3 Schematic diagram of the variation of interaction energy (W) with particle separation (D) according to the DLVO theory.

1.4.1. The charge regulation model

The DLVO approach considers either the charge or the potential, of two interacting surfaces immersed in an aqueous solution, to be constant.[7,8] This assumption is valid when the dissociating groups of the substance are strong acids or bases, inasmuch their thermodynamic equilibrium is shifted completely to the dissociate form. But in the majority of real systems (i.e. biological interfaces), the chargeable groups at the interface undergo an equilibrium between dissociate and undissociate forms. The assumption of a constant charge and potential in DLVO theory, was made since no relationships for the calculation in interacting systems were available.[8] In 1971 Ninham and Parsegian[9] proposed a model where the electrostatic potential between two surface is regulated (during approach), by the equilibria at the surface that are responsible for the formation of the surface charge itself. The

mechanism of the 'charge regulation', extended and generalized by others authors to include a wide variety of situations,[10–12] can be explained taking into account a planar surface in contact with a solution of 1:1 electrolyte whose bulk pH may be controlled. In this approach the change of the potential is completely attributed to the potential determining ion (*p.d.i.*), represented in this case by the hydrogen ion. The equilibria at the interface for a generic amphoteric group of the substance are described by the following equations:

$$AH_2^+ \rightleftarrows AH + H^+ \qquad K_+ = \frac{[AH] \cdot [H_s^+]}{[AH_2^+]} \qquad (1.19)$$

$$AH \rightleftarrows A^- + H^+ \qquad K_- = \frac{[A^-] \cdot [H_s^+]}{[AH]} \qquad (1.20)$$

where K_+ and K_- are the effective acid ionization constants for the equilibria, $[AH_s^+]$, $[AH]$ and $[A^-]$ are the concentrations of the surface species and $[H_s^+]$ is the concentration of the *p.d.i.* at the surface. For a rigorous treatment, the activities rather than the concentrations should be used. In this model, however, the activity coefficients of the species reported in eqs. 1.19 and 1.20 are considered constant and close to unity during the approaching of the surfaces. According to this assumption, K_+ (K_-) can be considered to be equal to the thermodynamic constants K_+° (K_-°). On the basis of those approximations the surface charge density of the particle (σ_0) can be calculated as a function of the fraction of total sites (N_s) positively (θ_+) and negatively (θ_-) ionized:

$$\sigma_0 = N_s e(\theta_+ - \theta_-) \qquad (1.21)$$

$$\theta_+ = \frac{[AH_2^+]}{N_s} \quad ; \quad \theta_- = \frac{[A^-]}{N_s}$$

(1.22)

Substituting the fraction of sites with the expressions obtained by the eqs. 1.19, 1.20 and reordering, the expression for the surface charge density $\frac{\sigma_0}{N_s e}$ as a function of the dissociation constants and of the *p.d.i.* concentration is obtained:

$$\frac{\sigma_0}{N_s e} = \frac{\left(\dfrac{H_s^+}{K_+} - \dfrac{K_-}{H_s^+} \right)}{1 + \dfrac{H_s^+}{K_+} + \dfrac{K_-}{H_s^+}}$$

(1.23)

H_s^+ can be calculated by using the equation:

$$[H_s^+] = [H_b^+] \exp\left(-\frac{e\psi_0}{k_b T} \right)$$

(1.24)

where $[H_b^+]$ represents the bulk concentration of hydrogen ions and ψ_0 is the surface electrostatic potential that can be calculated by solving the Poisson-Boltzmann equation (see Sec. 1.2) by imposing the opportune boundary conditions.[9,11–13]

1.5.   Success and limitations of DLVO theory

The DLVO was the first theory thought to give an explanation of the various phenomena that occurs in colloidal systems. Despite the narrow range of

electrolyte's concentrations for which the DLVO validity was claimed (< $5 \cdot 10^{-2}$ M [3]), the theory had been able to explain qualitatively many effects that occur in colloidal systems.

One of the most popular successes of the DLVO was the explanation of the Shulze-Hardy rule (1900) for the critical coagulation concentration (*c.c.c.*) of a colloidal system. The *c.c.c.* represents the minimum electrolyte concentration required to coagulate a colloid. Its value for a particular electrolyte is essentially determined by the valence of the counter ion regardless of the nature of the ion (with the same charge as the surface). For example to coagulate a negative colloid as As_2S_3, the coagulation power of different cations decreases in the order Al^{3+} > Mg^{2+} > Na^+ leading to higher concentrations of electrolyte needed for the coagulation. The DLVO repulsion energy for two spheres of equal size (eq. 1.18) is proportional to the square of the Debye length ($w_{rep} \propto \kappa^{-2}$). When the Debye length decreases as a result of an increase in concentration or in the charge of the ions (eqs. 1.7 and 1.8), the energy barrier in (Fig. 1.3) will reduce favoring the coagulation of the colloidal system.

Other experimental measurements of DLVO forces have been performed in various electrolytes,[14–17] between surfactant and lipid bilayers,[18–21] across soap films,[22–24] and between silica and sapphire and metal surfaces [25–27] showing a semi-quantitative agreement with the theory.

All the measurements reported, however, are made in a range of concentrations far from that relevant for biological systems (~ 0.15 M), where the assumptions made at the base of the theory are not valid anymore. At this concentration deviations from the expected behavior have been observed, for example if the type of electrolyte is changed with another having the same valence. These effects can be classified in terms of ion specific (Hofmeister) phenomena.

2. *Chapter*:   Ion-specific effects

2.1.   The Hofmeister's series

2.1.1.   Background

Ion interactions with charged interfaces play a key role in many biological and technological processes.[28] These effects are usually framed in terms of the 'Hofmeister' or 'lyotropic' ([1]) series which traditionally order anions and cations according to their ability to precipitate proteins.

The first who observed the occurrence of ion-specific effects was Poiseuille when, in 1847, published a paper about the viscosity of aqueous solutions containing different salts.[29] The matter rested until 1888, when Franz Hofmeister found that the precipitation of egg white proteins and other colloids, in solutions at fixed ionic strength, was salt specific.[30]
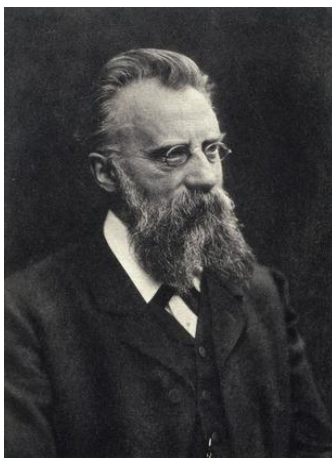
Figure 2.1 Portrait of Franz Hofmeister (1850-1922). Image by Science and Society picture library.

([1]) The lyotropic series was introduced for the first time by A. Voet in 1936 [112] and concerns the ability of different electrolytes to influence the properties of the solvent and the rate of the chemical reactions and physicochemical processes occurring in it.

He performed a series of experiments determining the weight of salt necessary to produce the clouding of the protein solution. Experiments were complicated, due to the impurities contained in the reagents and the low precipitation rates. Sometimes clouding was observed only after several days.[30] Despite that, Hofmeister found that salts, with different anion but fixed cation, could be ordered as a function of the weight of salt used to produce the clouding of the solution. Hence, anions efficiency to precipitate egg proteins followed the series:

$$\text{Citrate}^{3-} > \text{HPO}_4^{2-} > \text{SO}_4^{2-} > \text{F}^- > \text{Cl}^- > \text{Br}^- > \text{I}^- > \text{NO}_3^- > \text{ClO}_4^- > \text{SCN}^-$$

Salting-out   Salting-in

Analogously for salts having the same anion but different cation:

$$\text{N(CH}_3)_4^+ > \text{NH}_4^+ > \text{Cs}^+ > \text{Rb}^+ > \text{K}^+ > \text{Na}^+ > \text{Ca}^{2+} > \text{Mg}^{2+} > \text{Al}^{3+}$$
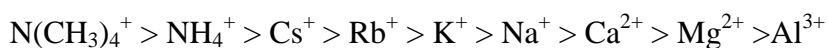
Salting-out   Salting-in

Hofmeister, however, didn't find an universal series. Later it was found that this classical representation is valid only for particular conditions of pH and salt concentration,[31] and is closely related to the type of considered interface.[32–34]

Since its discovery, the Hofmeister series was found to occur in several systems such as: the viscosity of electrolyte solutions,[35] the activity coefficient of non-electrolytes,[36] the structure of water in ionic solutions,[37] the adiabatic compressibilities of liquids,[38] the conductance of aqueous solutions,[39] etc.[40–43]

The interest towards Hofmeister phenomena is currently living a renaissance due to the huge amount of experimental and theoretical papers related to ion specific effects. There is now a full awareness that salts affect a myriad of systems both in science and technology. Recent experimental works

have investigated how ion specificity affects: the crystallization of proteins,[44] enzyme activities,[45] silica and alumina interactions,[46] bacterial growth,[47] cloud points of lysozyme,[48] the water structure adjacent to surfactant or protein monolayers[49] and many other examples.[46,50–58]

Although so many experimental data concerning Hofmeister phenomena in different chemical and biological systems have been collected, the understanding of these effects at a molecular level is still object of a wide scientific debate.[28] However, the starting point to understand ion specificity is the knowledge of the behavior of a salt when dissolved in water.

2.1.2. First attempts of interpretation: the Debye-Hückel theory and its extensions

Hofmeister was a pharmacologist and related the ability of salts to precipitate proteins and colloids with their laxative and diuretic properties. He suggested that the phenomenon observed was dependent on the capacity of salts to bind water.[30] In the 19th century it was not easy to explain these effects but, despite that, his intuition put the basis for the first attempts to rationalize ion-specific effects. In the following years new salt specific experiments were carried out, but the first theory of electrolytes due to P. Debye and E. Hückel became available only in 1923.

The Debye-Hückel theory considers anions and cations as point charges immersed in a medium of dielectric constant ε and surrounded by an ionic atmosphere of counter-ions. Ions interact through electrostatic forces only.[59] By using these assumptions it is possible to calculate the average activity coefficient, $\gamma_\pm$, through the so called: 'Debye-Hückel limiting law':

$$\log\gamma_\pm = -A\left|z_+ z_-\right|\sqrt{I}$$

(2.1)

where z_+ and z_- are the charges of the ions, I is the ionic strength, and A is a coefficient that depends on the dielectric properties of the solvent. The limiting law is valid only for very diluted systems (condition of infinite dilution).

In order to extend the range of validity of that law to higher concentrations, a slightly more complicated treatment was then proposed.[59] It uses the same assumptions of a continuum dielectric medium but, instead of point charges, ions are considered as spherical hydrated charges having a finite radius a. The so called 'extended Debye-Hückel law' is then:

$$\log \gamma_\pm = -\frac{A|z_+ z_-|\sqrt{I}}{1 + Ba\sqrt{I}}$$

(2.2)

where B is a parameter that depends on the temperature and the dielectric constant of the solvent. For very dilute solutions, $Ba\sqrt{I} \ll 1$ and eq. 2.2 become equal to eq. 2.1. Despite the ions are considered not to be point charges, this extended Debye-Hückel law is valid for electrolyte concentrations < 0.01 M and still does not consider ion specificity as shown by the values of ion size parameter, a, reported in table 2.1.

**Table 2.1** Values of the ion size parameter a for cations and anions having different valence.[60]

a (Å)	Monovalent	Bivalent	Trivalent
3	Rb^+, F^-, Cl^-, NO_3^-, Br^-, I^-, SCN^-	---------------	---------------
6	Li^+, Et_4N^+, CCl_3COO^-	Ca^{2+}, Ni^{2+},	$Co(ethylendiammine)_3^{3+}$
9	H^+	---------------	Al^{3+}, Ce^{3+}, La^{3+}

An attempt of including ion-specific effects in the classical electrolyte theory, was made by Guggenheim in 1935:[61]

$$\log \gamma_{\pm} = -\frac{A|z_+z_-|\sqrt{I}}{1+Ba\sqrt{I}} + bI \approx -A|z_+z_-|\sqrt{I} + (A|z_+z_-|Ba+b)I$$

(2.3)

where the coefficients A, B, a are described above and the coefficient b is a parameter that reflects the ion-specificity.

In 1938 Davies modified the equation 2.3 by expressing the b parameter as $b=0.1 \cdot z_1 z_2$.[59,62] This form of the equation was able to reproduce the differences due to the valence of the involved ions up to 0.1 M, but not the trend of the activity coefficients for 1:1 electrolytes reported by Robinson in 1935 for higher concentrations of electrolyte (Fig. 2.2).
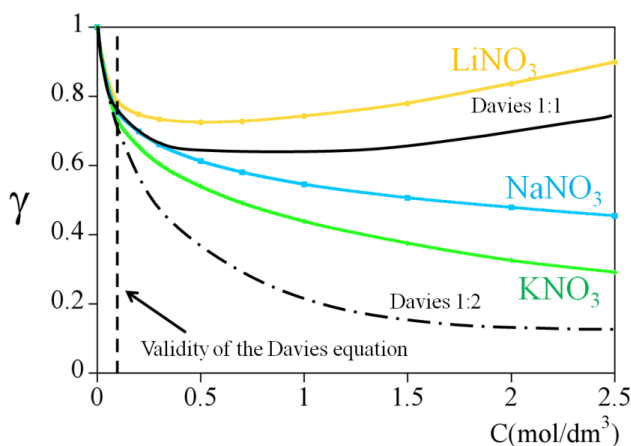
Figure 2.2 Activity coefficient of several alkali nitrate solutions as a function of the salt concentration[63] and Davies activity coefficient for 1:1 and 1:2 electrolytes.

2.1.3. Use of Debye-Hückel-like equations to quantify ion specific effects

Another milestone in the story of ion-specific effects was put in 1929 by G. Jones and M. Dole.[35] They extended Poiseuille's work by measuring the

viscosity of different salt solutions in comparison with that of pure water, at constant temperature. For a wide range of concentrations (between 5 mM and 0.1 M) the specific viscosity, η, of a salt aqueous solution is related to that of pure water η_0 by:

$$\frac{\eta}{\eta_0} - 1 = A\sqrt{c} + Bc$$

(2.4)

where c is the salt concentration. The coefficients A and B are obtained as fitting parameters of the eq. 2.4 which has a mathematical form similar to that of the extended Debye-Hückel equation (eq. 2.3). In particular, A reflects the viscous drag due to the ionic atmosphere which should delay the motion of an ion and makes the solution more viscous. The term B, known as the Jones-Dole B viscosity coefficient, becomes important in more concentrated solutions and is ion specific. Some typical values of the B coefficient are reported in table 2.2.

Table 2.2 Selected Ionic Jones-Dole B coefficients obtained from viscosity measurements of salt aqueous solutions at 25 °C. [64]

Cations	B (M^{-1})	Anions	B (M^{-1})
Li^+	0.146	Cl^-	-0.005
Na^+	0.085	Br^-	-0.033
K^+	-0.009	NO_3^-	-0.043
Rb^+	-0.033	I^-	-0.073
Cs^+	-0.047	SCN^-	-0.022
Mg^{2+}	0.385	SO_4^{2-}	0.206
Ca^{2+}	0.284		

Another remarkable example of a system where ion-specific effects are involved was reported by A. A. Green in 1931. He studied the solubility of human hemoglobin in different aqueous salt solutions.[40,65]
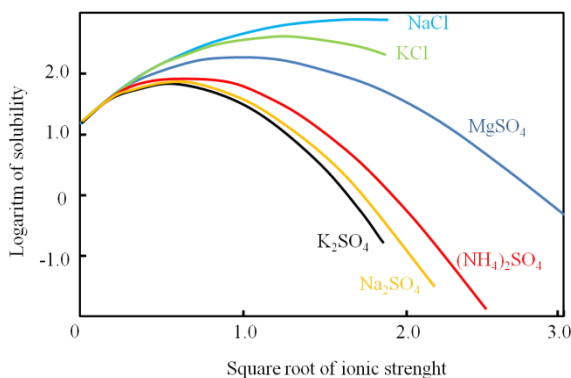
Figure 2.3 Solubility of carboxy hemoglobin in various electrolyte solutions at 25 °C.[40]

By considering S and S_0 the solubilities of hemoglobin in the presence and in the absence of salt respectively, the term $log\ S/S_0$ followed a bell shaped trend as a function of the square root of the ionic strength (Fig. 2.3). As expected different curves for different salts were obtained. Experimental solubilities could be fitted by using an empirical equation which has the same form of the Debye-Hückel equation:

$$\log \frac{S}{S_0} = \frac{0.5 z_1 z_2 \sqrt{I}}{1 + B\sqrt{I}} - K_s I$$

(2.5)

where K_s is the "salting out" coefficient, analogous of the b coefficient in eq. 2.3 or Jones-Dole B coefficient in eq. 2.4.

The use of equations which recall the classical Debye-Hückel electrolyte theory and its extensions gives an empirical description of the properties influenced by the presence of ions. But these approaches fail, since the fitting

parameters that must be invoked vary, even for the same electrolyte, depending on the system under investigation.[28]

As an alternative approach - due to the lack of a consistent theoretical model able to explain and predict the behavior of a specific electrolyte in a given situation - the extensive analyses of correlations between different experimental results and different physicochemical properties (Jones-Dole B coefficients, molar refractivities, surface tensions, etc.) that are specific "fingerprints" for different ions, have been attempted.[66–69]

Based on this approach, the most diffuse empirical set of rules is certainly the law of "Matching water affinities" developed by Kim D. Collins. [70] Before discussing that rule and its limitations, let us introduce an useful, although in part misleading, classification of ions.

2.1.4. First attempts of classification: Kosmotropic and Chaotropic ions

In their studies, Jones and Dole observed that some salts cause an increase and others a decrease of aqueous solutions viscosity.[35] The effect of the ions on the viscosity of water solutions can be related to the modifications that ions produce to a hypothetical 'water structure'. Ions are divided into two classes depending on the sign of the B coefficient and hence, as a function of their ability to promote the order (kosmotropes, $B > 0$) or the disorder (chaotropes, $B < 0$) of water molecules. The classification of ions into 'water structure maker' and 'water structure breaker' was mentioned for the first time in 1938 by Kujumzelis[71] and successively by Stewart,[37] Frank et al.,[72] Corey,[38] and Gurney.[73] Kosmotropes (*order maker*) are small ions which carry a high charge density and interact with water molecules more strongly than water molecules do among themselves. Differently, chaotropes (*disorder maker*) are large ions

with a low charge density which interact with water more weakly than water molecules do among themselves.

The description of kosmotropic and chaotropic ions in terms of hydration is supported by the values of absolute enthalpies of hydration ($\Delta H°_{hyd}$) reported in (Tab. 2.4).

Table 2.3 Ionic radii [59] and absolute hydration enthalpies[74] for a range of cations and anions classified as kosmotropes and chaotropes

	Cations	Ionic radius (Å)	$\Delta H°_{hyd}$ / (KJ/mol) at 298K	Anions	Ionic radius (Å)	$\Delta H°_{hyd}$/ (KJ/mol) at 298K
Kosmotropes	Li$^+$	0.60	-520	F$^-$	1.36	-506
	Na$^+$	0.95	-405	------	------	------
Chaotropes	K$^+$	1.33	-321	Cl$^-$	1.81	-364
	Rb$^+$	1.48	-300	Br$^-$	1.95	-337
	Cs$^+$	1.69	-277	I$^-$	2.16	-296

Kosmotropes have very negative values of $\Delta H°_{hyd}$. This means that the hydration process is thermodynamically more favorable than for chaotropic ions which have less negative values of $\Delta H°_{hyd}$. The consequence is that kosmotropic ions in water are strongly hydrated while chaotropes are only weakly hydrated. The $\Delta H°_{hyd}$ of the single ions, can be also considered in terms of "affinity for water molecules" as reported by Collins, but this formalism is not rigorous, as will be discussed below.

If the solution enthalpies at infinite dilution (ΔH°_{sol}) of a range of salts are reported versus the difference (anions minus cations) in absolute enthalpies of hydration, a typical "volcano's plot" is obtained (Fig. 2.4).
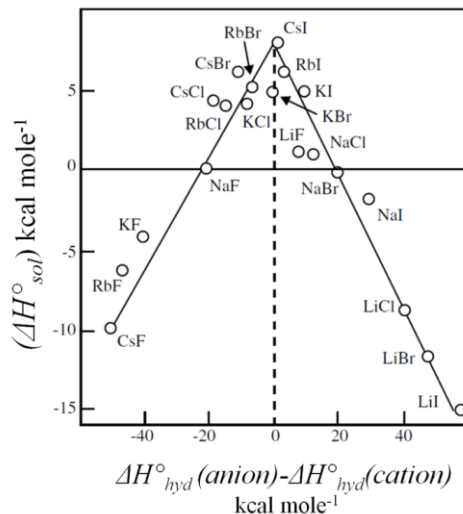

Figure 2.4 Standard solution enthalpy at infinite dilution for a range of salts (ΔH°_{sol}) reported as a function of the difference between the enthalpies of hydration of the corresponding gaseous anion and cation [ΔH°_{hyd} (anion)- ΔH°_{hyd}(cation)] according to D. F. C. Morris (1969).[73]

The 'Volcano plot' shows that when a cation and an anion have similar values of ΔH°_{hyd}, - i.e. they are both kosmotropic (Li$^+$F$^-$) or both chaotropic (Cs$^+$I$^-$) - salt dissolution is an endothermic process ($\Delta H^\circ_{sol} > 0$). On the contrary, when a cation and an anion have different ΔH°_{hyd}, - i.e. an ion is chaotropic and its counterion is kosmotropic (Cs$^+$F$^-$) or (Li$^+$I$^-$) - salt dissolution is an exothermic process ($\Delta H^\circ_{sol} < 0$).

2.2.   The law of 'Matching water affinities' (Collins)

In 1997 Kim D. Collins proposed an empirical rule based on the previous classification of ions in kosmotropic and chaotropic and on the observation of volcano plots.[75]
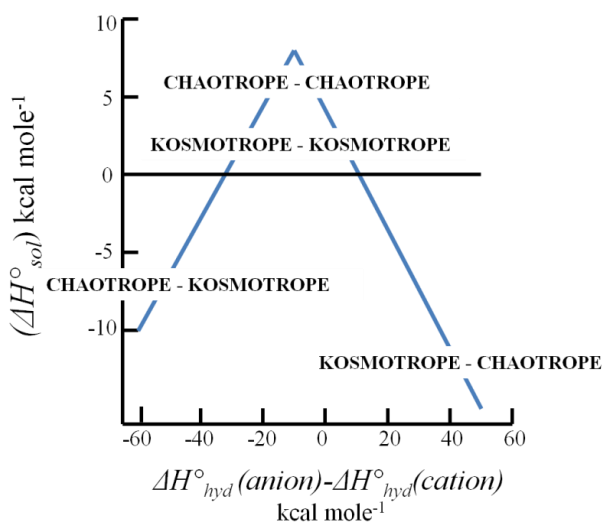

Figure 2.5 Schematization of the volcano plot by using the kosmotropic-chaotropic classification of ions.[70]

When a salt is dissolved in water, the constituent ions can either form ion-pairs or stay in solution as hydrated ions. The salts which have positive ΔH°_{sol} and similar ΔH°_{hyd} of the constituents ions tend to form ion-pairs (Fig. 2.5). In the case of a salt constituted by kosmotropic ions (K-K), the formation of ion-pairs is attributed to the strong electrostatic interaction between the two small ions that is higher than the energy of interaction between the dissociated ion and the water molecules. In the case of a salt formed by two chaotropic ions (C-C) the electrostatic interaction between the ions is weak,

nevertheless they are squeezed together by water molecules since they interact among them more strongly than with chaotropes.

The salts which have negative $\Delta H°_{sol}$ and different values of $\Delta H°_{hyd}$ of the constituent ions, tend to stay in solution as hydrated ions (Fig. 2.5). These salts are constituted by a chaotropic ion and a kosmotropic counter-ion (C-K or K-C) and the formation of ion-pairs is energetically unfavorable since the energy consumed for breaking a kosmotrope-water bond is higher than the energy gained to break a chaotrope-water bond.

By considering the enthalpies of hydration as a measure of the water affinity of the single ions, Collins summarized the previous observations in an empirical rule called "the law of Matching Water Affinities" (MWA). This rule states that: "*opposite charged ions in free solution form inner sphere ion pairs spontaneously only when they have equal water affinities*". Collins' rule is schematized in Fig. 2.6.
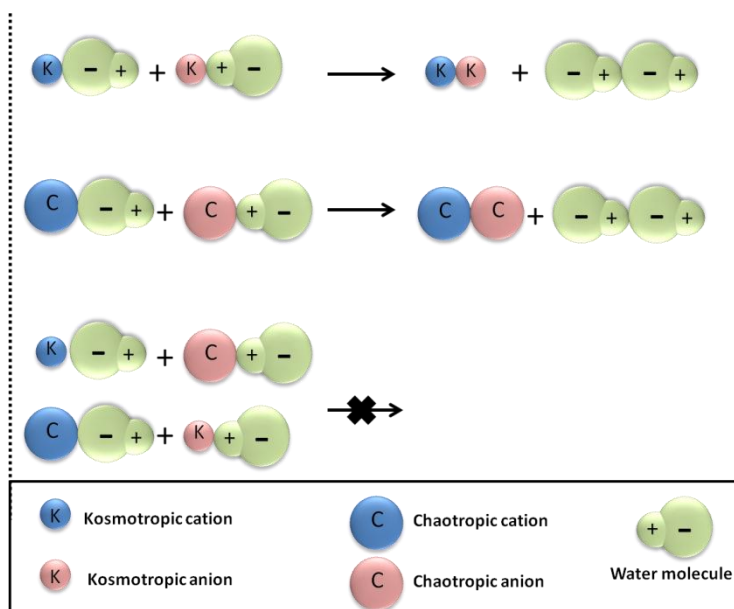
Figure 2.6 Schematic representation of the law of "matching water affinities".[70]

This empirical law is able to explain in a simple way some ion-specific phenomena. One of the success of this approach is the qualitative explanation of the Hofmeister series reversal in the activity coefficients of simple aqueous alkali metal salt solutions (Fig. 2.7).
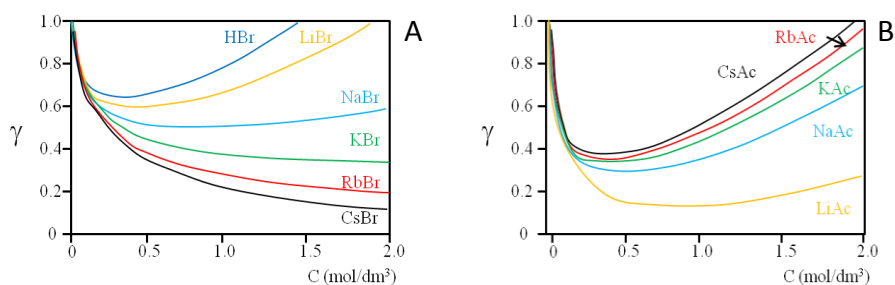
Figure 2.7 A) Activity coefficients of HBr and several alkali bromide solutions as a function of salt concentration. B) Activity coefficients of several alkali acetate solutions as a function of salt concentration.[59]

For bromide salt solutions the activity coefficients increase with increasing the kosmotropic character of the cations, whereas for the acetates the order is reversed. According to Collins' law, bromide ions (which are considered to be chaotropes) would form stable ion-pairs with chaotropic cations (i.e. Cs^+) while would have less affinity for kosmotropic cations (i.e. Li^+). On the contrary, acetate ions (which are considered to be kosmotropes) would form stable ion-pairs with kosmotropic ions (i.e. Li^+) rather than with chaotropic ions (i.e. Cs^+). Indeed activity coefficients reflect this tendency giving lower values for salts formed by ions with similar water affinities (C-C and K-K).

Collins' law can also be used to understand the behavior of some head groups very popular in biological systems, such as sulphates or carboxylates.[76] The classification of a headgroups as chaotropic or kosmotropic allows to extend the MWA law also to more complicated systems. An example is given by the selective binding of alkali counterions to anionic Sodium Dodecyl Sulfate

(SDS) surfactant films by ion floating technique.[77] Similarly to the case of activity coefficients of salts, a reversed series of cation binding is observed when SDS micelles are replaced by dodecanoate micelles, supporting respectively the attribution of a chatropic and kosmotropic character to the head groups of surfactants. The MWA approach has been proved to be also useful to explain the binding of ions to lipid membranes,[78] the swelling or deswelling of hydrogels,[79] and other examples.[27,37,54]

2.2.1.   Criticism of Collins' rule

The success of Collins' rule is due to its simplicity and easy applicability to predict and explain some experimental observations. Despite that, this phenomenological rule is unable to explain the true nature of the ion-specific effects and have some serious limits. One of the most interesting observation that can be moved in this direction is related to the thermodynamic cycle reported in Fig. 2.8. [81]
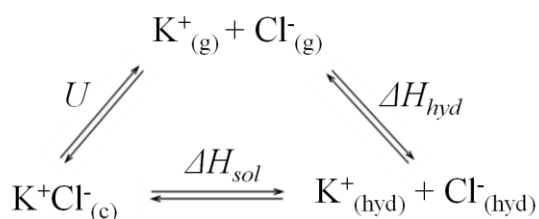
Figure 2.8 Thermodynamic cycle for the dissolution of potassium chloride in water [81]

The standard enthalpy of solution of a salt at infinite dilution (ΔH°_{sol}) is the heat change that takes place when a mole of salt is completely dissolved in a very large excess of water, measured under standard conditions. It can be calculated as the sum of the salt lattice energy (internal) U plus the sum of the hydration enthalpies of the single ions (ΔH°_{hyd}):

$$\Delta H_{sol} = U + \Delta H_{hyd}$$

(2.6)

At infinite dilution, an ion will never interact with its counter-ion effectively. The enthalpy of solution then, will not be influenced by the interaction energy between the ions in water (and hence by their propensity to form ion-pairs).

Also, the calculated enthalpy of hydration (Fig. 2.4) is not really a measure of the ion-water molecule affinity, but rather, is a measure of the average electrostatic interaction of the ion with the bulk water and not just an individual molecule with which it is in contact.[81]

For those and other reasons[82] Collins' law is not able to explain all the variety of effects that can be ascribed to the ion-specific effects.[51,83] A more rigorous approach for the explanation of Hofmeister effects is the consideration of dispersion forces acting among ions and between ions and charged interfaces.

2.3. The correct treatment of dispersion forces (Ninham)

Turning the attention to the intermolecular forces considered in terms of pair potentials, in 1997 Ninham and Yaminsky proposed an improved alternative to DLVO theory (See Sec. 1.4) where ion-ion and ion-interface interactions are affected not only by electrostatics but also by dispersion forces.[84] This approach involves the introduction of an additional potential $U_i(x)$, due to dispersion forces, directly in the Poisson-Boltzmann relationship. Hence both electrostatic and dispersion interactions are consistently expressed via the same exponential equation:

$$\nabla^2 \psi = \frac{1}{\varepsilon_0 \varepsilon_r} \sum_i n_i z_i e^{\left(\frac{-z_i e \psi(x) + U(x)_i}{k_b T} \right)}$$

(2.7)

where ε_r is the medium permittivity, ε_0 the vacuum permittivity, z_i the charge of the ion and c_{0i} is the bulk concentration of the electrolyte. The term $U_i(x)$ can be obtained by the relationship:

$$U_i(x) = \frac{B_i f(x)}{x^3}$$

(2.8)

where B_i is the dispersion coefficient, x is the distance of the ion from the interface, and $f(x)$ is a function of the reciprocal of the size of the ion (a):

$$f(x) = 1 + \frac{2x}{\sqrt{\pi} a} \left[\frac{2x^2}{a^2} - 1 \right] \exp\left(\frac{-x^2}{a^2} \right) - \left[1 + \frac{4x^4}{a^4} \right] erfc\left(\frac{x}{a} \right)$$

(2.9)

The dispersion coefficient (B_i)[85] is specific of the interface considered and depends on the ion dynamic polarizability α_i^* and the dielectric properties of both the interface ε_r and the solvent ε_w:

$$B_i = \frac{k_b T}{4} \sum_{n=0} (2 - \delta_{0,n}) \frac{\alpha_i^*(i\omega_n)}{\varepsilon_w(i\omega_n)} \left(\frac{\varepsilon_w(i\omega_n) - \varepsilon_s(i\omega_n)}{\varepsilon_w(i\omega_n) + \varepsilon_s(i\omega_n)} \right)$$

(2.10)

Where the term $i\omega_n$ represents the set of imaginary frequencies for a given ion (derived from the Lifshitz theory).[84]

The ionic sizes, static ion polarizabilities and dispersion coefficients (for instance at the water-protein interface) for some of the most common ions are listed in Table 2.5.

Table 2.4 List of ionic sizes (hard sphere radius), a, static ionic polarizabilities, α_0, and dispersion constants B *(water-protein like interface)*, for the ions.

Ion	a (Å)	α_0 (Å^3)	B (10^{-50} Jm^3)
F$^-$	1.12	1.218	n.a.
Cl$^-$	1.86	4.220	-1.26
Br$^-$	2.16	6.028	-1.70
ClO$_4^-$	2.35	5.488	-1.53
SCN$^-$	2.39	7.428	-2.27
Li$^+$	0.42	0.028	n.a.
Na$^+$	0.67	0.131	-0.20
K$^+$	1.06	0.795	n.a
Cs$^+$	1.62	2.354	n.a.

Hofmeister effects are hence the result of a delicate interplay between hydration, non-electrostatic potentials and ionic size effects.

Experimental verification of this theory has been hindered by the lack of accurate values of ion polarizabilities. Recently, progress in calculating B_i coefficients from *ab initio* ion polarizabilities for some interfaces (i.e. air-water,[86] water-silica, water-alumina,[87] and water-protein[88]) were made.

## 2.3.1. Toward consistency between theory and experiment

The new theory of ion specificity based on the correct treatment of dispersion forces is being able to explain both qualitatively and quantitatively the Hofmeister phenomena observed in several systems. Here two of the most important examples of the success of that theory are reported.

2.3.1.1.   Prediction of activity coefficients of some salts

As reported above, the theories of electrolytes consider ion-ion interactions due to electrostatic forces only. Extensions of Debye-Hückel limit law that permit to improve the agreement between theory and experiment only for concentrations below 0.1 M have been reported but the use of a set of adjustable parameters that change depending on the system is generally required.[69]

Recently, Parsons and Ninham compared the activity coefficients of a range of alkali halides calculated by using the modified Poisson-Boltzmann equation approach, with the experimental values reported by Robinson and Stokes in 1959.[59]
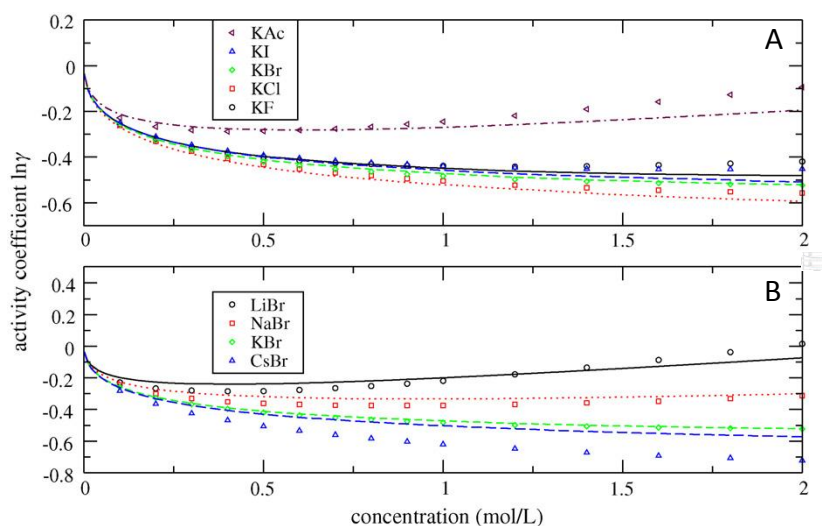
Figure 2.9 Experimental activity coefficients for a range of potassium salts (A) and bromides (B) (single points). Continuous lines indicate theoretical calculations according to the Poisson-Boltzmann modified equation.[86]

The calculated activity coefficients show a good agreement with the experimental data over a wide range of concentration for anions (Fig.2.9A) and

cations (Fig.2.9B) series. The trend is verified also for concentrations of electrolyte higher than $1 molL^{-1}$ where the activity coefficients are more spread. Some discrepancies were found for the alkali bromides (especially for Li^+ and Cs^+) and are attributed to the special model used to estimate the hard sphere radii of metal cations.[86]

Differently from Collins' rule, which explains only qualitatively the trend of the activity coefficients in the experiments of Robinson et al., this approach reproduces semi-quantitatively the values of activity coefficients thus revealing the fundamental contribute of dispersion forces in Hofmeister phenomena.

2.3.1.2. *Hofmeister series reversal with protein precipitation*

Another interesting successful example of the approach proposed by Ninham concerns the explanation of the Hofmeister series reversal. This effect was observed for the first time by Robertson[31] in 1911, but similar trends were found for different systems and different conditions. [89–91]

In an important study, Cremer and coworkers investigated the cloud point temperature of lysozyme in presence of different sodium salts (Fig. 2.10).
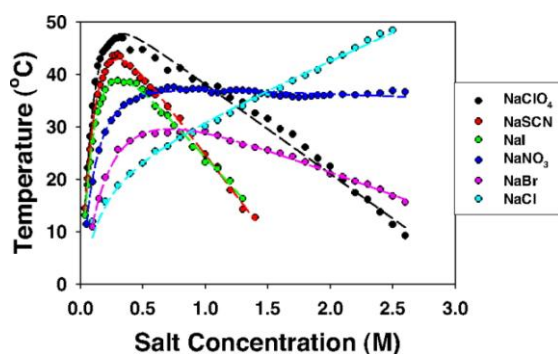

Figure 2.10 The cloud-point temperature of lysozyme as a function of anion type and concentration.[48]

They found that the cloud point temperature for the liquid-liquid phase transition of lysozyme (pI=11) at pH 9 (positive net surface charge) follows two distinct Hofmeister series depending on salt concentration: direct for low salt concentration and reversal for high salt concentrations. Below the cloud point protein molecules aggregate into a cloudy protein-rich phase, and above it the protein molecules are dispersed into a clear solution. The temperature at which the cloud point occurs can be correlated with the forces acting among protein molecules. In particular, the higher the temperature at which cloud point occurs, the stronger the attractive forces among proteins will be (or the weaker the repulsive forces will be). Zhang and Cremer related the effects of the anions to two factors: the attenuation of electrostatic repulsion through the specific association of chaotropic anions to the positively charged groups at lysozyme surface and the specific ability of the ions to alter the surface tension of the protein/aqueous interface.[48]

In a recent paper Boström et al. proposed an alternative explanation of the series inversion, invoking the charge-reversal mechanism.[88] These authors modified Poisson-Boltzmann equation according to Ninham's theory, showing that at low salt concentrations more polarizable (chaotropic) anions are more strongly adsorbed due to non-electrostatic interactions. At high salt concentrations, the effective surface charge is reversed in sign. The electrostatic potential switches from positive to negative due to anion adsorption, and a reversal series is observed (Fig.2.11A). The inversion of the series due to surface properties is known as charge reversal, and can be invoked also to explain the inversion that occurs with changing pH.

Figure 2.11B shows the force between two globular proteins with a fixed separation for different salt types as a function of the electrolyte concentration.
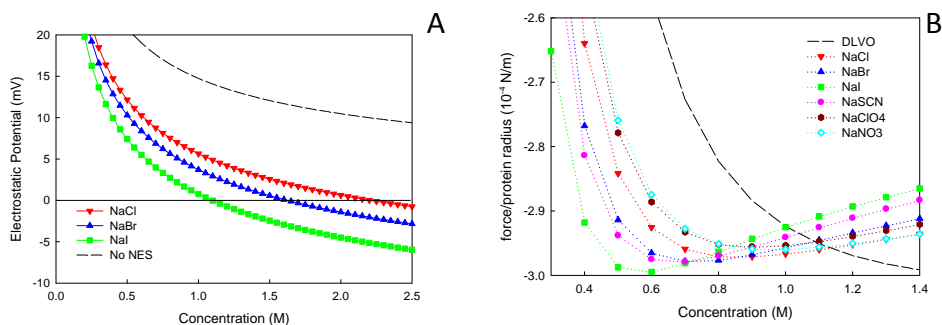
Figure 2.11 A) Electrostatic potential at a protein-like surface as a function of salt concentration for different ionic species. B) Total force (normalized with protein radius) versus salt concentration for two lysozyme proteins with closest distance 20 Å apart at pH 9.

In good agreement with the experimental results of Cremer, the interaction between proteins in a lysozyme suspension was found to follow a reversed Hofmeister series at low salt concentrations (I^- > SCN^- > Br^- > Cl^- > ClO_4^- > NO_3^-) and a direct Hofmeister series at high salt concentrations (I^- < SCN^- < Br^- $\approx$ ClO_4^- < NO_3^- $\approx$ Cl^-). At low salt concentrations the most polarizable anions are more strongly adsorbed due to the ion-surface dispersion interactions reducing the electrostatic repulsion between protein molecules and making easier for them to aggregate. This is the same effect observed for the cloud point temperature of lysozyme.[48] As more salt is added, at a certain concentration, the force curves reveal a minimum which is ion specific similarly to the experimental maximum in cloud point temperatures. A further increase of the salt concentration produces an inversion in the curves of force giving a reversal Hofmeister series, again in agreement with the experiments.

The approach of the correct treatment of dispersion forces by using a modified Poisson-Boltzmann equation developed by Ninham is being used for the explanation of other experimental cases. Some of them will be discussed in the following chapters of the present thesis.

3. *Chapter*: Experimental Techniques

3.1.   Introduction

In the present thesis Hofmeister phenomena on charged interfaces were investigated by means of potentiometric titrations (PT), electrophoretic light scattering (ELS) and differential pulse voltammetry (DPV).

− Potentiometric titrations were used to study the net proton charge of two different types of interface: proteins (BSA) and silica-based ordered mesoporous materials (SBA-15).

− Electrophoretic light scattering was used to study the electrophoretic mobility of a protein (BSA) aqueous solution. The obtained mobilities were then used to calculate the zeta potential and the effective charge of BSA by means of Henry equation.

− Differential-pulse voltammetry was used to explore the electrochemical properties of a redox protein (cytochrome c). The electrochemical process occurs when the diffusing redox protein approaches an interface constituted by a modified gold electrode.

The basic principles of these techniques are reported in the following paragraphs.
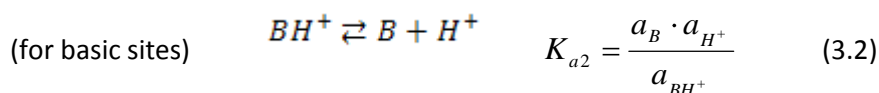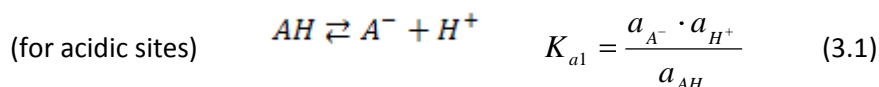
3.2.   Potentiometric titrations (PT)

In potentiometric titrations (PT) the activity of a certain ion in a solution is recorded as a function of the volume of the added titrant. The activity is estimated by measuring the potential of the sample solution with respect to that of a reference solution. The device used to measure the ionic activity is a potentiometric cell constituted by a combined electrode (composed by a measuring and a reference electrode) dipped in the sample solution, and connected to a potentiometer. The difference of potential, measured by the

potentiometer, is converted into the ion activity by means of the Nernst equation.

3.2.1. Determination of the surface charge of an interface

Potentiometric titrations can be used to determine the charge of an interface. According to the mechanism reported in the sec. 1.4.1, an interface can become charged due to the dissociation of either acidic or basic surface groups:

(for acidic sites) $\qquad AH \rightleftarrows A^- + H^+ \qquad K_{a1} = \dfrac{a_{A^-} \cdot a_{H^+}}{a_{AH}}$ (3.1)

(for basic sites) $\qquad BH^+ \rightleftarrows B + H^+ \qquad K_{a2} = \dfrac{a_B \cdot a_{H^+}}{a_{BH^+}}$ (3.2)

The net proton charge will be determined by the algebric sum between positive and negative surface groups at any pH.

In a common experiment a sample, the surface charge of which has to be measured, is suspended/dissolved in a water solution (containing a supporting electrolyte). The initial pH of the sample (pH_{init}) is recorded and then, a measured amount of a strong acid is added up to reach the desired acidic pH. During this procedure the interface is protonated becoming either neutral - if acidic sites are present (eq. 3.1) - or positively charged - if basic sites are present (eq. 3.2) -.

In order to obtain a surface charge/pH curve a "blank" sample (which does not contain the substance which generates the charged interface) has to be brought at the same acidic pH of the sample. Then, both the sample and the

blank are titrated by adding successive amounts of titrant solution, and recording pH after each addition, up to the final basic pH. It is worth noticing that during the initial acidification step the volume of added acid to the sample and to the blank solution can be either different (if the same initial pH is being reached Fig. 3.1A), or equal, (resulting in a different initial pH for the two solutions Fig.3.1B).
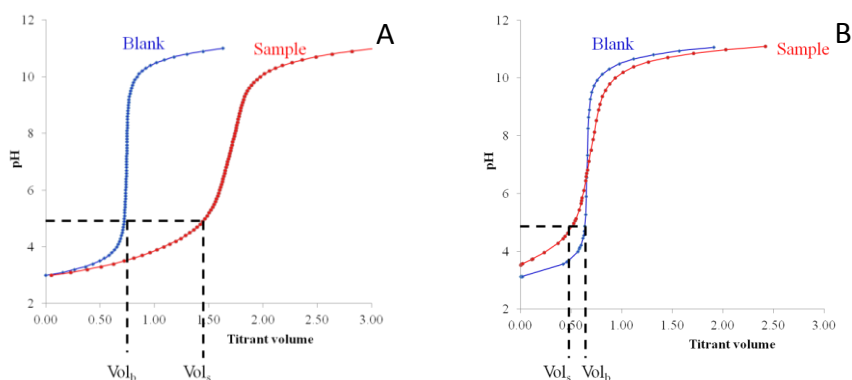
Figure 3.1 Two general examples of sample and a blank titration: A) solutions treated with different volume of acid to reach the same initial pH, B) solutions treated with fixed volume of acid.

The titration could be carried out also from basic to acidic pHs. This titration modality can be used to determine the "range of reversibility" of particular samples, but this will be discussed in more detail later.

Potentiometric titration allows the determination of the surface charge/pH curve by taking into account the difference of acid/base amount between the sample and the blank. The moles of hydrogen ions bound/removed from an interface (α_H), if different additions of acid are carried out (Fig. 3.1A), can be calculated at any pH by the equation:

$$\alpha_H = (mol_s^{acid} - mol_b^{acid}) - (mol_s^{base} - mol_b^{base}) =$$
$$= [(Vol_s^{acid} - Vol_b^{acid}) \cdot c_{acid}] - [(Vol_s^{base} - Vol_b^{base})_{pH} \cdot c_{base}] \qquad (3.3)$$

where Vol_s^{acid}, Vol_b^{acid}, Vol_s^{base} and Vol_b^{base} are the volumes of the acid/base used for the sample and the blank at the same pH and $c_{acid/base}$ is the concentration of the acid/base used in the titration.

In the case of fixed addition of acid (Fig.3.1B), the term $mol_s^{acid} - mol_b^{acid}$ in eq. 3.3 is zero, and the moles of hydrogen ions bound/removed from an interface (β_H) are calculated by the equation:

$$\beta_H = mol_b^{base} - mol_s^{base} = [(Vol_b^{base} - Vol_s^{base})_{pH} \cdot c_{base}] \qquad (3.4)$$
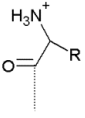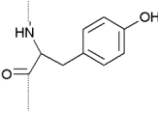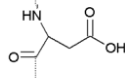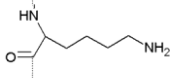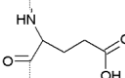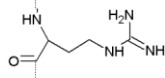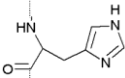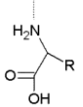
The calculation of the surface charge depends on the particular interface which is being investigated. The moles of hydrogen ions bound/removed from the interface (α_H and β_H) at any pH are the basic information needed to calculate the surface charge. These quantities, however, are not absolute values, but rather are relative to the number of hydrogen ions bound to the interface at the initial pH of the sample (pH_{init}). In next paragraphs surface charge calculations for of two types of interface will be illustrated in detail.

3.2.2. Titration of proteins

A protein in an aqueous solution constitutes a biological interface which can be characterized through potentiometric titrations. Proteins are ampholytic molecules that acquire a charge in aqueous media due to the dissociation of acidic and basic amino acids (Tab. 3.1) occurring at their

surface. The protein surface charge (Z_p) / pH curve can be determined by means of potentiometric titrations.

Table 3.1 Charged amino acid groups of protein and their thermodynamic pKa.[92]

Acidic/basic groups		pKa	Acidic/basic groups		pKa
	α-Amino group	7.9		Tyrosine	10.0
	Aspartic acid	4.5		Lysine	10.4
	Glutamic acid	4.7		Arginine	12.0
	Histidine	6.1		α-Carboxilic group	3.6

The moles of hydrogen ions bound/removed at any pH from a protein during a potentiometric titration are determined by α_H (eq. 3.5). Since α_H depends on the number of hydrogen ions bound at the initial pH of the solution (pH_{init}), for the determination of the surface charge it is necessary to choose a "reference point", that is an initial pH which has a physical significance for the protein under study.[93] There are three possible "reference points" which can be used:

- The pH of protein's maximum acidic capacity;
- The pH of protein's maximum basic capacity;
- The isoionic point of the protein.

The first two points represent the pH at which the surface groups of the protein are completely undissociated (maximum positive charge) or completely dissociated (maximum negative charge) respectively. These two reference points, however, are not of practical use since the proteins can be subjected to denaturation due to exposure to extreme pH values.([2]) For this and other reasons it is preferable to refer α_H to the isoionic point (*IIP)* of the protein.
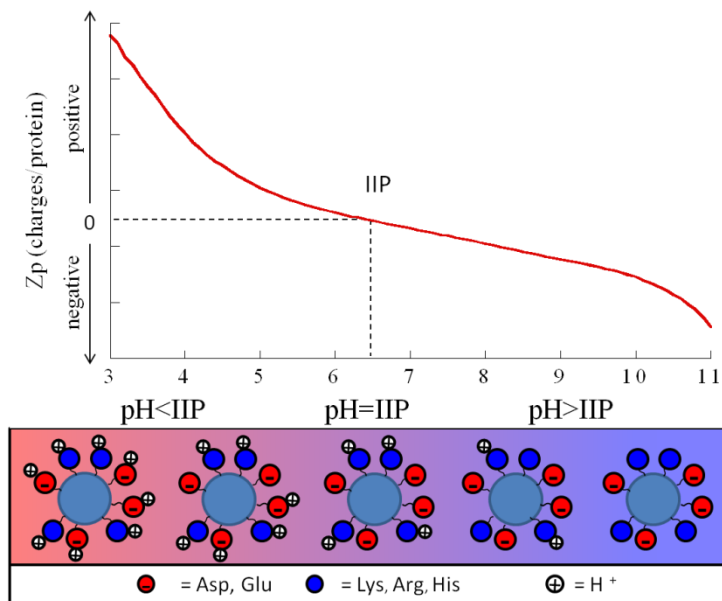
The isoionic point is the pH at which the protein, in the absence of other adsorbed ions except hydrogen, has the same number of positive and negative charges. Solutions made from commercial proteins are usually not at the IIP, due to the presence of stabilizing electrolytes (salts and buffers). The IIP can be reached by using a process of dialysis through which all the other ions are removed from the solution of the protein. Alternatively, the simplest way to bring the protein solution at its isoionic pH is to carry out a preliminary titration where the pH is brought to the value of IIP reported in the literature. By setting the IIP as the initial pH of the sample (and blank) solution, the moles of hydrogen ions bound/removed α_H (eq. 3.3) divided by the moles of protein in the sample, gives the protein charge (Z_p):

$$Z_p = \frac{\alpha_H}{mol_p}$$

(3.5)

---

[2] At high or low pH values, some irreversible changes in protein structure can occur. The loss of protein's native structure can bring to the exposure of internal groups, thus modifying protein properties and producing changes in the shape of the charge/pH curve. To avoid denaturation it is necessary establish the "range of reversibility" of the surface charge curve of the protein, that is the ability to obtain the same Z_p values after exposure of the protein solution to high or low pHs.[93]

Z_p is an adimensional number and represents the net proton charge of a protein molecule at a given pH. Figure 3.2 shows a schematic representation of the protein titration process.([3])

Figure 3.2 Graphical representation of the zwitter-ionic model for protein titration. Big circles (pale blue) represent a generic protein. Small red circles represent the acidic residues of the protein (i.e. Asp, Glu); small blue circles represent the basic residues (i.e. Lys, Arg, His); small white circles represent hydrogen ions.

---

[3] At low pH values ($pH<IIP$), all the acidic and basic sites are protonated; that is, carboxilate are neutral ($z^-_{pH}=0$) and aminelike residues are positively charged ($z^+_{pH}>0$). The net charge of the protein is then positive $Z_p>0$. By increasing the pH, due to the addition of the base, the acidic residues lose their protons, thus becoming negatively charged (R-COO⁻). This will decrease the positive net charge of the protein. When pH equals the *IIP*, $Z_p=0$ because of the presence of the same number of positive and negative charges ($z^+_{pH}=z^-_{pH}$). A further addition of titrant solution removes protons by the basic sites which becomes uncharged. The net charge of the protein then becomes negative ($Z_p<0$), not because of the generation of new negative charges but due to the neutralization of the positively charged basic groups.

3.2.3. Potentiometric titrations of silica based powder materials

The second type of interface investigated in this thesis by means of potentiometric titrations, is a silica based ordered mesoporous material (OMM), namely SBA-15.[94] OMMs are characterized by an ordered structure, a high surface area and a narrow distribution of the pore size. When a silica based powder material is suspended in an aqueous media (suspension), it acquires a surface charge due to the amphoteric behavior of surface silanol groups.[95] Silica surface charge can be neutral, positive or negative depending on pH, according to Figure 3.3.
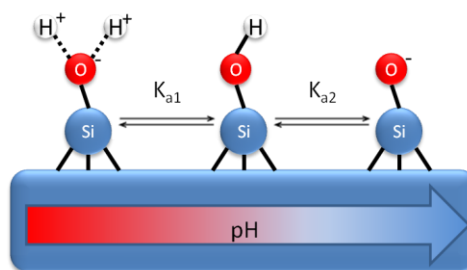
Figure 3.3 Graphical representation of the surface groups of silica and their dissociation as a function of pH.

The pK_a values of silica fall generally at acidic pHs, but they can change depending on the particular structure which is being considered, due to the different interactions among the surface silanol groups.[96] From the values of the pK_a it is possible to calculate the point of zero charge (pzc) of the material:

$$pzc = \frac{pK_{a1} + pK_{a2}}{2}$$

(3.6)

pzc represents the pH at which the material has a zero net charge. The pzc of silica based OMMs was found to be in the range between 3.6 - 4.[97] In this work the surface charge of the material was investigated in the range of pH 4 - 10. In this conditions, the equilibrium involved is mainly that due to the second dissociation (K_{a2}), at which the surface silanol groups change from uncharged to negatively charged form (Fig. 3.3).

As remarked above, silica based OMMs have complex structures and the process of diffusion of a substance inside the pores is a slow process. This means that, in a potentiometric titration, every variation in the proton activity of the suspension requires a long equilibration time with the internal interface of the material. Here, according to the methods reported in the literature,[98,99] a fixed volume of acid was added to the samples (and to the blanks). The solutions are then stirred and kept at constant temperature over-night to allow the equilibration of the interface with the bulk solution. The solutions then are titrated to the final basic pH.

For a fixed addition of acid, the amount of hydrogen ions bound/removed from the interface (β_H) in a potentiometric titration can be calculated by the equation 3.6. OMMs are characterized by high surface areas and then their charge is better expressed as surface charge density σ (C m^{-2}):

$$\sigma = \frac{F \cdot \beta_H}{S_{BET} m}$$

(3.7)

where F (96485 C mol^{-1}) is the Faraday constant, S_{BET} (m^2 g^{-1}) is the surface area of the material determined by the BET method[100] and m (g) is the mass of material used in the titration experiment.
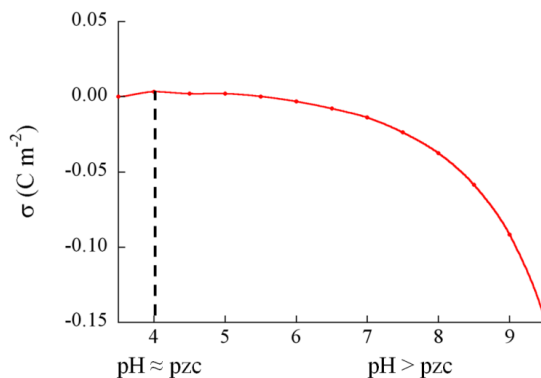
Figure 3.4 Graphical representation of the surface charge density σ of an OMM (SBA-15) as a function of the pH.

Fig. 3.4 shows a plot of σ as a function of pH for a SBA-15 sample. At pH $\approx$ pzc the silanol groups are in the uncharged form (-Si-OH) and the material has a zero surface charge density. The addition of the base results in a pH increase, then the silanol groups start to dissociate and the surface charge becomes negative.

At acidic pHs silica-based materials are chemically stable[95] for indefinite time. At basic pHs, instead, silica based materials start to dissolve, due to the basic hydrolysis of the internal siloxane groups forming the structure.[95] Indeed pH = 10 was the highest value reached in these investigations.

3.2.4. Experimental equipment: the glass electrode and the automatic titrator

As reported above, a potentiometric titration is a plot relating the pH of a solution to the volume of an added titrant solution. The pH of the solution can be determined by means of an ion-selective electrode for H^+ ions (glass electrode).

The glass electrode is characterized by the presence of a thin glass membrane, sensitive to the changes of H⁺ activity. H⁺ sensitive glasses are composed mainly of SiO_2, doped with different amounts of other metal oxides (i.e. Na_2O, CaO). When the membrane is in contact with two different solutions (an unknown external solution and a known internal solution) both surfaces become hydrated, and an equilibrium is established between the two sides of the layer as a function of their respective H⁺ activity (Fig.3.5A).
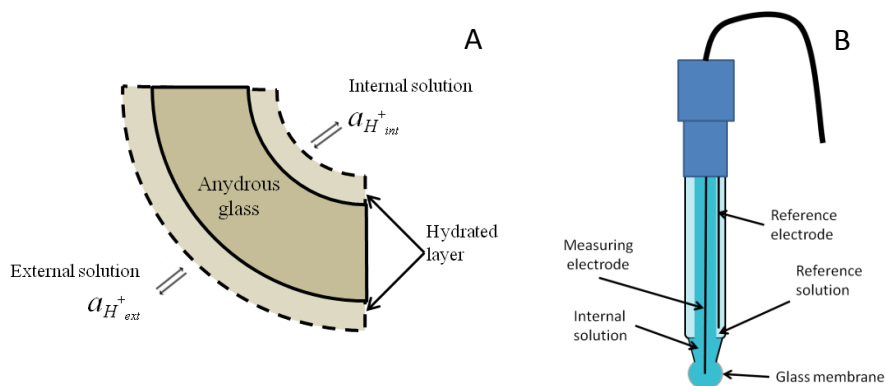
Figure 3.5 Representation of A) pH sensitive membrane of a glass electrode B) a combined glass electrode.

The potential generated between the two sides of the membrane can be determined as a function of a reference potential (generated by an Ag/AgCl reference electrode) and the hydrogen ion activities of the external and the internal solution according to the Nernst equation.[101] The device constituted by the glass electrode and the reference electrode is usually referred as combined electrode (Fig.3.5B). The difference of potential between the external solution and the reference electrode can be detected by a potentiometer.

If in a measurement the temperature is set up to *298K*, the theoretical potential across the glass membrane varies by 59.2 mV for a change of a pH unit and the Nernst equation assumes the form:

$$E = K - 0.0592 pH \qquad (3.8)$$

where K is a constant of the electrode that must be determined through a standard calibration procedure. The calibration requires the measure of the potential of different solutions having a stable and known pH (pH Buffers). The calibration of the pH electrode has to be done before each set of measurements.

Potentiometric titrations can be carried out manually as well as automatically by means of an automatic titrator. The advantage of using an automatic equipment is that the titration parameters, such as the addition of a preset volume of titrant or the evaluation of the pH after each addition, can be automatized by setting up a priori these parameters in the software.

In this work potentiometric titrations were carried out using an automatic titrator Titrando 836 from Metrohm (Fig.3.6). The titrator is composed by a central unit (1) that deals with different devices, such as different dosing units (2), a stirrer (3) and the electrode for the measure of pH (4) that along with a thermostatic vessel, constitutes the sample cell (5). The central unit is connected with a computer (6) equipped with a software (Tiamo 1.3) that controls automatically the different devices, by means of a suitable operative system.

The parameters chosen for the preliminary and the effective titrations (i.e. drift, initial and end point of titration) are set up in the system together with the speed of stirring. Automatic titrations have been proved to be very useful for the determination of the surface properties of the interfaces. The high sensitivity that can be reached using an automatic titration, allows to reveal even very small changes in the bulk activity of H^+ which results into very accurate surface charges.
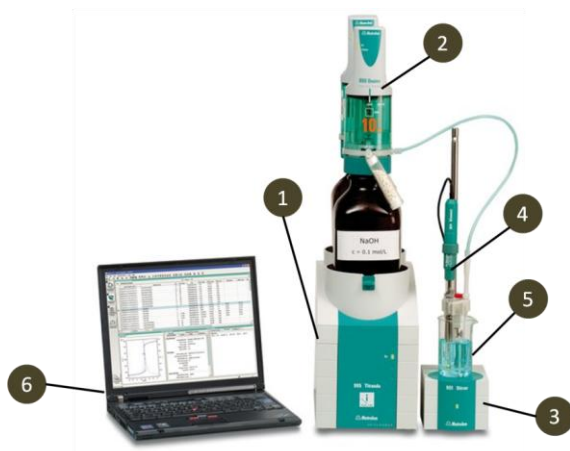
Figure 3.6 Picture of the automatic titrator Titrando 836: (1)central unit, (2) Dosing devices (acid and base), (3) magnetic stirrer, (4) glass electrode, (5) sample cell, (6) computer.

3.3. Electrophoretic light scattering (ELS)

In this technique an electric field is applied across a colloidal electrolyte solution. The suspended charged colloidal particles are attracted toward the electrode of opposite charge. Viscous forces acting on the particles tend to oppose to this movement. When the equilibrium between these two opposing forces is reached, the particles move with a constant velocity (mobility). As will be discussed later, the electrophoretic mobility of the colloidal particle can be determined by means of light scattering measurements.

3.3.1. Electrophoretic unity and Henry's equation

A colloidal particle dispersed in an electrolyte solution generates an electrical double layer that can be studied by solving the Poisson-Boltzmann equation for a spherical symmetry with the Debye-Huckel approximation (see

Sec. 1.2). When an electric field is applied across the solution, the charged particles will move toward the electrode of opposite charge carrying some of the ions in their surroundings (Fig. 3.7).
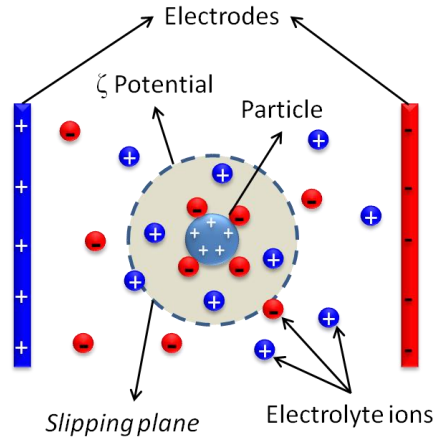
Figure 3.7 Graphical representation of an electrophoretic unity in the experiments of electrophoretic light scattering.

The colloidal particle and the electrolyte ions present in its surroundings up to the "*slipping plane"*, constitutes the "electrophoretic unity". The *slipping plane* is a theoretical boundary surface localized in the diffuse part of the double layer. The distance of the slipping plane from the surface of the particle cannot be measured but the potential measured at this point is referred as zeta potential (ζ).

The electrophoretic mobility (μ_e) of a charged colloidal particle is related to the zeta potential, and to the physico-chemical properties of the medium and of the particles by the Henry's equation:[102]

$$\mu_e = \frac{\zeta 2\varepsilon_0 \varepsilon_r f(\kappa R_p)}{3\eta}$$

(3.9)

55

where R_p is the hydrodynamic radius of the particle, κ is the Debye length (see Sec. 1.2), η is the viscosity of the medium and $f(\kappa R_p)$ is the Henry's function. The Henry's function is an asymptotic series derived from the PB equation[102] and can be calculated by the approximated relationship:[103]

$$f(\kappa R_p) = 1 + \frac{0.5}{1 + \exp[d\{1 + \log(\kappa R_p)\}]}$$

(3.10)

with d = 2.8 for κR_p <10 and 2.5 for κR_p >10.

Rearranging the Henry's equation, the electrophoretic mobility can also be related to the effective charge of the particle (Z_{eff}):[104]

$$\mu_e = \frac{Z_{eff}\, ef(\kappa R_H)(1 + \kappa R_b)}{6\pi\eta R_p(1 + \kappa R_p + \kappa R_b)}$$

(3.11)

where R_b is the average radius of the electrolyte.

3.3.2. 'Electrophoretic titration' of proteins

ELS is an useful technique for carrying out acid-base titration of colloidal particles if they change their effective charge as a function of pH. In this work the electrophoretic mobility of BSA protein was studied by changing the pH through the addition of an acid or a base. In this type of measurement the protein modifies its surface charge as a function of pH by means of the mechanism reported in Sec. 1.4.1.

A typical curve of electrophoretic mobility as a function of the pH is reported in Fig. 3.8.
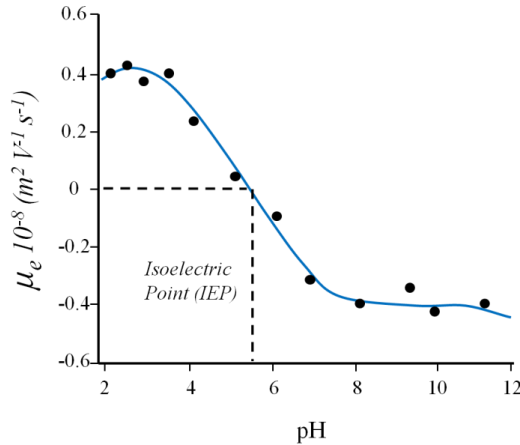
Figure 3.8 Electrophoretic mobility curve of a protein as a function of the pH.

For low pHs, the particle carries a positive charge and moves toward the cathode (μ_e>0). Increasing the pH, the mobility of the particle decreases up to become stationary in the electric field (μ_e=0). This particular pH is defined as the isoelectric point (*IEP*) of the particle. A further increase of pH, the surface becomes negative and the protein moves in the opposite direction, toward the anode (μ_e<0). Due to the adsorption of the electrolyte ions to the protein surface (ion binding), the value of the isoelectric point of a protein (*IEP*) is different from the isoionic point (*IIP*), but this effect will be discussed later in more detail.

3.3.3. Experimental equipment

In electrophoretic light scattering (ELS), the mobility of the charged particle under the influence of an applied electric field, is measured by monitoring the Doppler frequency shift (Δv) of the light scattered by the particle. The light scattered from stationary particles will have the same frequency and wavelength of the incident light, whereas light scattered by particles in motion

will be Doppler shifted. In ELS, the electrophoretic mobility (μ_e) of the particle is calculated from the Doppler frequency shift using the equation:

$$\Delta \nu = 2\mu_e \frac{\sin\left(\dfrac{\theta}{2}\right)}{\lambda}$$

(3.12)

where θ is the scattering angle and λ is the wavelength of the incident light.

The electrophoretic light scattering instrument is constituted by the following parts (Fig.3.9):

  − Laser light source

  − Sample cell

  − Detector for the scattered light

  − Computer
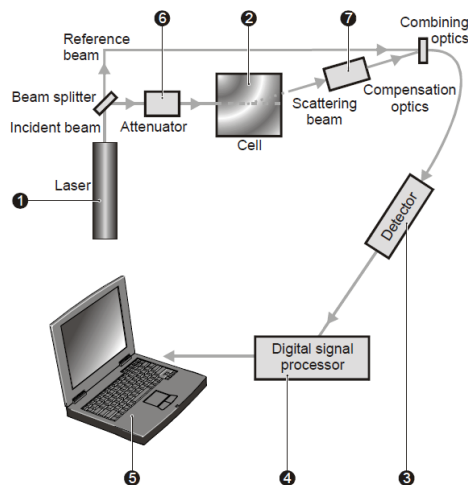
Figure 3.9 Schematic representation of a electrophoretic light scattering equipment: 1) laser source, 2) sample cell, 3) detector, 4) signal processor, 5) computer, 6) attenuator, 7) scattering beam.

The laser source (1) provides the light to illuminate the particles contained in the sample cell (2). This light source is split to provide an incident and reference beam. The laser beam passes through the centre of the sample cell, and the scattering at an angle of 17° is detected (3). When an electric field is applied to the cell, the particles moving through the cell will cause a Doppler shift to the frequency of the scattered light from which the corresponding value of electrophoretic mobility is calculated (eq. 3.12).

3.4. Voltammetry

Voltammetry is an electrochemical technique based on the measure of the current flowing through two electrodes (a working and a counter electrode) dipped in a solution containing an electro-active substance, while a potential scanning is imposed upon it. The resulting 'current-potential' and 'current-time' curves are analyzed to obtain information about the composition and the concentration of the electro-active species in the solution.

3.4.1. The faradaic process

The transfer of electrons between the electro-active species in solution and the electrode surface can be studied by considering a generic redox reaction:

$$Ox + ne^- \rightleftarrows Red$$

(3.13)

The pathway of the redox reaction at the electrode surface usually takes place in a sequence that involves several steps. In the simplest case a redox reaction at the electrode surface involves the mass transport of the electroactive specie to the electrode surface, the electron transfer across the

interface, and the transport of the product back to the bulk solution. The rate of the redox reaction is determined by the slowest step in the sequence (rate determining step). The net rate of the reaction may be limited either by mass transport of the electroactive specie or by the rate of the electron transfer. Whether a given reaction is controlled by the mass transport (*diffusive regime*) or electron transfer (*kinetic regime*) is usually determined by the type of compound being measured and by several experimental conditions (electrode material, medium, operating potential, mode of mass transport, time scale).

When the reaction is in diffusive regime (the rate at which the electroactive specie reaches the surface is the rate determining step) the reaction is defined as nernstian or reversible[101] since it follows the thermodynamic relationships. The discharging potential of the electroactive species at the electrode surface ($E°'$) can be used to determine the activity of the electro-active species at the surface (a_{ox} and a_{red}) according to the Nernst equation:

$$E°' = E° - \frac{RT}{nF} \ln \frac{a_{ox}}{a_{red}} \tag{3.14}$$

where R is the ideal gas constant and T is the absolute temperature. The $E°$ is the standard reduction potential of the redox couple, which is related to the difference in free energy between the reduced and the oxidized species (ΔG^0) by the equation:

$$E^0 = -\frac{\Delta G^0}{nF} \tag{3.15}$$

When a potential E is applied between two electrodes the discharging process of the *Ox*/*Red* species generates an electrical current and the respective activities *Ox* and *Red* species in a thin layer of solution close to the

electrode surface are modified. The current resulting from a change of the oxidation state of the electro-active species is referred as *faradaic current* since it obeys to Faraday's law.[101] The modification of the activities at the solution/electrode interface will lead to a flow of molecules from and to the electrode surface. In particular, by considering the reduction process, the production of *Red* species provides the driving force for their diffusion from the electrode surface towards the bulk of the solution. On the contrary, the decreased concentration of *Ox* species promotes the diffusion of new molecules from the bulk solution to the electrode surface (Fig. 3.10).
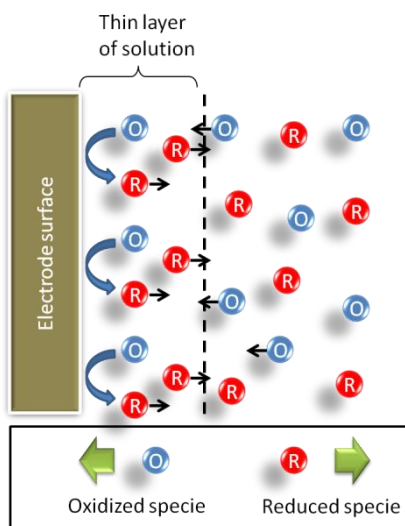
Figure 3.10 Graphical representation of the flux of matter followed by an electrochemical reaction onto to the electrode surface.

The flux of mass toward the electrode surface J (mol cm^{-2} s^{-1}) depends on the concentration gradient of *Ox* species and is described by first Fick's law:

$$J = -AD_0 \left(\frac{\partial c_0}{\partial x} \right)$$

(3.16)

where D_0 (cm^2 s^{-1}) is the diffusion coefficient of the oxidized specie, A (cm^2) is the electrode active surface area and x (cm) is the distance from the electrode surface.

When an electrochemical experiment is in a steady state, the diffusion of the electrochemical species toward the electrode surface is the rate determining step of the process and the system is in conditions of *diffusive regime*. In these conditions the current intensity produced in an electrochemical experiment is proportional to the flux of electrochemical species toward the electrode surface:

$$i = nFAD_0\left(\frac{\partial c_0}{\partial x}\right)$$

(3.17)

where n is the number of electrons exchanged in the redox reaction and F is the Faraday constant. The differential equation (3.17) can be solved as a function of the experimental conditions of the system (the stirring of the sample solution and the geometry of the electrode surface). A fundamental role is played by the type of "excitation signal", that is the variation of the potential applied to the working electrode during the electrochemical experiment.

3.4.2.   Types of excitation signals. The differential pulse voltammetry (DPV)

In a typical voltammetry experiment the voltage of the working electrode is varied systematically while the current response is measured. Different voltage-time functions, called excitation signals, can be applied to the working electrode (Fig.3.11). The classical voltammetric excitation signal is a linear scan (Fig.3.11A) where the potential of the working electrode is changed linearly

with time. For particular applications however it is preferable to use other types of excitation signal as differential pulse (Fig. 3.11B), square wave (Fig. 3.11C) and triangular wave (Fig. 3.11D).
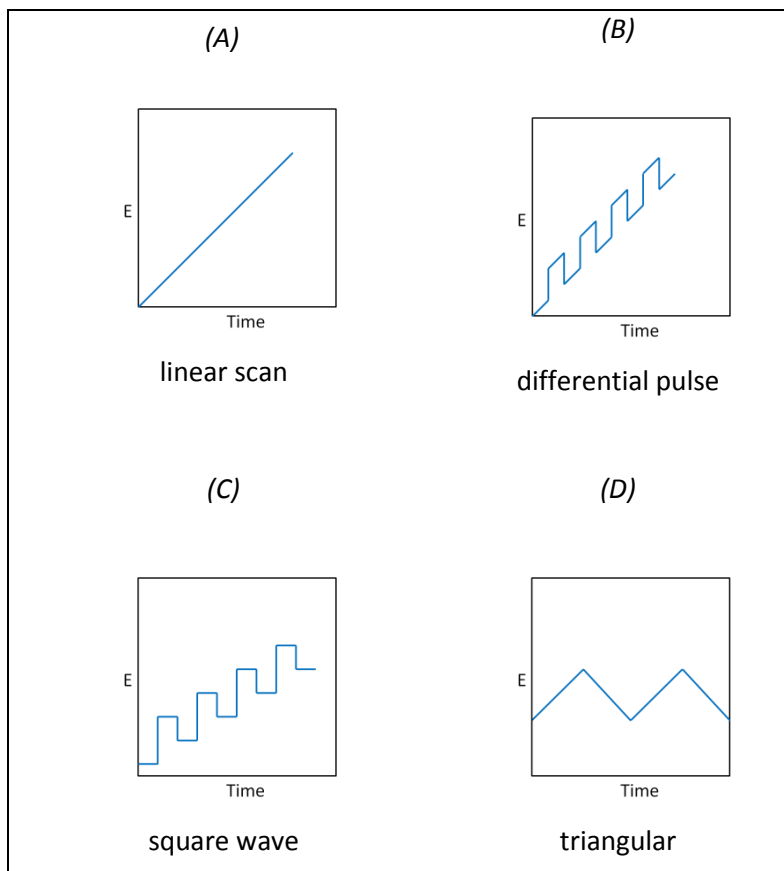
Figure 3.11 Most common types of excitation signal used in electrochemical experiments: A) Linear voltammetry, B) Differential pulse voltammetry, C) Square wave voltammetry, D) Cyclic voltammetry.
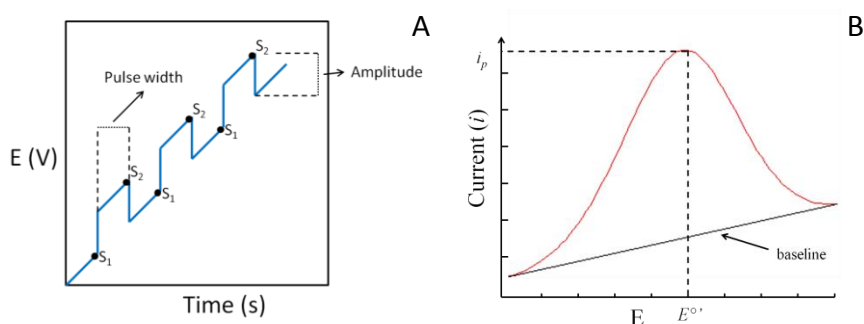
In this work differential pulse voltammetry (DPV) was used. The excitation signal used in DPV has two important advantages:

- It has high sensitivity
- It allows to reach low detection limits

These advantages derive from the particular waveform used in DPV, which eliminates the charging current generated at the electrode interface.[101]

The DPV's waveform (variation of potential as a function of time) is obtained by imposing a periodic pulse on a linear scan. Usually a small pulse, (E_{S2}-E_{S1}=50 mV), is applied. As shown in Fig 3.12A the current is measured alternately in two points of the signal: the first point (S_1) before the application of the pulse, and the second (S_2) before the end of the pulse (Fig 3.12A).

Figure 3.12 A) Excitation signal for differential pulse voltammetry B) voltammogram for a DPV experiment.

The difference in current intensity per pulse i = i_{S2}-i_{S1} is recorded as a function of the linearly increasing voltage. A differential curve is obtained (Fig. 3.13B) where the height of the peak (i_p) is proportional to the concentration of the electro-active specie (c):

$$i_p = \frac{nFAc\sqrt{D_0}}{\sqrt{\pi \cdot t_{S2}}}\left(\frac{1-\sigma}{1+\sigma}\right)$$

(3.18)

where n, F, A and D_0 are defined above, t_{S2} is the time (after the application of the pulse) at which the current is sampled. σ is an exponential

term that depends on the amplitude of the pulse (ΔE) according to the equation:

$$\sigma = e^{\frac{nF\Delta E}{2RT}}$$

(3.19)

The peak potential ($E°'$) can be used to obtain useful information about the investigated system. Indeed by eq. 3.16 $\Delta G^{°'}$ can be expressed through an enthalpic ($\Delta H^{°'}$) and an entropic ($\Delta S^{°'}$) term:

$$E^{°'} = -\frac{\Delta G^{°'}}{nF} = \frac{-\Delta H^{°'}}{nF} + \frac{T\Delta S^{°'}}{nF}$$

(3.20)

The information that can be obtained from this approach is specific of the system under investigation (i.e. redox proteins) and will be discussed in more detail.

3.4.3.   DPV of redox proteins

Due to the low detection limits and high sensitivity, DPV is a useful technique for a wide variety of molecules that can show an electro-active behavior, including redox proteins.

Electrochemical measurements can provide useful information about small variations of protein structure that can be revealed by a shift in the redox potential. Changes in the solvent properties (dielectric properties, type and concentration of electrolytes) can produce distortions of the protein structure modifying, for example, the coordination of the metal ion in the prostetic group and thus the relative stability of the *Red* and the *Ox* forms. The shift in the potential of a redox protein can give precious information about its stability and behavior in physiological systems.[105–107] As reported above, the

faradaic current measured in an electrochemical experiment is proportional to the amount of the electro-active species at the electrode interface (eq. 3.19). Electrochemical studies of proteins, however, can not be carried out with the same type of working electrodes as for classical electrochemical species (i.e. $Fe(CN)_6^{3-}$, $Fe(C_5H_5)_2^{2+}$). Two main difficults occur: the low rates of electron transfer between the protein and the electrode, and the unwanted adsorption of proteins ("fouling") on the electrode surface. The rate of electron transfer is influenced generally by the factors reported above such as electrode material, medium, operating potential, mode of mass transport and time scale. In the case of redox proteins, however, the electron transfer depends also on the orientation of the adsorbed proteins with respect to the electrode surface. Indeed, redox proteins as cytochrome c, allow for the electron transfer only when the side containing the electroactive specie (heme-coordinated Fe^{2+}/ Fe^{3+}) is oriented toward the electrode surface as discussed in the next paragraph. Equally important for the electrochemistry of the proteins, is the irreversible adsorption leading to a layer of electro-inactive proteins onto the electrode surface that prevents the adsorption of new electrochemical active protein molecules.

For these reasons the electrodes used to study the electrochemical properties of redox proteins, need to be chemically modified with a substance that increases the electron transfer rate between the protein and the electrode and allows for the reversible adsorption of the protein.

3.4.3.1.   Chemical modified electrodes (C.M.E.)

The use of chemically modified electrodes (CME) to promote electron transfer between a redox protein and an electrode has been widely studied.[108] One of the most common approaches to chemically modify the electrode surface is to use a "bifunctional" molecule able to interact with both the

electrode surface and with the surface groups of the protein (electronic mediator). The first work on CME reported the investigation of the electrochemical properties of cytochome c using a gold electrode modified with 4,4' bipyridyl (Fig.3.13).[109] Eddowes and Hill proposed that interaction between the lysines present in the surface region surrounding the heme edge and the pyridyl nitrogens at the modified electrode surface stabilize the transient protein-electrode.[110] They demonstrated that the binding step provides approximately half of the activation free energy for electron transfer, which is a crucial factor to enhance the rate of the process.
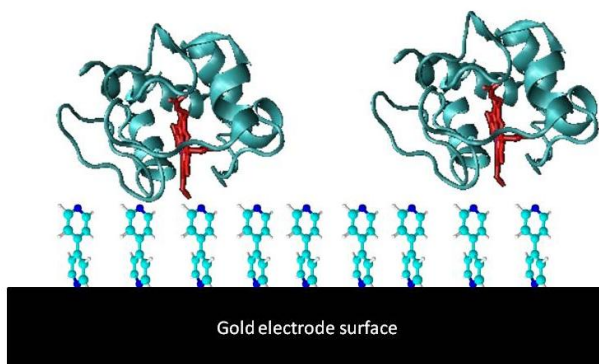
Figure 3.13 Graphical representations of the oriented-adsorption of a citochrome c molecule onto a 4,4' bipyridyl modified electrode.

A monolayer of 4,4' bipyridyl is formed by simply immersing the electrode in a solution containing the electronic mediator. Hence the 4,4' bipyridyl mediator can be directly added to the sample solution.

Another remarkable example of chemical modified electrodes concerns the spontaneous adsorption of n-alkanethiols monolayers ($X(CH_2)_nSH$ with $n > 10$) on gold electrode surfaces (Fig.3.14).
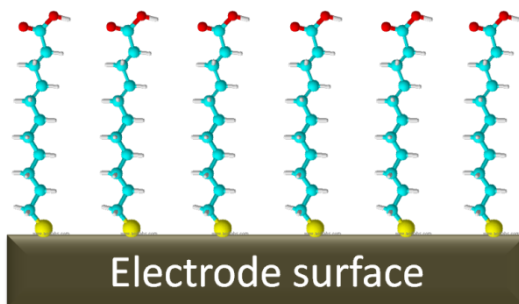
Figure 3.14 Graphical representation of a chemically modified electrode with 11-mercapto undecanoid acid.

This chemical modification is based on the strong bond between gold and sulfur. The mechanism of action of this type of Self Assembled Monolayers (SAM) is similar to that already seen for 4,4' bipyridyl layers, that is the orientation of the redox proteins (i.e. cytochrome c) in a way favorable for the electron transfer. In this case, however, the SAM tends to form covalent bonds between the terminal groups (i.e. carboxylic groups) and the surface groups of the protein (i.e. the lysines of the cytochrome c) thus producing stable electrochemical devices that can be re-used for several experiment.[111]

3.4.4. Experimental equipment

The electrochemical process takes place in a voltammetric cell connected to a potentiostat. The voltammetric cell (Fig. 3.15A) is constituted by three electrodes immersed in a solution containing the redox protein, the electronic mediator and a supporting electrolyte. The first element of the cell is the working electrode that transmits the proper potential for the excitation signal to the electroactive species contained in the sample solution. The most used working electrodes in voltammetry are made by platinum, graphite or gold.
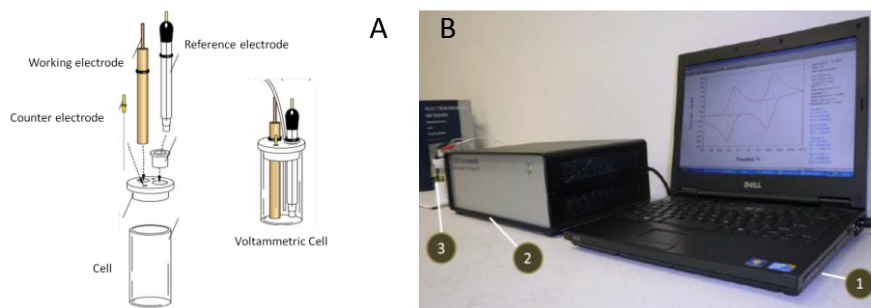
Figure 3.15 A) Graphical representation of the Voltammetric cell used for the experiments; B) A picture of the equipment used for electrochemical measurements: 1) PC equipped with a software, 2) potentiostat CH instruments 630C, 3) voltammetric cell.

The reference electrode maintains an invariant potential during the electrochemical measurement and allows the observation, the measurement, and the control of the working electrode potential. The most common reference electrode for aqueous solutions is the Ag/AgCl electrode. The third electrode is the counter electrode whose function is to allow the current flow through the cell. Most often the counter electrode consists of a platinum or graphite wire. A potentiostat, controlled by a suitable software that runs in a PC, applies the voltage between the working electrode and the counter electrode according to the method set up in the software and as a function of the potential of the reference electrode (Fig.3.15B). The intensity current measured will be recorded and plotted as a function of the applied potential.

References

(1)   Hiemenz, P. C. *Principles of colloid and surface chemistry*; Dekker, M., Ed.; 10th ed.; New York, 1977; p. 516.

(2)   Shaw, D. J. In *Introduction to Colloid and surface chemistry*; 1985; pp. 148–182.

(3)   Israelachvili, J. *Intermolecular and Surface forces*; 1991; pp. 238–249.

(4)   Stern, O. *Z. Elektrochem.* **1924**, *30*, 508.

(5)   Shaw, D. J. In *Introduction to Colloid and surface chemistry*; 1985; pp. 183–212.

(6)   Hamaker, H. C. *Physica* **1937**, *4*, 1058–1072.

(7)   Derjaguin, B. V.; Landau, L. *Acta Physicochim. URSS* **1941**, *14*, 633–662.

(8)   Verwey, E. J. W.; Overbeek, J. T. G. *Theory of stability of lyophobic colloids*; Elsevier: Amsterdam, 1948.

(9)   Ninham, B. W.; Parsegian, V. A. *J. Theor. Biol.* **1971**, *31*, 405–428.

(10) Healy, W.; Yates, D. E.; Levine, S. *Trans. Farad. Soc. I* **1974**, *70*, 1807.

(11) Boström, M.; Deniz, V.; Franks, G. V; Ninham, B. W. *Adv. Coll. Int. Sci.* **2006**, *123–126*, 5–15.

(12) Healy, T. W.; Chan, B. Y. D.; White, L. R. *J. Chem. Soc. Farad. I* **1977**, *76*, 2844–2865.

(13) Chan, B. Y. D.; Perram, J. W.; White, L. R.; Healy, T. W. *J. Chem. Soc. Farad. Trans.* **1975**, *71*, 1046–1057.

(14) Pashley, M. R. *J. Coll. Int. Sci.* **1981**, *80*, 531–545.

(15) Pashley, M. R. *J. Coll. Int. Sci.* **1981**, *83*, 531–545.

(16) Israelachvili, J.; Pashley, M. R. *J. Coll. Int. Sci.* **1984**, *97*, 446–455.

(17) Horn, R. G.; Israelachvili, J. *Macromolecules* **1988**, *21*, 2836–2841.

(18) Pashley, M. R.; Israelachvili, J. *J. Coll. Surf.* **1981**, *2*, 169–187.

(19) Marra, J. *J. Phys. Chem.* **1986**, *90*, 2145–2150.

(20) Marra, J. *Biophys. J.* **1986**, *50*, 815–25.

(21) Marra, J.; Israelachvili, J. *Biochem.* **1985**, *24*, 4608–4618.

(22) Derjaguin, B. V.; Titijevskaia, A. S.; Abrxcossova, I. I. *Discuss. Farad. Soc.* **1954**, *18*, 24–41.

(23) Lyklema, J.; Mysels, K. J. *J. Am. Chem. Soc.* **1965**, *87*, 2539–2546.

(24)   Donners, W. A. B.; Rinjnbout, J. B.; Vrij, A. *J. Coll. Int. Sci.* **1977**, *61*, 249–260.

(25)   Horn, R. G.; Hirz, S. J.; Hadziioannou, G.; Frank, C. W.; Catala, J. M. *J. Chem. Phys.* **1989**, *90*, 6767.

(26)   Horn, R. G.; Smith, D. T.; Haller, W. *Chem. Phys. Lett.* **1989**, *162*, 404–408.

(27)   Horn, R. G.; Clarke, D. R.; Clarkson, M. T. *J. Mater. Res.* **1988**, *3*, 413–416.

(28)   Ninham, B. W.; Lo Nostro, P. *Molecular forces and Self Assembly -In colloid, Nano Sciences and Biology*; Cambridge University Press: Cambridge, 2010.

(29)   Poiseuille, J. L. M. In *Ann. Chim. Phys.*; 1847; pp. 76–110.

(30)   Kunz, W.; Henle, J.; Ninham, B. W. *Curr. Op. Coll. Int. Sci.* **2004**, *9*, 19–37.

(31)   Robertson, T. B. *J. Biol. Chem.* **1911**, *9*, 303–326.

(32)   Diamond, J. M.; Wright, E. M. *Ann. Rev. Physiol.* **1969**, *31*, 581–646.

(33)   Leontidis, E. *Curr. Op. Coll. Int. Sci.* **2002**, *7*, 81–91.

(34)   Zhang, Y.; Cremer, P. S. *Curr. Opin. Chem. Biol.* **2006**, *10*, 658–63.

(35)   Jones, G.; Dole, M. *J. Am. Chem. Soc.* **1929**, *51*, 2950–2964.

(36)   Randall, M.; Failey, C. F. *Chem. Rev.* **1927**, *4*, 285–290.

(37)   Stewart, G. W. *J. Chem. Phys.* **1939**, *7*, 869.

(38)   Ber, D.; Corey, V. B. *Phys. Rev.* **1943**, *64*, 350.

(39)   Jones, G.; Bickford, F. *J. Am. Chem. Soc.* **1934**, *56*, 602–611.

(40)   Green, A. A. *J. Biol. Chem.* **1932**, *95*, 47–66.

(41)   McCall, D. W.; Douglass, D. C. *J. Chem. Phys.* **1965**, *69*, 2001–2011.

(42)   Chambers, J. F. *J. Phys. Chem.* **1958**, *62*, 1136–1138.

(43)   Long, F. A.; McDevit, W. F. *J. Am. Chem. Soc.* **1952**, *74*, 1773–1781.

(44)   Curtis, R. A.; Montaser, A.; Prausnitz, J. M.; Blanch, H. W. *Biotech. Bioeng.* **1998**, *58*, 451.

(45)   Pinna, M. C.; Salis, A.; Monduzzi, M.; Ninham, B. W. *J. Phys. Chem. B* **2005**, *109*, 5406–5408.

(46)   Dishon, M.; Zohar, O.; Sivan, U. *Langmuir* **2009**, *25*, 2831–2836.

(47)   Nostro, P. Lo; Ninham, B. W.; Nostro, A. Lo; Pesavento, G.; Fratoni, L.; Baglioni, P. *Phys. Biol.* **2005**, *2*, 1–7.

(48)   Zhang, Y.; Cremer, P. S. *Proc. Natl. Acad. Sci.. U.S.A.* **2009**, *106*, 15249–53.

(49)   Chen, X.; Flores, S. C.; Lim, S.-M.; Zhang, Y.; Yang, T.; Kherb, J.; Cremer, P. S. *Langmuir* **2010**, *26*, 16447–54.

(50) Murgia, S.; Portesani, F.; Ninham, B. W.; Monduzzi, M. *Chem. Eur. J.* **2006**, *12*, 7689.

(51) Nostro, P. Lo; Severi, M.; Ninham, B. W. *J. Am. Chem. Soc.* **2010**, *132*, 6571–6577.

(52) Salis, A.; Pinna, M. C.; Bilanicová, D.; Monduzzi, M.; Lo Nostro, P.; Ninham, B. W. *J. Phys. Chem. B* **2006**, *110*, 2949–56.

(53) Voinescu, A. E.; Bauduin, P.; Pinna, M. C.; Touraud, D.; Ninham, B. W.; Kunz, W. *J. Phys. Chem. B* **2006**, *110*, 8870–6.

(54) Petersen, P. B.; Saykally, R. J. *J. Phys. Chem. B* **2006**, *110*, 14060–14073.

(55) Weckström, K.; Papageorgiou, A. C. *J. Coll. Int. Sci.* **2007**, *310*, 151–62.

(56) Lagi, M.; Nostro, P. Lo; Fratini, E.; Ninham, B. W.; Baglioni, P. *J. Phys. Chem. B* **2007**, *111*, 589–97.

(57) Schott, H. *J. Coll. Int. Sci.* **1995**, *173*, 265–277.

(58) Baldwin, R. L. *Biophys. J.* **1996**, *71*, 2056–63.

(59) Robinson, R. A.; Stokes, R. H. *Electrolyte solutions*; Butterwhorths: London, 1959.

(60) Kielland, J. *J. Am. Chem. Soc.* **1937**, *59*, 1675.

(61) Guggenheim, E. A. *Phil. Mag.* **1935**, *19*, 588.

(62) Davies, C. W. *J. Chem. Soc.* **1938**, 2093–2098.

(63) Robinson, A. *J. Am. Chem. Soc.* **1935**, *57*, 1165–1168.

(64) Marcus, Y. *Chem. rev.* **2009**, *109*, 1346–70.

(65) Green, A. A. *J. Biol. Chem.* **1931**, *93*, 495–516.

(66) Setschenow, J. *Z. Phys.* **1889**, *4*, 117.

(67) Lo Nostro, P.; Fratoni, L.; Ninham, B. W.; Baglioni, P. *Biomacromol.* **2002**, *3*, 1217–24.

(68) Jungwirth, P.; Tobias, D. J.; Heyrovsky, J. *J. Phys. Chem. B* **2002**, *106*, 6361–6373.

(69) Kunz, W.; Lo Nostro, P.; Ninham, B. W. *Curr. Op. Coll. Int. Sci.* **2004**, *9*, 1–18.

(70) Collins, K. D. *Methods* **2004**, *34*, 300–11.

(71) Kujumzelis, T. G. *Z. Phys.* **1938**, *110*, 742.

(72) Frank, H. S.; Evans, M. W. *J. Chem. Phys.* **1945**, *13*, 507.

(73) Gurney, R. W. *IONIC PROCESSES IN SOLUTION*; McGraw-Hill: New York, 1953.

(74) Atkins, P. *Physical Chemistry*; 8a ed.; Oxford university press, 2006.

(75) Collins, K. D. *Biophys. J.* **1997**, *72*, 65–76.

(76) Vlachy, N.; Jagoda-Cwiklik, B.; Vácha, R.; Touraud, D.; Jungwirth, P.; Kunz, W. *Adv. Coll. Int. Sci.* **2009**, *146*, 42–7.

(77) Schulz, J. C.; Warr, G. G. *J. Chem. Soc. Farad. Trans.* **1998**, *94*.

(78)   Garcia-Celma, J. J.; Hatahet, L.; Kunz, W.; Fendler, K. *Langmuir* **2007**, *23*, 10074–80.

(79)   Xu, L.; Li, X.; Zhai, M.; Huang, L.; Peng, J.; Li, J.; Wei, G. *J. Phys. Chem. B* **2007**, *111*, 3391–7.

(80)   Collins, K. D. *Biophys. Chem.* **2006**, *119*, 271–81.

(81)   Lo Nostro, P.; Ninham, B. W. *Chem. rev.* **2012**, *112*, 2286–322.

(82)   Leberman, R.; Soper, A. K. *Nature* **1995**, *378*, 364.

(83)   Bostrom, M.; Tavares, F. W.; Finet, S.; Skouri-panet, F.; Tardieu, A.; Ninham, B. W. *Biophys. Chem.* **2005**, *117*, 217–224.

(84)   Ninham, B. W.; Yaminsky, V. *Langmuir* **1997**, *13*, 2097–2108.

(85)   Parsons, D. F.; Ninham, B. W. *Langmuir* **2010**, *26*, 6430–6436.

(86)   Parsons, D. F.; Deniz, V.; Ninham, B. W. *Coll. Surf. A Physicochem. Eng. Aspects* **2009**, *343*, 57–63.

(87)   Parsons, D. F.; Ninham, B. W. *Langmuir* **2010**, *26*, 1816–1823.

(88)   Boström, M.; Parsons, D. F.; Salis, A.; Ninham, B. W.; Monduzzi, M. *Langmuir* **2011**, *27*, 9504–11.

(89)   Schwierz, N.; Horinek, D.; Netz, R. R. *Langmuir* **2010**, 372–381.

(90)   Heyda, J.; Lund, M.; Oncák, M.; Slavícek, P.; Jungwirth, P. *J. Phys. Chem. B* **2010**, *114*, 10843–52.

(91)   Salis, A.; Cugia, F.; Parsons, D. F.; Ninham, B. W.; Monduzzi, M. *Phys. Chem. Chem. Phys.* **2012**, *14*, 4343–6.

(92)   Tanford, C.; Swanson, S. A.; Shore, W. S. *J. Am. Chem. Soc.* **1955**, *77*, 6414–6421.

(93)   Tanford, C. In *Adv. Prot. Chem.*; 1955; pp. 69–165.

(94)   Zhao, D.; Feng, J.; Huo, Q.; Melosh, N.; Fredrickson, G.; Chmelka, B.; Stucky, G. *Science* **1998**, *279*, 548–52.

(95)   Stumm, W. *Chemistry of the solid-water interface: Processes at the Mineral-Water and Particle-Water Interface in Natural Systems*; John Wiley & Sons: New York, 1992.

(96)   Leung, K.; Nielsen, I. M. B.; Criscenti, L. J. *J. Am. Chem. Soc.* **2009**, *131*, 18358–18365.

(97)   Bui, T. X.; Choi, H. *J. Haz. Mater.* **2009**, *168*, 602–8.

(98)   Bourikas, K.; Kordulis, C.; Lycourghiotis, A. *Adv. Coll. Int. Sci.* **2006**, *121*, 111–30.

(99)   Bourikas, K.; Vakros, J.; Kordulis, C.; Lycourghiotis, A. *J. Phys. Chem. B* **2003**, *107*, 9441–9451.

(100)   Brumaner, S.; Emmet, P. H.; Teller, E. *J. Am. Chem. Soc.* **1938**, *60*, 309.

(101)   Wang, J. *Analytical electrochemistry*; 2nd ed.; WILEY-VCH Verlag: New York, 2000.

(102)   Henry, D. C. *Proc. Roy. Soc. London Sec. A* **1931**, *133*, 106–129.

(103)   Rodbard, D.; Chrambach, A. *Anal. Biochem.* **1971**, *40*, 95–134.

73

(104) Winzor, D. *Anal. Biochem.* **2004**, *325*, 1–20.

(105) O'Reill, N. J.; Magner, E. *Langmuir* **2005**, *21*, 1009–1014.

(106) Battistuzzi, G.; Borsari, M.; Menabue, L.; Saladini, M.; Sola, M. *Inorg. Chim. Acta* **1998**, *273*, 397–402.

(107) Kranich, A.; Ly, H. K.; Hildebrandt, P.; Murgida, D. H. *J. Am. Chem. Soc.* **2008**, *130*, 9844–9848.

(108) Baldwin, R. P.; Thomsen, K. N. *Talanta* **1991**, *38*, 1–16.

(109) Eddowes, M. J.; Hill, H. A. O. *J. Chem. Soc. Chem. Comm.* **1977**, 771.

(110) Albery, W. J.; Eddowes, M. J.; Hill, H. A. O.; Hillman, A. R. *J. Am. Chem. Soc.* **1981**, *103*, 3904–3910.

(111) Armstrong, F. A.; Heering, H. A.; Hirst, J. *Chem. Soc. Rev.* **1997**, *26*, 169–179.

(112) Voet, A. *Chem. Rev.* **1936**, *20*, 169–179.

PAPER I

Measurements and Theoretical Interpretation of Points of Zero Charge/Potential of BSA Protein

Andrea Salis,*,[†] Mathias Boström,*,[†,‡] Luca Medda,[†] Francesca Cugia,[†] Brajesh Barse,[†] Drew F. Parsons,[‡] Barry W. Ninham,[‡] and Maura Monduzzi[†]

[†]Department of Chemical Science, University of Cagliari-CSGI and CNBS, Cittadella Universitaria, S.S. 554 bivio Sestu, 09042- Monserrato (CA), Italy

[‡]Research School of Physical Sciences and Engineering, Australian National University, Canberra, 0200 Australia

ABSTRACT: The points of zero charge/potential of proteins depend not only on pH but also on how they are measured. They depend also on background salt solution type and concentration. The protein isoelectric point (IEP) is determined by electro-kinetical measurements, whereas the isoionic point (IIP) is determined by potentiometric titrations. Here we use potentio-metric titration and zeta potential (ζ) measurements at different NaCl concentrations to study systematically the effect of ionic strength on the IEP and IIP of bovine serum albumin (BSA) aqueous solutions. It is found that high ionic strengths produce a shift of both points toward lower (IEP) and higher (IIP) pH

values. This result was already reported more than 60 years ago. At that time, the only available theory was the purely electrostatic Debye−Hückel theory. It was not able to predict the opposite trends of IIP and IEP with ionic strength increase. Here, we extend that theory to admit both electrostatic and nonelectrostatic (NES) dispersion interactions. The use of a modified Poisson−Boltzmann equation for a simple model system (a charge regulated spherical colloidal particle in NaCl salt solutions), that includes these ion specific interactions, allows us to explain the opposite trends observed for isoelectric point (zero zeta potential) and isoionic point (zero protein charge) of BSA. At higher concentrations, an excess of the anion (with stronger NES interactions than the cation) is adsorbed at the surface due to an attractive ionic NES potential. This makes the potential relatively more negative. Consequently, the IEP is pushed toward lower pH. But the charge regulation condition means that the surface charge becomes relatively more positive as the surface potential becomes more negative. Consequently, the IIP (measuring charge) shifts toward higher pH as concentration increases, in the opposite direction from the IEP (measuring potential).
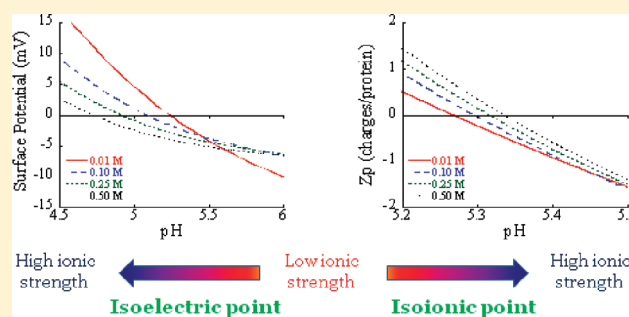
1. INTRODUCTION

The net electrical charge of proteins is a parameter that strongly affects their physicochemical behavior in living organisms. Protein surfaces in an aqueous medium naturally charge to form an electrical double layer. The most common surface charge-determining ions are H^+ and OH^-. In this case, the net surface charge is affected by the pH of the medium in which the protein is dispersed. Of particular importance is the pH value at which the protein surface is electrically neutral. At this pH, the electric repulsion between proteins is minimal. Hence, they can easily coagulate and precipitate. Protein precipitation can also be induced by the addition of salts through the "salting out" phenomenon, following a Hofmeister series.[1]

In all cases, electrolytes (acids, bases, and salts) are responsible for either protein stabilization or precipitation because they strongly affect forces between colloidal particles.[2] Knowledge of these phenomena can help biochemists interested in protein purification. Moreover and intriguingly, protein aggregation/precipitation seems to play a role in several neurodegenerative disorders, such as Alzheimer's disease, prion disease, Parkinson's disease, and amyotrophic lateral sclerosis.[3] The pH value at which protein electrical neutrality occurs is termed either as the

isoionic point (IIP) or, alternatively, as the isoelectric point (IEP). The conceptual difference between these two points is in principle known, but they are often used interchangeably without too much thought on the subtleties associated with them. This is the matter we explore here. It leads to a useful and rigorous demarcation.

The isoionic point is defined as the pH value at which a zwitterionic molecule has an equal number of positive and negative charges and no adsorbed ionic species.[4] The isoelectric point, instead, is the pH value at which the zeta potential (or surface potential), equivalent to the net charge of the molecule including bound ions, is zero. Thus, the isoelectric and isoionic points should, in principle, coincide when the concentration of electrolytes is zero.

The two points can be determined with different kinds of experimental measurements. The isoelectric point is measured by electrokinetical methods. It is determined by the value of pH at which the protein molecule remains stationary in an electrical

field. The isoionic point, instead, can be measured through potentiometric titrations carried out at different ionic strengths.[5-9] IIP can be obtained as the intersection point among the different titration curves.[6]

Going through the literature, several different values of IEP and IIP for the same protein, depending on the experimental method used and also on the experimental conditions, have been reported. For example, it was found that IEP of bovine serum albumin (BSA) is either 5.1 or 4.7 if Tris or MES buffer is used, respectively.[10] An IEP of 4.6 was also found by electroosmotic flow measurements.[11] Tanford and Swanson instead measured an IIP of BSA (by means of potentiometric titrations) of about 5.5.[6] Hence, for the same protein, the point at which it is electrically neutral can change by almost 1 pH unit depending on both the experimental method and experimental conditions.

The differences between protein IEPs and IIPs, and their shifts with salt type and concentration, was the subject of intense research activity at the end of the 1940s. Scatchard and Black[12] reported that the effect of an increase in ionic strength would result in an increase of IIP of human serum albumin. The same shift was caused by different sodium salts at fixed ionic strength according to the Hofmeister series.[12] Longsworth and Jacobsen[13] found that the IEP of β-lactoglobulin and BSA, obtained by electrophoretic measurements in sodium acetate buffers, decreases with increasing ionic strength and, at constant ionic strength, with the substitution of chloride, iodide, or thiocyanate for acetate. What emerges and is surprising in these old papers is that the commonly accepted explanation, by the biophysical and colloid chemistry community of that age, is that the effects "... are probably to be ascribed to specific binding, by the protein, of the salt ions, especially anions."[13] Hence, no (ion induced) change of water structure was invoked. The theoretical model that was proposed considered a purely electrostatic Debye−Hückel approach.[12] This was the only possible approach at that time since DLVO theory was only just becoming available.[14,15] Now a new theory[16-22] and a huge amount of new experimental data are available. Applications range over colloid stability[23] to enzyme activities,[24-28] protein adsorption on solid surfaces,[29] as well as from pH of buffers[30] to the surface charge of silica.[31]

These new insights are pushing researchers to revisit what had already been investigated several years ago.[1] For example, a recent paper of Zhang and Cremer showed that salt-induced protein (lysozyme) precipitation follows different Hofmeister series at low and high concentration.[32] In fact, the effect was observed by Robertson almost 100 years before.[33] A new possible explanation has just been proposed.[34] In this paper, the IIP and IEP of BSA with both experimental and theoretical approaches were determined. Four different ionic strength values (from 0.01 to 0.5 M) were used to show that protein surface neutrality varies with ionic strength. This is an important fact in real systems. It will be also shown that the IIP coincides with the crossing points among different ionic strength titration curves only if a pure electrostatic model is considered. But for experimental results, except at very low salt concentrations, there is a shift between these points. The shift can be predicted when dispersion (non-electrostatic or NES) forces are included in the Poisson−Boltzmann equation. This approach also allows us to predict correctly the opposite shifts observed when comparing the IEP from zeta potential measurements and IIP from titration measurements.

2. EXPERIMENTAL SECTION

2.1. Chemicals. Bovine serum albumin (BSA, 99%) and sodium chloride (>98%) were from Sigma Aldrich (Milan, Italy). Buffers (pH 1, 4, 6, 9, 10) were purchased from Hanna instruments (Szeged, Hungary). Sodium hydroxide standard solution (0.1 M) was from Merck (Milan, Italy). All samples and blanks were prepared by using purified water (conductivity ≤ 0.054 mS cm^{-1}), prepared by means of a Millipore water purification system (Millipore, U.K.). In order to remove any interference on pH by carbonic acid, CO_2 was removed by bubbling argon for 2 h before the preparation of each solution.

2.2. BSA Sample Preparation. Potentiometric titrations and zeta potential measurements were done by preparing BSA dispersions (1 g/L) in NaCl solution at different ionic strengths (0.01, 0.10, 0.25, and 0.50 M). Sodium chloride was dried overnight at 110 °C, cooled at room temperature in a desiccator, and dissolved in CO_2-free Millipore water.

2.3. Potentiometric Titration Experiments. Potentiometric titrations of BSA suspensions were performed using an automatic titrator, titrando 836 from Metrohm (Herizau, Switzerland), interfaced to a PC with software Tiamo 1.3. The pH electrode was calibrated by a five-point calibration. The sample and blank solutions were first pretitrated to pH 2.65 with a standard HCl solution (0.1 M). Samples and blanks were then titrated with a standard solution of NaOH (0.1 M) up to pH = 11. In order to allow the equilibration of the solution after titrant addition, the automatic titrator was set with a delay of 300−600 s between two consecutive titrant additions, and a maximal signal drift of 4 mV/min. Blank titrations were carried out on a solution having the same composition of the sample (HCl 0.1 M and NaCl) but without dispersed BSA. All experiments were performed in a thermostatted room ($T = 25$ °C). Surface charge of BSA (Z_p) was calculated at different pH values by using the data obtained by potentiometric titrations, of both proteins samples and blanks, according to the following equation:

$$Z_p = \frac{\text{mol } H^+_{\text{boundtoBSA}}}{\text{mol}_{\text{BSA}}}$$

$$= \frac{(V_{\text{HClsample}} - V_{\text{HClblank}})[\text{HCl}] - (V_{\text{NaOHsample}} - V_{\text{NaOHblank}})[\text{NaOH}]'}{m_{\text{BSA}}/MW_{\text{BSA}}}$$

(1)

where V_{HCl} is the volume of HCl in the pretitration at pH 2.65 for the sample and the blank. V_{NaOH} is the volume of NaOH used in the titration of both the sample and the blank. m_{BSA} is the mass of the BSA sample, and MW_{BSA} is the molecular weight of BSA. [HCl] and [NaOH] are the molar concentrations of hydrochloric acid and sodium hydroxide respectively.

2.4. Zeta Potential Measurements. A Zetasizer nano series (Malvern Instruments) was used for the determination of zeta potential (ζ) of BSA as a function of pH at different ionic strengths. A volume of 2.5 mL of 0.1 M HCl was initially added to the BSA dispersion, which was then titrated by adding NaOH 0.1 M through a digital buret (BRAND, Germany). After each titrant addition, the pH was measured then a small volume of the solution was put in the analytical cell for zeta potential measurement. The temperature of the scattering cell was fixed at 25 °C, and the data were elaborated with the Zetasizer software version 6.01. Five zeta potential measurements were made at each pH value, and the average value ($\pm$ standard deviation) was reported.

3. THEORETICAL METHODS: MODIFIED DOUBLE LAYER THEORY FOR A GLOBULAR BSA PROTEIN IN NaCl SALT SOLUTIONS

The experimentally observed deviations between the isoelectric point (IEP, from zeta potential measurements) and isoionic point (IIP, from titration) presented in the next section have

motivated us to investigate theoretically the average protein charge and the surface potential of a BSA-like colloidal particle under different conditions. We outline here the basic ideas used in our theoretical calculations for a single protein in NaCl salt solutions. The results of our calculations will be presented in section 4.2.

We consider a single globular BSA protein surrounded by an aqueous solution of negatively charged anions and positively charged cations each with bulk concentration c and charge $\pm ze$. The protein is modeled as a homogeneous dielectric sphere of radius r_p (35 Å) with ionizable surface groups. The electrostatic potential on the model protein surface is averaged over the spherical surface. On a real protein, charges are localized and there will clearly be local variations in charge density and there will, of course, be counterions clustering at the charged groups.[35] Despite its obvious simplifications, it has been demonstrated that the simple model used here can explain qualitatively many trends in protein solutions, for instance, accounting for the ion specific charge of lysozyme protein,[36] and the second virial coefficients of protein solutions.[37,38] The experimentally observed Hofmeister reversal in lysozyme protein solutions as a function of pH[39−41] and salt concentration[37,42] can be explained in terms of ion specific NES potentials. Recently, the availability of ab initio quantum chemical estimates for the excess polarizabilities and radii of ions in salt solutions has made it possible to go from qualitative comparison with experiments to quantitative and predictive theories in colloid chemistry.[18,31,43]

The distribution of ions near the protein surface is determined by a modified Poisson—Boltzmann equation that includes both electrostatic ($\phi(r)$) and NES ($U_{i(r)}$) potentials acting on the ions[16,31,42]

$$\frac{1}{r^2}\frac{d}{dr}\left(r^2\frac{d\phi}{dr}\right) = \frac{-e\sum_i z_i c_{i,0}\exp\left[-[z_i e\phi(r) + U_i(r)/kT]\right]}{\varepsilon_0\varepsilon_w} \tag{2}$$

where $c_{i,0}$, z_i, k, and T denote, respectively, the bulk concentration, valency of ionic species i, Boltzmann constant, and temperature.

Cations and anions with no excess polarizability are also considered to compare our results with traditional theories. The modified Poisson—Boltzmann equation can be solved numerically using charge regulated boundary condition at the protein surface,

$$r_p\frac{d\phi}{dr}\bigg|_{r=r_p} = \frac{-eZ_p}{4\pi\varepsilon_0\varepsilon_w(0)} \tag{3}$$

$$Z_p = \sum_{base}\frac{N_b\times 10^{-pH_s}}{10^{-pH_s}+10^{-pK_a}} - \sum_{acid}\frac{N_a\times 10^{-pK_a}}{10^{-pH_s}+10^{-pK_a}} \tag{4}$$

where Z_p is the protein surface charge, and N_b and N_a are the number of basic and acidic groups, respectively. We use an "ion-embedded" model where the ion is permitted to embed into the interface. This may be justified on the grounds that the actual protein surface contains pits and bumps. Following Parsegian,[44] we neglect any changes in the hydronium ion bulk activity coefficient. In other words, we take the local pH at the BSA surface to be given by the following expression:

$$10^{-pH_s} = 10^{-pH}\exp\left[-e\phi(r_p)/kT\right] \tag{5}$$

The number of amino acid charged groups and their pK_a values of BSA[6] can be found in Table 1. The pK_a values of the ionizable groups may change with salt concentration[45,46] and

Table 1. Values of pK_a and Number (N) of Each Charge Group from Tanford[6] Used in the Charge Regulation Model for a Globular BSA Protein

acidic/basic group	N	pK_a
α-COO$^-$	1	3.75
β,γ-COO$^-$	99	3.92
phenolic	19	10.35
α-amino	1	7.75
ε-amino	57	9.8
imidazole	16	6.9
guanidine	22	12

Table 2. Effective (Excess) Static Polarizabilities ($\alpha^*(0)$), Dispersion Constants (B), and Ion Gaussian Radii (a) for the Ions Used in This Study

ion	$\alpha^*(0)$ (Å^3)	B (10^{-50} J m^3)	a (Å)
Na$^+$ (hydrated)	−7.31	−0.20	2.25
Cl$^-$	−3.03	−1.26	1.86

with protein charge.[6] Results including Tanford's correction,[6] which changes the pK_a's in accordance with the average protein charge, were found to give very similar results (see below). Since the BSA protein has a quite large average radius (35 Å), we can approximate the NES potential with that acting between a polarizable ion with finite Gaussian radius (a) and a planar charged surface:[31]

$$U(r) = \frac{Bf(r-r_p)}{(r-r_p)^3} \tag{6}$$

where

$$f(r) = 1 + \frac{2r}{\sqrt{\pi}a}\left[\frac{2r^2}{a^2}-1\right]\exp\left(\frac{-r^2}{a^2}\right) - \left[1+\frac{4r^4}{a^4}\right]\mathrm{erfc}\left(\frac{r}{a}\right) \tag{7}$$

$$B = \frac{kT}{4}\sum_{n=0}^{}(2-\delta_{0,n})\frac{\alpha^*(i\omega_n)\varepsilon_w(i\omega)-\varepsilon_p(i\omega)}{\varepsilon_w(i\omega_n)\varepsilon_w(i\omega)+\varepsilon_p(i\omega)} \tag{8}$$

$\omega_n = \pi kTn/\hbar$, and k and T are Boltzmann's constant and temperature, respectively. $\varepsilon_w(i\omega)$ and $\varepsilon_p(i\omega)$ are the dielectric functions of water[47] and protein[48] surface, respectively. $\alpha^*(i\omega)$ is the excess polarizability of the ion.

The excess polarizability describes the difference between the intrinsic dielectric response of the ion from that of the surrounding medium (water). The magnitudes, and even the signs, of the dispersion potentials near the two interfaces depend in a sensitive way on these frequency-dependent entities. The ionic parameters, $\alpha^*(i\omega)$ (excess dynamic polarizabilities), B values, and ion sizes a, were calculated elsewhere.[19,43] Those useful for the present work, related to hydrated Na$^+$ and Cl$^-$, are reported in Table 2, with the static excess polarizability $\alpha^*(0)$ at zero frequency given to indicate the relative strengths of the dynamic polarizabilities.

4. RESULTS

4.1. Experimental Results. Table 3 reports the IEP and IIP values for three proteins, namely BSA, β-lactoglobulin, and
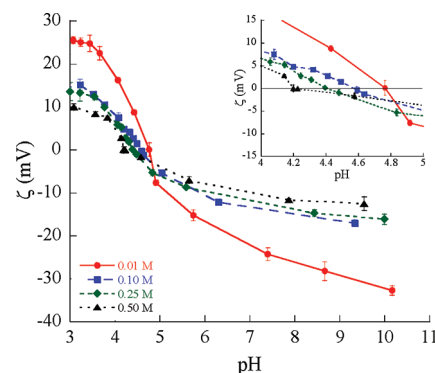
Table 3. Isoelectric (IEP) and Isoionic (IIP) Points, Type of Experimental Method, and Salt Type and Concentration Used for a Set of Proteins

protein	IEP/IIP	experimental method	electrolyte	ref.
bovine serum albumin	5–5.6	potentiometric titration	0.01–0.15 M NaCl	6, 7
	4.7–4.9	isoelectric focusing	not available	49
	4.75	isoelectric focusing	not available	50
	4.7–5.1	zeta potential	0.001–0.15 M NaCl	10
β-lactoglobulin	5.48	potentiometric titration	0.01 M KCl	51
	5.1–5.34	isoelectric focusing	not available	52
	5.18	potentiometric titration	0.01 M KCl	53
ribonuclease	9.3	isoelectric focusing	not available	49
	9.60	potentiometric titration	0.001 M KCl	8
	9.45	electrophoresis	0.01 M sodium barbiturate	54
	8.88	isoelectric focusing	not available	52
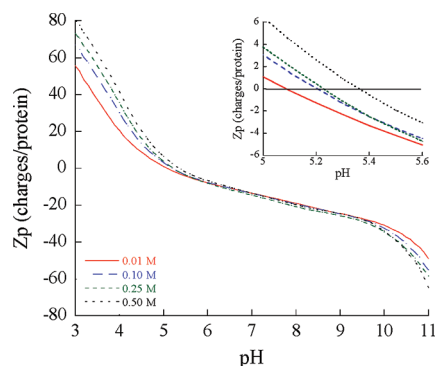
Figure 1. Experimental titration curves of BSA at different NaCl concentrations in a wide range of pH values and for pH values close to the point of zero charge (inset).

Figure 2. Experimental zeta potential of BSA versus pH at different NaCl concentrations and for pH values close to the point of zero charge (inset).

ribonuclease, found in the literature. These were chosen as an example of the different values of IEP and IIP that can be found depending on the experimental method and conditions used. According to classical theory, the IIP and IEP should coincide and be independent of salt concentration. As a general observation, we note that IIP values, obtained through potentiometric titrations, are generally higher than IEPs obtained through electrokinetic methods. Here we have carried out potentiometric titrations and zeta potential measurements of BSA as a function of pH at different NaCl concentrations (namely, 0.01, 0.1, 0.25, and 0.5 M). Experimental titration curves are shown in Figure 1. IIP values depend on ionic strength. The effect of increasing ionic strength is to shift IIP to higher pH values. Indeed the IIP ranges from 5.15 at 0.01 M to 5.4 at 0.5 M. Zeta potential measurements versus pH are shown in Figure 2. If IEP values are compared with IIP obtained by potentiometric titrations, we see that the IEP are found to take on significantly lower pH values.

In particular, at ionic strength 0.01 M, the IEP is 4.7 whereas the IIP is 5.1. As opposed to what was observed for potentiometric titrations, the increase of ionic strength has the effect of shifting IEP values to lower pH. Specifically, the IEP values are 4.5 and 4.2 at 0.1 and 0.5 M respectively. This trend agrees with previous studies.[12,13] Looking in more detail at both kinds of measurements (inset in Figures 1 and 2), we see that there is no common intersection point for the ionic strengths investigated.

Different curves crossing at different points at a range of pH values rather than at single intersection point are obtained. Moreover, intersections all occur below both $Z_P = 0$ (potentiometric titrations) and $\zeta = 0$ mV (zeta potential measurements). A final observation on experimental data for pH values close to the IIP is that the increase of salt concentration results in a higher BSA surface charge at a certain pH. As opposed to that, a lower BSA ζ potential is obtained as salt concentration is increased. This will be discussed below.

4.2. Theoretical Results. The theoretical titration curves for low concentrations of NaCl (below 10 mM) are shown in Figure 3. We note a unique intersection point between the curves, which occurs at the point of zero charge. This is in line with the practice used by Tanford and others that suppose one can use the intersection point to find the IIP. However, as discussed in the Experimental Section, this is not true in real experimental systems at physiological and higher salt concentrations.

The experimental results can be understood including ion specific NES potentials acting between the ions and the protein surface. Figure 4 shows the theoretical titration curves for higher NaCl concentrations obtained including ion–protein NES potentials. Here, it is seen that there is not a unique intersection point, but, in fact, there are different crossing points for different
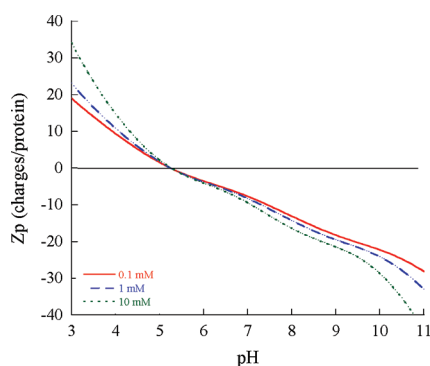
Figure 3. Theoretical titration curves of BSA protein in the pH range close to the point of zero charge in the presence of low salt concentrations of NaCl (using NES potentials and no Tanford correction).
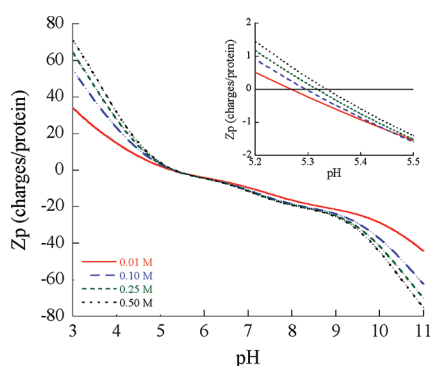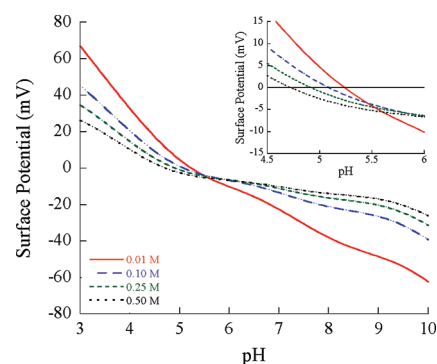

Figure 4. Theoretical titration curves of BSA protein in a wide range of pH values and for pH values close to the point of zero charge (inset); in the presence of different salt concentrations (from 0.01 to 0.5 M) of NaCl (using NES potentials and no Tanford correction).
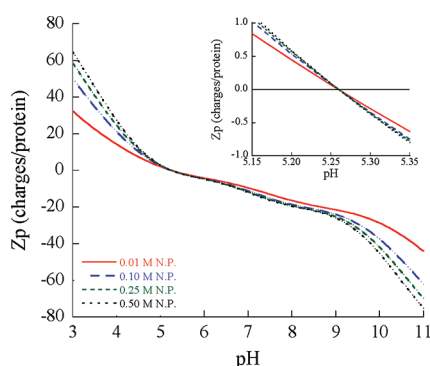
Figure 5. Theoretical titration curves of BSA protein in a wide range of pH values and for pH values close to the point of zero charge (inset); in the presence of different concentrations (0.1 to 0.5 M) of artificial salt solutions with nonpolarizable (NP) ions (no Tanford correction).

concentrations, and in general not at the point of zero charge. There is also reasonable agreement between the theoretical model system and experiments. This supports the view that NES potentials, obtained from ab initio quantum chemical calculations,[18] are required to obtain agreement between theory and experiments. On the contrary, when NES potentials (Figure 5) are ignored, there is for all salts with nonpolarizable (NP) ions a unique intersection point at the point of zero charge.


Figure 6. Theoretical electrostatic surface potential of BSA protein in a wide range of pH values and for pH values close to the point of zero surface potential (inset; in the presence of different salt concentrations (from 0.01 to 0.5 M) of NaCl (using NES potentials and no Tanford correction).

The same intersection point also occurs for the point of zero surface potential when salts with NP ions are considered (data not shown). Figure 6 shows the electrostatic surface potential as a function of pH at different concentrations of NaCl. We observe that the theoretical surface potential is larger than the measured zeta potential (Figure 2). The zeta potential is effectively measured at some distance from the protein surface. The trends with increasing salt concentration, on the other hand, match the experimental data. An important point observed in the literature is that the real "point of zero charge" from titration usually occurs at a higher pH value compared to the "point of zero potential" obtained from ζ measurements. This can now be understood to be due to the effect of ion–protein NES potentials.

5. DISCUSSION

Our modeling based on the modified Poisson–Boltzmann equation considering both electrostatic and NES forces allowed us to reproduce experimental trends of IIP and IEP values at different NaCl concentrations. The two calculated quantities are (i) the protein charge (Z_p) that is directly comparable with the same experimentally obtained quantity and (ii) the surface potential ϕ that is related to the experimental zeta potential. A better quantitative agreement is obtained for IIP values coming from potentiometric titrations than for IEPs from zeta potential; that is, IIPs vary less than IEPs with increasing salt concentration. The resulting points of zero charge/zero surface potential, as a function of salt concentration, in our model system are shown in Figure 7a. From these data, we can argue that IIP and IEP values tend to the same limit value (about 5.27) at zero salt concentration. But they tend to diverge as salt concentration is increased. Results shown in Figures 3–6 were obtained with a model that ignored protein charge related shifts in pK_a values. Here, we compare the resulting points of zero charge/zero potential using also Tanford correction to the pK_a values. We note that the differences between IIP and IEP increase with added salt and are close to those observed experimentally. The differences between the two models including or neglecting Tanford correction are small (Figure 7a). Experimental IIPs and IEPs are shown in Figure 7b. There is a qualitative agreement with theoretical results, although experimental variations of points of zero charge/potential are more pronounced.
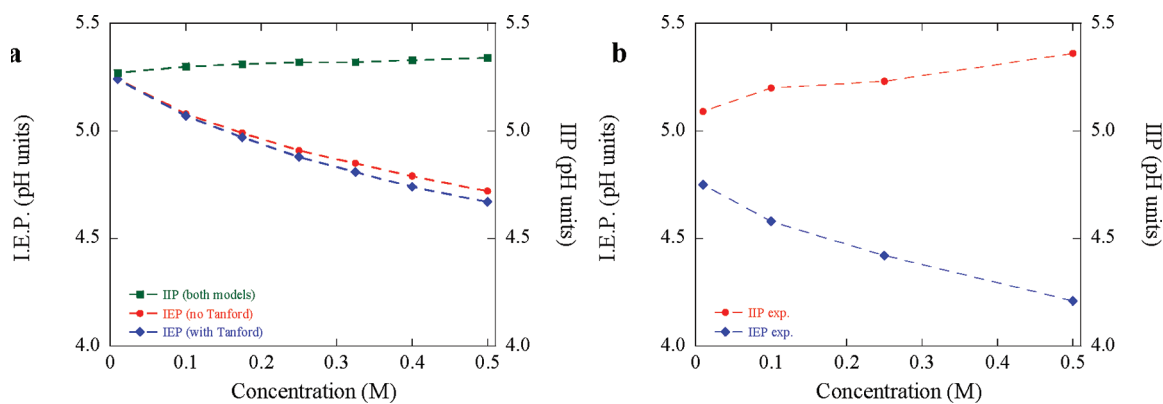
Figure 7. Variation of IIP and IEP of as a function of NaCl concentration. (a) Theoretical results (comparison between results with and without Tanford correction to the pK_a of the protein charge groups); (b) experimental results.

Our results for BSA protein charges in the presence of different NaCl concentrations (Figures 1 and 4) are in good agreement with previous work of Boström et al.[55] and with the papers published by Tanford and co-workers.[5−9] There is, instead, an apparent contradiction with the recent results presented for lysozyme by Gokarn et al.[56] These authors found that the positive lysozyme protein "effective charge" decreases with increasing salt NaCl concentration. However, the difference should be due to the fact that different quantities are measured. Gokarn et al. deduced their protein charge from electrophoretic mobility.[56] Their work should therefore be closely related to the measured zeta potentials which measure the dressed protein charge including counterions close to the protein surface. On the contrary, potentiometric titrations measure the bare protein charge.

In any case, there is no contradiction that the fact that, at fixed pH, Z_p increases with salt concentration increase, whereas ζ decreases. This, apparently counterintuitive, result can be explained by the charge regulation boundary condition[57] (eq 4) used to solve the modified Poisson−Boltzmann equation (eq 2). Z_p depends on surface potential ϕ according to eq 5. At a fixed pH, the surface potential decreases as ionic strength increases. At the limit of very high ionic strength, ϕ tends to zero and the exponential terms in eq 3 tends to 1. Thus, Z_p is maximized (being proportional to the sum of N_b or N_a depending on acidic or basic pH). An ionic strength decrease will produce an increase of surface potential and a consequent decrease of Z_p. This means that the surface hydronium concentration is increasing (decreasing) with increasing salt concentration at low pH (high pH). This leads to an increase in the magnitude of the protein charge with increasing salt concentrations both at high and low pH.

On the contrary, the electrostatic potential becomes more and more screened as salt concentration increases, leading to a decrease of surface potentials and zeta potentials. In their pioneering work, Scatchard and Black proposed a purely electrostatic approach based on Debye−Hückel theory to explain shifts of the IIP, but not the IEP, at high ionic strengths. The model accommodates ion specificity through ion size.[12] Both IIP and IEP shifts (obtained with salt concentration increase, Figure 7) can be predicted once NES forces are inserted into the modified Poisson−Boltzmann equation (eq 2).

One of the fundamental parameters of NES forces is the B dispersion coefficient, determined independently (through ab initio calculations) by ion polarizability in conjunction with properly defined ion size.[58] Anions generally have stronger NES interactions

than cations, as is the case here for Cl$^−$ compared with Na$^+$ (Table 2). Hence, at both isoionic and isoelectric points (zero charge and zero surface potential), one would expect, if only electrostatics is considered, that the same number of cations and anions would interact with the protein surface. This would happen both at low and high ionic strengths. However, due to NES forces, anions (here Cl$^−$) are more strongly adsorbed than cations (here Na$^+$) at the protein surface. This would mean that the protein surface potential is not zero anymore, and adsorbed negative charges could be compensated only by a higher bulk hydrogen ion concentration.

It follows that this will result in a shift at lower pH of IEP as salt concentration is increased. The same phenomenon, that is, chloride adsorption, would also affect the IIP since the negative charges would provide an attractive electrostatic potential that drives positively charged H$^+$ ions toward the protein surface. Therefore, a lower bulk H$^+$ concentration (i.e., higher pH) is required to obtain protein charge neutrality. Again, this effect becomes more pronounced at higher salt concentrations, leading to the observed opposite trends for IIP and IEP. Although the description of these phenomena seems to be complicated, it comes out easily when NES forces are properly taken into account in the correct theoretical framework. We remark that the parameters used to characterize these interactions have been obtained from direct ab initio computations and are not adjustable.

Our simple modeling does not consider two additional effects related with geometry and dipole moment of BSA. First, the BSA shape would be better approximated with a revolution ellipsoid rather than a sphere.[59] Bratko and Dolar showed how the ellipsoid geometry can be used to calculate some thermodynamic properties, as the pK_a's, from numerical solutions of the Poisson−Boltzmann equation, obtained by the finite difference method.[60] Here, we tested corrections on pK_a proposed by Tanford and Swanson,[6] obtaining no substantial differences in the IIPs compared with those uncorrected. Nevertheless, ellipsoid geometry corrected pK_a's would result in an equal shift of IIPs for all salt concentrations. We remark that what is important here is the inclusion of the dispersion potential in a modified Poisson−Boltzmann equation. This allows one to predict the experimental shift of both IIPs and IEPs. Hence, although the ellipsoidal geometry, rather than a spherical one, might help to get a better quantitative agreement between theory and experiment (through a better estimation of pK_a's), our goal, that is, the prediction of IIP and IEP shifts, can be obtained only by the proper inclusion of dispersion forces.

Additional effects due to the large BSA dipole moment, of about 350 D,[59] were not included here. BSA dipole corrections will be relatively small, since their impact is attenuated by the large size (35 Å radius) of the BSA globule. We estimate BSA dipole interactions to be 3 orders of magnitude smaller than electrostatic interactions due to the excess protein charge. An additional possible consequence (or cause) of the large BSA dipole moment is that the surface charge may be distributed inhomogeneously across the surface of the protein, resulting in a nonspherically symmetric electric field. This effect requires more complex modeling and is out of scope for the spherically symmetric model applied here.

6. CONCLUSIONS

We have used titration and zeta potential measurements on a suspension of BSA proteins to study systematically the shifts of isoionic and isoelectric points of BSA protein in different concentrations of NaCl. It was known already 60 years ago that the points of zero protein charge/potential occur at different pH values in their dependence on background salt solution mixture and on the technique used.[12,13] However, while some very insightful comments were made already in the original papers concerning the origin of these effects, a deeper understanding had to await the new theory for intermolecular forces.[16] We have provided what appears to be a possible explanation to the salt concentration effects in terms of ion–protein nonelectrostatic potentials and a modified Poisson–Boltzmann equation for a charge regulated spherical colloidal particle in NaCl salt solutions. This simple model enables us to understand, at a semiquantitative level, the opposite trends observed for the isoelectric point (zero zeta potential) and isoionic point (zero protein charge) with added salt.

■ AUTHOR INFORMATION

Corresponding Author
*(A.S.) Telephone: +39 070 6754362. Fax: +39 070 6754388. E-mail: asalis@unica.it. (M.B.) E-mail: mtb110@physics.anu. edu.au.

■ REFERENCES

(1) Ninham, B. W.; Lo Nostro, P. *Molecular Forces and Self Assembly - In Colloid, Nano Sciences and Biology*; Cambridge University Press: Cambridge, 2010.
(2) Israelachvili, J. *Intermolecular & Surface Forces*, 2nd ed.; Academic Press: London, 1992.
(3) Kakizuka, A. *Trends Genet.* **1998**, *14*, 396.
(4) Sørensen, S. P. L.; Linderstrøm-Lang, K.; Lund, E. *J. Gen. Physiol.* **1927**, *8*, 543.
(5) Tanford, C.; Wagner, M. L. *J. Am. Chem. Soc.* **1954**, *76*, 3331.
(6) Tanford, C.; Swanson, S. A.; Shore, W. S. *J. Am. Chem. Soc.* **1955**, *77*, 6414.
(7) Tanford, C.; Buzzell, J. G. *J. Phys. Chem.* **1956**, *60*, 225.
(8) Tanford, C.; Hauenstein, J. D. *J. Am. Chem. Soc.* **1956**, *78*, 5287.
(9) Tanford, C.; Roxby, R. *Biochemistry* **1972**, *11*, 2192.
(10) Jachimska, B.; Wasilewska, M.; Adamczyk, Z. *Langmuir* **2008**, *24*, 6866.
(11) Chaiyasut, C.; Tsuda, T. *Chromatography* **2001**, *22*, 91.
(12) Scatchard, G.; Black, E. S. *J. Phys. Colloid Chem.* **1949**, *53*, 88.
(13) Longsworth, L. G.; Jacobsen, C. F. *J. Phys. Colloid Chem.* **1949**, *53*, 126.
(14) Derjaguin, B.; Landau, L. *Acta Physicochim. URSS* **1941**, *14*, 633.
(15) Verwey, E. J. W.; Overbeek, J. T. G. *Theory of the stability of lyophobic colloids*; Elsevier: Amsterdam, 1948.
(16) Ninham, B. W.; Yaminsky, V. *Langmuir* **1997**, *13*, 2097.
(17) Parsons, D. F.; Deniz, V.; Ninham, B. W. *Colloids Surf., A* **2009**, *343*, 57.
(18) Parsons, D. F.; Ninham, B. W. *Colloids Surf., A* **2011**, *383*, 29.
(19) Parsons, D. F.; Ninham, B. W. *J. Phys. Chem. A* **2009**, *113*, 1141.
(20) Parsons, D. F.; Ninham, B. W. *Langmuir* **2010**, *26*, 1816.
(21) Parsons, D. F.; Ninham, B. W. *Langmuir* **2010**, *26*, 6430.
(22) Parsons, D. F.; Boström, M.; Maceina, T. J.; Salis, A.; Ninham, B. W. *Langmuir* **2010**, *26*, 3323.
(23) Boström, M.; Deniz, V.; Ninham, B. W.; Franks, G. *Adv. Colloid Interface Sci.* **2006**, *5*, 123.
(24) Kim, H.-K.; Tuite, E.; Nordén, B.; Ninham, B. W. *Eur. Phys. J. E* **2001**, *4*, 411.
(25) Pinna, M. C.; Bauduin, P.; Tourand, D.; Monduzzi, M.; Ninham, B. W.; Kunz, W. *J. Phys. Chem. B* **2005**, *109*, 16511.
(26) Pinna, M. C.; Salis, A.; Monduzzi, M.; Ninham, B. W. *J. Phys. Chem. B* **2005**, *109*, 5406.
(27) Salis, A.; Bilanicova, D.; Ninham, B. W.; Monduzzi, M. *J. Phys. Chem. B* **2007**, *111*, 1149.
(28) Bilanicova, D.; Salis, A.; Ninham, B. W.; Monduzzi, M. *J. Phys. Chem. B* **2008**, *112*, 12066.
(29) Salis, A.; Bhattacharyya, M. S.; Monduzzi, M. *J. Phys. Chem. B* **2010**, *114*, 7996.
(30) Salis, A.; Pinna, M. C.; Bilanicova, D.; Monduzzi, M.; Lo Nostro, P.; Ninham, B. W. *J. Phys. Chem. B* **2006**, *110*, 2949.
(31) Salis, A.; Parsons, D. F.; Bostrom, M.; Medda, L.; Barse, B.; Ninham, B. W.; Monduzzi, M. *Langmuir* **2010**, *26*, 2484.
(32) Zhang, Y.; Cremer, P. S. *Proc. Natl. Acad. Sci. U.S.A.* **2009**, *106*, 15249.
(33) Robertson, B. T. *J. Biol. Chem.* **1911**, *9*, 303.
(34) Boström, M.; Parsons, D. F.; Salis, A.; Ninham, B. W.; Monduzzi, M. *Langmuir* **2011**, *27*, 9504.
(35) Lund, M.; Jungwirth, P. *J. Phys.: Condens. Matter* **2008**, *20*, 4.
(36) Boström, M.; Williams, D. R.; Ninham, B. W. *Biophys. J.* **2003**, *85*, 686.
(37) Lima, E. R. A.; Biscaya, E. C., Jr.; Boström, M.; Tavares, F. W.; Prausnitz, J. M. *J. Phys. Chem. C* **2007**, *111*, 16055.
(38) Lima, E. R. A.; Biscaia, E. C.; Bostrom, M.; Tavares, F. W.; Prausnitz, J. M. *J. Phys. Chem. C* **2008**, *112*, 8741.
(39) Finet, S.; Skouri-Panet, F.; Casselyn, M.; Bonneté, F.; Tardieu, A. *Curr. Opin. Colloid Interface Sci.* **2004**, *9*, 112.
(40) Boström, M.; Tavares, F. W.; Finet, S.; Skouri-Panet, F.; Tardieu, A.; Ninham, B. W. *Biophys. Chem.* **2005**, *117*, 217.
(41) Wernersson, E.; Kjellander, R. *J. Chem. Phys.* **2006**, *125*, 154702.
(42) Zhang, Y.; Cremer, P. S. *Annu. Rev. Phys. Chem.* **2010**, *61*, 63.
(43) Borah, J. M.; Mahiuddin, S.; Sarma, N.; Parsons, D. F.; Ninham, B. W. *Langmuir* **2011**, *27*, 8710.
(44) Parsegian, V. A. *Ann. N.Y. Acad. Sci.* **1974**, *238*, 362.
(45) Lee, K. K.; Fitch, C. A.; Lecomte, J. T. J.; Garcia-Moreno, E. B. *Biochemistry* **2002**, *41*, 5656.
(46) Kuehner, D. E.; Engmann, J.; Fergg, F.; Wernick, M.; Blanch, H. W.; Prausnitz, J. M. *J. Phys. Chem. B* **1999**, *103*, 1368.
(47) Dagastine, R. R.; Prieve, D. C.; White, L. R. *J. Colloid Interface Sci.* **2000**, *231*, 351.

(48) Tavares, F. W.; Bratko, D.; Blanch, H.; Prausnitz, J. M. *J. Phys. Chem. B* **2004**, *108*, 9228.

(49) Malamud, D.; Drysdale, J. W. *Anal. Biochem.* **1978**, *86*, 620.

(50) Gelsema, W. J.; Ligny, C. L. d.; Veen, N. G. v. d. *J. Chromatogr., A* **1978**, *154*, 161.

(51) Nozaki, Y.; Bunville, L. G.; Tanford, C. *J. Am. Chem. Soc.* **1959**, *81*, 5523.

(52) Righetti, P. G.; Caravaggio, T. *J. Chromatogr.* **1976**, *127*, 1.

(53) Cannan, R. K.; Palmer, A. H.; Kibrik, A. C. *J. Biol. Chem.* **1942**, *142*, 803.

(54) Anderson, A. *J. Phys. Colloid Chem.* **1948**, *52*, 1315.

(55) Boström, M.; Lonetti, B.; Fratini, E.; Baglioni, P.; Ninham, B. W. *J. Phys. Chem. B* **2006**, *110*, 7563.

(56) Gokarn, Y. R.; Fesinmeyer, R. M.; Saluja, A.; Razinkov, V.; Chase, S. F.; Laue, T. M.; Brems, D. N. *Protein Sci.* **2011**, *20*, 580.

(57) Ninham, B. W.; Parsegian, V. A. *J. Theor. Biol.* **1971**, *31*, 405.

(58) Parsons, D. F.; Bostrom, M.; Lo Nostro, P.; Ninham, B. W. *Phys. Chem. Chem. Phys.* **2011**, *13*, 12352.

(59) Soetewey, F.; Rosseneu-Motreff, M.; Lamote, R.; Peeters, H. *J. Biochem.* **1972**, *71*, 705.

(60) Bratko, D.; Dolar, D. *J. Chem. Phys.* **1984**, *80*, 5782.

PAPER II

Hofmeister Challenges: Ion Binding and Charge of the BSA Protein as Explicit Examples

Luca Medda,[†] Brajesh Barse,[†,‡] Francesca Cugia,[†] Mathias Boström,[§] Drew F. Parsons,[∥] Barry W. Ninham,[∥] Maura Monduzzi,[†] and Andrea Salis*[,†]

[†]Department of Chemical and Geological Sciences, University of Cagliari-CSGI and CNBS, Cittadella Universitaria, S.S. 554 bivio Sestu, 09042 Monserrato (CA), Italy

[‡]Evalueserve Pvt. Limited Tower B, Infospace, (SEZ), Sector-21, Gurgaon 122001, Haryana, India

[§]Department of Materials Science and Engineering, Royal Institute of Technology, SE-100 44 Stockholm, Sweden

[∥]Research School of Physical Sciences and Engineering, Australian National University, Canberra 0200, Australia

ABSTRACT: Experiments on bovine serum albumin (BSA) via potentiometric titration (PT) and electrophoretic light scattering (ELS) are used to study specific-ion binding. The effect is appreciable at a physiological concentration of 0.1 M. We found that anions bind to the protein surface at an acidic pH, where the protein carries a positive charge ($Z_p > 0$), according to a Hofmeister series ($Cl^- < Br^- < NO_3^- < I^- < SCN^-$), as well as at the isoionic point ($Z_p = 0$). The results obtained require critical interpretation. The measurements performed depend on electrostatic theories that ignore the very specific effects they are supposed to reveal. Notwithstanding this difficulty, we can still infer that different 1:1 sodium salts affect the BSA surface charge/pH curve because anions bind to the BSA surface with an efficiency which follows a Hofmeister series.
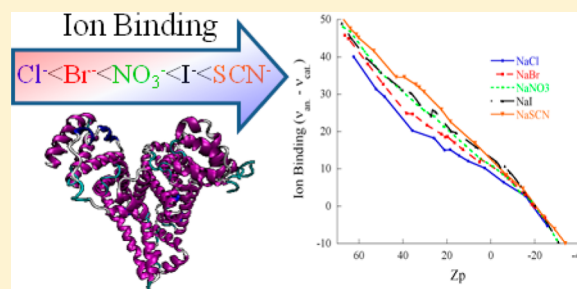
1. INTRODUCTION

1.1. Background. The earliest report on ion specificity dates back to Napoleon's expedition to the Nile in 1798. Claude L. Berthollet, an accompanying scientist, observed rocks covered with soda lime, precipitated sodium carbonate, in the river bed. The expectation was that it was calcium carbonate rather that should be precipitated, leaving sodium chloride in solution. This reaction reversal, due to high summer temperatures, probably marks the beginning of physical chemistry.[1]

Poiseuille studied ion specificity of viscosity of aqueous solutions in 1847.[2] The matter rested until Hofmeister studied ion specificity as measured by concentrations of salts needed to precipitate suspensions of proteins and other colloids in the 1880s.[3] Hofmeister phenomena permeate all of chemistry and biology.[1,4]

A definition of the term Hofmeister effects, like that of "hydrophobic effects", is necessarily vague and certainly confusing. At first, it meant specificity as embodied in the Hofmeister's series for the relative efficiency of sodium salts in precipitation of egg white protein

$$HPO_4^{2-} > SO_4^{2-} > F^- > Cl^- > Br^- > NO_3^- > I^- > ClO_4^- > SCN^-$$
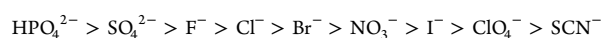
Early on, it became clear that the series is not universal. It depends on the nature of the suspension and sometimes reverses in order.[5] Later, it came to mean specificity not accounted for by the classical theory of strong electrolytes and colloids. At first this meant the Debye−Hückel theory, extended to include hard core interactions in the primitive

model. Later still, it meant further extensions to include the civilized model of electrolytes, namely Gurney potentials due to ionic hydration shell overlap, and surface hydration. Theory and experiment still failed to accommodate the phenomena.

In the last 15 years, more data from a plethora of experiments has emerged. The state of affairs can be gleaned from references in a book by Ninham and Lo Nostro[1] and in a more recent review article from the same authors.[4] A few of many such examples are with wool water absorption,[6] silica surface and alumina interactions,[7] bacterial growth,[8] enzyme activities,[9−13] surfactant interfaces,[14] electrophoretic mobilities,[15,16] cloud points of lysozyme[17,18] and nonionic surfactants,[19] optical activity of α-amino acids,[20] electrochemistry of cytochrome c,[21] the aggregation behavior of triblock copolymers,[22] the water structure adjacent to surfactant or protein monolayers,[23,24] and many other examples.[25−29] Different Hofmeister series, direct, inverse, or mixed, are observed.[5,17,30−35]

1.2. Theoretical Developments. Along with these new experimental data has been what appears to be substantial progress in the theory behind Hofmeister phenomena.[1,36−43] Simulation has provided useful modeling that provides a firmer basis for categorization like Collins' Rules.[37] This empirical law of "Matching Water Affinities"[44] has much appeal.[45] However, the law has some serious deficiencies.[4]

A complementary approach extends the classical theory of electrolytes to include additional ion-specific contributions from dispersion interactions. (These are missing from classical theory which include electrostatic forces and effective hydration).[46] These forces have now been built into emerging theories. They call on ab initio quantum mechanics to quantify frequency-dependent polarization, ion size, and ionic hydration. Ion size and hydration had until recently been effective parameters. The status of these theoretical developments can be seen in references 47 and 48. To complicate matters further, it is known that dissolved atmospheric gas plays a key role in the whole business.[1,49]

1.3. A Problem with Measurements: pH as an Example. It might be generally agreed that while parts of the phenomena can be accommodated, a lot can not. From the beginning of the Hofmeister saga, the outstanding test of modeling has been a parameter-free explanation for a reversal in the series.[1,5,17,33,50,51] This classic challenge to theory can be seen in pH measurements in electrolytes as a function of concentration.[52] A change in buffer from cacodylate to phosphate, at the same nominal pH, reverses the Hofmeister series. Similarly, a change in the cation from sodium to potassium, with a varying anion, reverses the series again.[34]

Evidently this phenomenon implies that not just bulk activities are involved. There has to be competition for the glass electrode surfaces of the cation−anion, buffer anion, and buffer anion−electrolyte interactions.[20] Again, with restriction enzyme activity the same phenomena occur, with the complication that dissolved gas may be involved.[31]

This problem of pH is fundamental. The work of Evens and Neidtz[53] shows that in a real complicated biological system, pH becomes a derived quantity and not meaningful as conventionally used. There is no problem with the measurement. The question is what it means. If we refer to the IUPAC standard reference on pH, we see that the theory behind the measurement rests on the extended Debye−Huckel theory and on the Poisson−Boltzmann distribution to describe ionic profiles near the glass-electrode surface. That is, it depends on an electrostatics-only foundation which can not account for the ion specificity of the Hofmeister effects. The advice of the IUPAC Committee[54] is to stay away from pH measurements above 0.1 M. It is of no help to standardize the electrode as usually done, as a function of concentration, say with NaCl; the results will change unpredictably with different salts and buffers (and with highly charged proteins and colloidal particles that also drastically modify the Debye length[55]).

It seems then that until we have a better underlying foundation that allows interpretation of the pH measurement, and of buffers, we remain in limbo.

1.4. Present Work. The dilemma of pH is known to biochemists but not so recognized by physical chemists. What is not recognized by both is that the difficulty underlies other standard techniques just as much. We illustrate the difficulties with experiments using potentiometric titrations (PT) and electrophoretic light scattering (ELS) applied to the study of specific-ion binding to the familiar protein bovine serum albumin (BSA).

Whatever be the explanation of Hofmeister effects that might occur in protein systems, it is widely recognized that (specific) ion binding to protein surface plays a fundamental role.[38] This is a very important issue in biochemical systems. Physiological media contain proteins and electrolytes (both salt and buffer) in water solution. The main function of buffers (but not the

only one)[12,31] is supposed to be to fix pH and thus the protonation state (i.e., the surface charge) of the protein. The effective charge can then be modulated by the salts due to the phenomenon of ion binding. Such an argument lies at the basis of a series of phenomena, such as protein aggregation and adsorption, relevant to applications in medicine, food science, biotechnology, and pharmaceutical and cosmetic industries.

In medicine, protein deposition (irreversible adsorption) is responsible for thrombosis in the cardiovascular system.[56] In the visual system of vertebrates, the (specific) electrolyte-mediated repulsive interactions between α-crystallins ensure a local liquidlike order that accounts for lens transparency, whereas the attractive interactions between γ-crystallins contribute to the lens refractive index and optical quality.[57] Moreover, some neurodegenerative disorders have been related to protein aggregation.[58,59] If the protein considered is an enzyme, ion binding may result in either an activation or a deactivation of its catalytic function.[10,11,60]

Hence, ions play a fundamental role in modulating protein functions and the study of their effects at physiological concentrations deserves investigation. The starting point would be the quantification of "ion binding" and possibly its effect on the net charge of the protein, a key determinant of the state of existence of the protein in disperse or aggregate forms.

In this work, we use two techniques, potentiometric titrations (PT) and electrophoretic light scattering (ELS), to study the Hofmeister effects on the surface charge/pH curve of bovine serum albumin (BSA) and to quantify the relative ion binding. Although we use conventional experimental techniques, we interpret the experimental data within the confines of classical theory (i.e., we keep in mind a caveat: theories behind measurements of pH or electrophoresis are based on electrostatic theories only and are therefore flawed). Notwithstanding this difficulty, we can still infer that different 1:1 sodium salts affect BSA surface charge/pH curve because anions bind to the BSA surface with an efficiency which follows a Hofmeister series.

2. EXPERIMENTAL SECTION

2.1. Chemicals. Bovine serum albumin (BSA) (99%), sodium chloride (>98%), sodium bromide (99%), sodium nitrate (99%), sodium iodide (≥99.5%), and sodium thiocyanate (≥98%) were from Sigma Aldrich (Milan, Italy). Buffer standard solutions (of unknown composition) at pH 1 (HI6001), pH 4 (HI6004), pH 7 (HI6007), pH 9 (HI6009), and pH 10 (HI6010) were purchased from Hanna instruments (Szeged, Hungary). Hydrochloric acid and sodium hydroxide standard solutions (0.1 M) were from Merck (Milan, Italy).

2.2. Preparation of BSA−Salt Solutions. All salts were dried overnight at 110 °C and cooled at room temperature in a desiccator. All sample (BSA and salt) and blank (salt with no BSA) solutions were prepared by using purified water (conductivity ≤0.054 mS cm^{-1}), prepared by means of a Millipore water purification system (Millipore, U.K.). Protein solutions were prepared by dissolving weighed amounts of BSA in different salt solutions (NaCl, NaBr, NaNO$_3$, NaI, and NaSCN) all at 0.1 M, reaching the final protein concentration of 1 mg/mL. Samples were filtered before carrying out the experiments.

2.3. Reversible Expansion of BSA. In the titration experiments described below, BSA was titrated in a pH range of 2.7−10. As reported by Tanford and co-workers,[61] BSA exists in a compact form between pH 4.3 and 10.5. Below and above those pHs, it undergoes a reversible expansion. There is no denaturation or irreversible unfolding. The "reversible expansion" phenomenon is due to the electrostatic repulsion between charged groups at extreme pH values and decreases as the ionic strength is increased. Hence, in our experimental conditions, we would have a change of BSA radius

between pH 2.7 and 4.3. On the basis of our own DLS measurement, we have used for the calculation of $f(\kappa R_p)$ and Z_{eff} (eqs 2 and 3) the following values of R_p: 3.8 nm (pH 3–4), 3.5 nm (pH 4–4.5), and 3.4 nm (pH > 4.5).

2.4. Potentiometric Titrations. Potentiometric titrations of sample and blank solutions were performed by using an automatic titrator, Titrando 836 from Metrohm (Herizau, Switzerland) interfaced to a PC with Tiamo 1.3. The pH electrode was calibrated by a 5-point calibration through the standard buffer solutions listed above. The protein titration curve reports the number of hydrogen ions attached to a protein molecule at any pH, relative to the number attached at an arbitrary reference pH. It is convenient to choose as the reference point a pH value which has physical significance for the protein.[62] The most-used reference point is the "point of zero net proton charge" which operatively corresponds to the isoionic point (IIP) of the protein.[63] The isoionic point would in principle be ion specific.[64] But due to the lack of such data, we assume the same IIP (i.e., pH ~5.3 for BSA) for all investigated salts. For these reasons, both the sample and the blank solutions were first set at pH 5.3, acidified to pH 2.7 (pretitration) with a standard HCl solution (0.1 M), and then titrated with a standard solution of NaOH (0.1 M) up to pH = 10. In order to allow the equilibration of the solution after a titrant addition, the automatic titrator was set with a delay of 300–600 s between two consecutive titrant additions and a maximal signal drift of 4 mV/min. Blank titrations were carried out on a solution having the same composition of the sample (HCl 0.1 M and the salt used for the experiment) but without BSA. All experiments were performed in a thermostatted cell ($T = 25\ °C$).

The surface charge of BSA (Z_p) was calculated at different pH values by using the data obtained by potentiometric titrations, of both proteins samples and blanks, according to the following equation:

$$Z_p(pH) = \frac{\text{mol H}^+_{\text{boundtoBSA}}(pH)}{\text{mol}_{BSA}}$$
$$= \frac{(V_{\text{HClsample}} - V_{\text{HClblank}})[\text{HCl}] - (V_{\text{NaOHsample}} - V_{\text{NaOHblank}})[\text{NaOH}]}{m_{BSA}/MW_{BSA}}$$

$$(1)$$

where m_{BSA} is the mass of the BSA sample, and MW_{BSA} is the molecular weight of BSA. V_{NaOH} is the volume of NaOH used in the titration of both the sample and the blank, and V_{HCl} is the volume of HCl used in the pretitration at pH 2.7 for both the sample and the blank.

We have here an apparent complication which would make the determination of Z_p difficult. Indeed we recognize that absolute pH measurements are affected by salt type and concentration[52] because ion adsorption at the glass electrode surface unpredictably modifies the electrochemical potential and, hence, the pH calculated through the conventional Nernst equation. What comes in our favor is the fact that Z_p is obtained as the difference between two titration experiments (protein sample and blank). Hence, we assume that the ions of the supporting electrolyte affect the potential measured by the glass electrode in the same way during sample and blank titration. Thus, the differences between the two (sample and the blank) curves can be ascribed only to the acid–base equilibrium of BSA-charged groups, suitably modulated by the presence of the different electrolytes (NaCl, NaBr, NaNO$_3$, NaI, and NaSCN). In doing so, we are not considering that the presence of the protein may affect pH measurements by modifying the Debye length of the sample solution.[55]

2.5. Electrophoretic Mobility Measurements. Electrophoretic mobility (μ_E) measurements of salt–BSA solutions were obtained through the electrophoretic light scattering (laser Doppler velocimetry) technique by means of a Zetasizer nano series (Malvern Instruments). The same sample of BSA (1 mg/mL) in a salt solution (0.1 M) was acidified to pH 3 then titrated with a NaOH solution to pH 10. After each addition of titrant, a small volume of the BSA–salt solution was put in a thermostatted (25 °C) scattering cell for the measurement of electrophoretic mobility. Each series of experiments was repeated 3–5 times. Each value of mobility is the average of 5–7

measurements for each salt concentration. Standard deviations were calculated and displayed as error bars.

Z_{eff} is considered to be the charge at the shear plane assumed to reside at a certain (unquantified and unquantifiable) distance away from the particle surface, which has a surface charge Z_p. On the basis of the conventional electrokinetic theory, the Henry equation allows the calculation of the Z_{eff} of a colloidal particle from the electrophoretic mobility, μ_E, data as[65]

$$\mu_E = \frac{Z_{eff} e f(\kappa R_p)(1 + \kappa R_b)}{6\pi\eta R_p(1 + \kappa R_p + \kappa R_b)}$$

$$(2)$$

where κ is the inverse Debye length calculated only considering the ionic strength due to the salt and not considering the contribution due to the presence of the multivalent protein;[55] R_p is the protein radius, and R_b is the average electrolyte radius. η is the solution viscosity and $f(\kappa R_p)$ is Henry's function, calculated through[65]

$$f(\kappa R_p) = 1 + \frac{0.5}{[1 + \exp\{a[1 - \log(\kappa R_p)]\}]}$$

$$(3)$$

Here, we have a familiar recurring difficulty: Henry's equation is derived by the purely electrostatic double-layer theory which ignores both hydration and dispersion forces. That is again the interpretation of the measurements depending on a theory that ignores the specific-ion effects it is supposed to measure. Nevertheless, since no complete theory is available, we are constrained to take Henry's equation as a rough guide to calculate the Z_{eff} of the BSA solutions.

3. RESULTS AND DISCUSSION

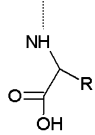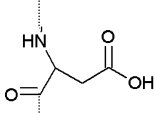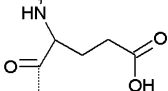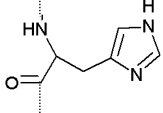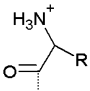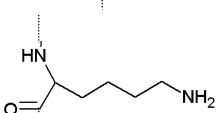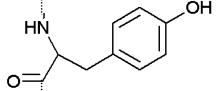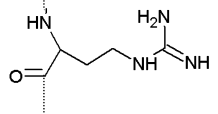**3.1. Potentiometric titration Versus Electrophoretic Light Scattering.** The dependence of protein charge by pH can be determined both by potentiometric titrations and electrophoretic light scattering measurements. In fact, the charge/pH curves obtained with these two methods do not coincide because different information is being obtained in each case. Potentiometric titrations allow the calculation of charge/pH curves based on a proton removal due to the OH$^-$ of the titrant solution.

Protein charge is given by the difference between the moles of titrant used to titrate the protein and those used for a blank solution, both previously brought to a low pH by adding a known amount of HCl. Hence, this technique considers the protein charges only due to bound (positive charges) or unbound (negative charges) protons, but it gives only an indirect response of the effect of the other ions eventually occurring in the system.

Electrophoretic mobility measurements, instead, are based on the motion of a protein in an electrical field and thus are also strongly influenced by bound ions besides H$^+$ and OH$^-$. Hence, the electrolytes present in the system affect the two types of measurements differently. Electrolytes affect potentiometric titrations because a change of the ionic strength affects the effective equilibrium dissociation constants of the titratable groups (see below) or, alternatively, because specific-ion effects driven by dispersion and electrostatic and hydration interactions affect the surface potential.[66] Mobilities are affected, instead, because ions bind to the protein surface, therefore, affecting its effective charge. Thus, protein charge versus pH curves obtained by the two methods are very different because of ion binding.

In addition, the two techniques allow for the determination of the pH value at which the protein surface is electrically neutral.[66] As originally defined, the isoionic point (IIP) is the pH value at which a zwitterionic molecule has an equal number of positive and negative charges and no adsorbed ionic species.

Table 1. Titratable Groups of Proteins and Number (N) of each Charge Group for BSA.[a]

Structure	Acidic/basic groups		N	pK$_{a(int)}$
	α-Carboxylic group	-	1	3.75
	Aspartic acid	ASP	40	3.92
	Glutamic acid	GLU	59	3.92
	Histidine	HIS	16	6.9
	α-Amino group	-	1	7.75
	Lysine	LYS	57	9.8
	Tyrosine	TYR	19	10.35
	Arginine	ARG	22	12

[a]The pK$_{a(int)}$ values of BSA are measured by Tanford et al.[63] at an ionic strength of 0.15 M in KCl.

The isoelectric point (IEP), instead, is the pH value at which the net charge of the molecule, including bound ions, is zero. On the basis of this definition, the isoionic point would exclude the presence of any ion by the system. But rather than the "theoretical" definition of isoionic point, we are interested in its "operative" definition. Indeed, the IIP is determined as the intersection point among potentiometric titration curves carried out at different ionic strengths. We consider this operative definition in the following parts of the paper.

3.2. Protein Charge from Potentiometric Titrations. Most proteins contain 8 different types of titratable amino acids. A full list of the titratable groups of BSA, their abundance, and their respective pK$_{a(int)}$ values is given in Table 1.

Figure 1 highlights, with different colors, the titratable groups of BSA. The terminal α-carboxyl and α-amino (green in Figure 1) are always present in each protein as the initial and terminal residues of the polypeptide chain. If the protein is constituted by more subunits their abundance is equal to the number of

these polypeptide chains. Aside from the initial and terminal residues, the other 4 types of titratable amino acids which [for the protein used (BSA)] are the main determinants of the charge dependence by pH. They are carboxylic acids (Asp and Glu; red in Figure 1), imidazole (His; purple), phenol (Tyr; pale blue), amino (Lys; blue), and guanidine (Arg; yellow).

Due to the zwitterionic nature of amino acids (and hence of proteins), the charge of a generic protein (Z_p), at any pH, is given by

$$Z_p = z^+ - z^- \tag{4}$$

where z^+ and z^- are the number of positive and negative charges at a given pH, respectively. More precisely they represent the number of bound or dissociated protons with respect to the isoionic point (IIP, the pH at which $z^+ = z^-$). The titration curve can then be described, according to Figure 2, as follows.
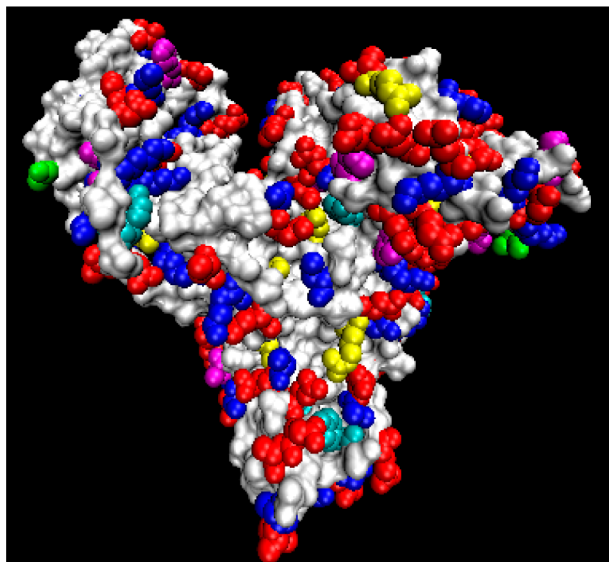
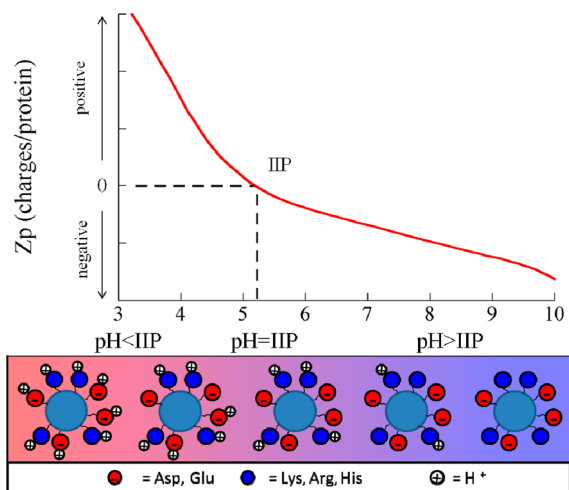**Figure 1.** Representation of the titratable amino acids of the Bovine Serum Albumin. Asp and Glu residues are red, His is purple, Lys is blue, Arg is yellow, Tyr is pale blue, and N and C terminal groups are green. White colored residues are untitratable amino acids (PDB code: 3V03).


Figure 2. Graphical representation of the zwitterionic model for protein titration. Big circles (pale blue) represent a generic protein. Small red circles represent the acidic residues of the protein (i.e., Asp and Glu); small blue circles represent the basic residues (i.e., Lys, Arg, and His), and small white circles represent hydrogen ions.

At low pH values (pH < IIP), all the acidic and basic sites are protonated; that is, carboxylates are neutral ($z_{pH}^- = 0$), and aminelike residues are positively charged ($z_{pH}^+ = $ max). The net charge of the protein is then positive ($Z_p > 0$). By increasing the pH, due to the addition of the sodium hydroxide solution, the acidic residues lose their protons, thus becoming negatively charged (R−COO$^-$). This will decrease the positive net charge of the protein. When pH equals the isoionic point (IIP), $Z_p > 0$ because of the presence of the same number of positive and negative charges ($z^+ = z^-$). A further addition of titrant solution removes protons by the basic sites which become uncharged. The net charge of the protein then becomes negative ($Z_p < 0$), not because of the generation of new negative charges but due to the neutralization of the positively charged basic groups.

3.3. Hofmeister Effects on Charge/pH Curves of BSA.
Although the effect of salt concentration on protein titrations has been widely investigated,[63,66−68] to the best of our knowledge, the effect of different ions at the same concentration has surprisingly not been reported yet, at least in the systematic framework of Hofmeister effects. Figure 3 shows the variation of BSA charge in the presence of a range of salts which can be ordered according to a Hofmeister series for anions.
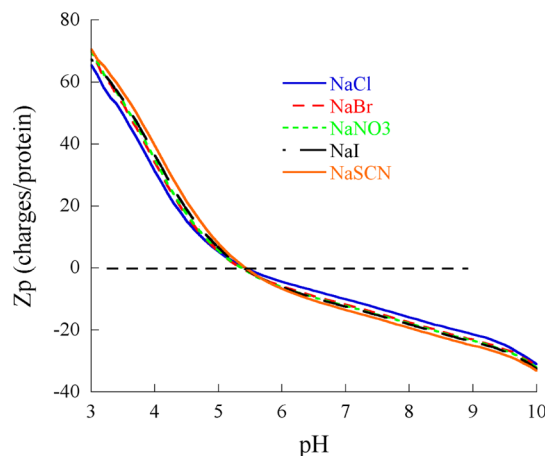
Figure 3. Ion-specific effects of BSA surface charge vs pH.

At pH < IIP, where anions are counterions, the surface charge increases in the order Cl$^-$ < Br$^-$ < NO$_3^-$ < I$^-$ < SCN$^-$. This trend is consistent with the increasing anion polarizability.[33] At pH > pI where anions are co-ions, the series is the same, so the surface charge increases in magnitude (more negative values) with an increase in anion polarizability. In Figure 3, it is possible to distinguish an inversion point around the isoionic point (IIP) of the protein. This inversion point has already been observed in experiments concerning the effect of salt concentration.[66] Hence, the effect of using salts with the same cation but a different anion at the same concentration seems to mimic the effect of increasing the NaCl concentration.

As reported by Tanford, an ionic strength increase results in a higher apparent pK_a^{app} for R−COOH groups and a lower pK_a^{app} for R−NH groups.[63] Indeed, pK_a^{app} depends on the charge of the protein Z and by a so-called electrostatic factor, w (which ultimately depends on the ionic strength and on the distribution of charges on the protein surface), according to

$$pK_{int} = pK_a^{app} - 0.868wZ \tag{5}$$

In the pH range (2.7−10) relevant to our work, BSA undergoes a conformational change at about pH 4.3.[61] This conformational change would affect pK_a values. The following equation considers this effect[63]

$$w = \frac{e^2}{\varepsilon_r \varepsilon_0 kTR_p}\left(1 - \frac{\kappa R_p}{1 + \kappa a}\right) \tag{6}$$

The parameter w is a function of the inverse of the Debye length (κ) and protein radius, R_p, and of the distance of closest approach, a. Conformational changes result in a variation of R_p and, hence, of w and pK_{int}. The experimental titrations already include the variation of those pK_a's whose values are reported in Table 1. Moreover, the increase of salt concentration affects the apparent dissociation equilibrium constants (K_a^{app}) and thus

the charge of the protein. In our study, the use of different sodium salts (i.e., NaBr, NaNO$_3$, NaI, and NaSCN) at the same concentration (0.1 M) mimics the effect of increasing the NaCl concentration. At pH < IIP, the substitution of Cl$^-$ with the more polarizable SCN$^-$ mimics the increase of the NaCl concentration.[66]

A more subtle argument has to be used to understand what happens at pH > IIP (Z_p < 0). Also, here SCN$^-$ results in higher (negative) Z_p compared to Cl$^-$ (Figure 3). In principle, we may expect the main effect is due to the binding of Na$^+$ cations. Hence, the effect of anions (Cl$^-$ and SCN$^-$), which are co-ions, would likely be less important. The experimental results can be explained only admitting that the more polarizable SCN$^-$ is bound to the BSA surface more than Cl$^-$, despite the net negative charge. This in turn would attract more Na$^+$ toward the protein surface, thus facilitating R−NH$^+$ neutralization (decrease of pK_a^{app}) as occurs by increasing the NaCl concentration.[66] Hence, in the negative branch of the titration curve, the anions would affect a net protein charge through an indirect mechanism.

3.4. Hofmeister Effects on Electrophoretic Light Scattering Measurements.
Electrophoretic light scattering measurements as a function of the pH of BSA in 0.1 M salt solutions were carried out. What we measure is the electrophoretic mobility from which we calculate, according to eq 2, protein charge/pH curves. Figure 4 shows that ion specificity is
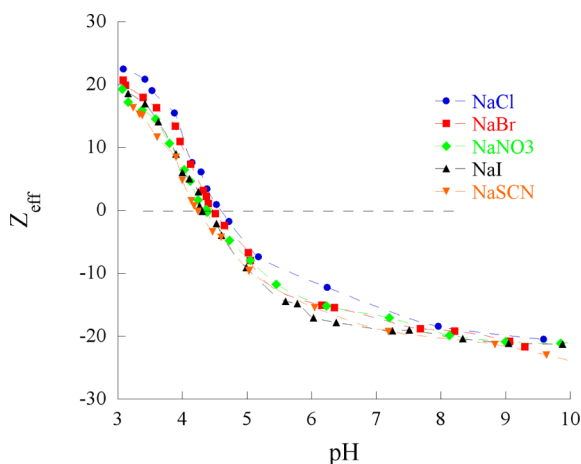
Figure 4. Ion-specific effects of the BSA surface charge (Z_{eff}) vs pH, in the presence of a range of 0.1 M sodium salts.

present also in these experiments. First of all, we note that the charge values are lower, in absolute terms, than those obtained with the PT experiments. At pH < IEP (isoelectric point), the charge decreases along the series: Cl$^-$ > Br$^-$ > NO$_3^-$ > I$^-$ > SCN$^-$ with a trend that is the opposite of what was obtained with PT experiments. On the other hand, at pH = IEP, we do not observe the crossing between the ion-specific curves as in the PT experiments. The different curves become negative being almost parallel in the region below and above the IEP.

The trends obtained by ELS can be explained by admitting that the effective charge (Z_{eff}) of BSA depends on ion binding. Highly polarizable SCN$^-$ binds more than less polarizable Cl$^-$, thus reducing the net charge in the positive branch of Z_{eff}/pH curve. The same mechanism is responsible for the more negative charge observed for SCN$^-$ in the negative branch of the curve.

3.5. Determination of Ion Binding.
The importance of ion binding in modulating protein−protein and protein−surface interactions has led to the search for methods for the estimation of the number of bound ions. Prausnitz and co-workers reported a method to estimate the number of chloride ions bound to the lysozyme surface in concentrated KCl solutions.[68] They carried out potentiometric titrations, much as we have in the present paper, thus determining the proton net charge of lysozyme as a function of pH. From the ionic strength dependence of Z_p, K$^+$ and Cl$^-$ binding was calculated through the molecular thermodynamic theory of Fraaije and Lyklema.[69] The theory ignores specific-ion effects, so that consistency is lost.

In a series of papers, Cremer and co-workers investigated the ion-specific behavior of the interfacial water structure by means of vibrational sum frequency spectroscopy (VSFS) in different systems.[23,35,70] Particularly relevant to the present work is their investigation on BSA at different pH values (pH = 2, 3, 5, and 9) and different sodium salts (namely, NaCl, NaBr, NaNO$_3$, NaClO$_4$, and NaSCN at 0.1 M and Na$_2$SO$_4$ at 0.03 M).[24] Their results suggest that the interfacial water structure is affected by the surface charge and of a preferential adsorption of more chaotropic monovalent anions over less chaotropic monovalent anions. They used a mathematical model, based on the combination of a Stern model and Langmuir isotherm,[24,70] for comparison with the experimental results reaching a good agreement between theory and experiment. Such a strategy had been used in quite a few papers, despite small differences in details, to account for ion binding, such as Saykally and co-workers[71] and Record and co-workers.[72]

Here, instead, we have taken advantage of the combined use of PT and ELS to directly quantify the number of bound ions as a function of pH. The two charges Z_p and Z_{eff} obtained by the two methods, are related by the following relationship[62]

$$Z_p - Z_{eff} = \nu_{anion} - \nu_{cation} \tag{7}$$

where ν_{anion} and ν_{cation} are the number of bound anions and cations, respectively. Plots showing the difference between Z_p and Z_{eff} which corresponds to the number of bound ions, are shown in Figure 5. Figures 5a and 5b show the ion binding as a function of pH and Z_p, respectively. The y axis in Figure 5 is in fact the difference between the number of bound anions minus the number of bound cations. So, in the hypothesis that at an acidic pH about the same number of sodium cations is bound for each salt to the protein surface, we obtain direct evidence of anion specificity. We are aware that this assumption is not rigorous, but nonetheless it is useful to disentangle the effect of anions from that of cations.

Indeed, at an acidic pH, where the protein is positively charged, we observe that the number of bound anions decreases along a Hofmeister series: SCN$^-$ > I$^-$ > NO$_3^-$ > Br$^-$ > Cl$^-$. This agrees with Collins' rule since positive charges are due to chaotropic (Arg, Lys, His) groups which can form a more stable ion pair with the highly chaotropic, SCN$^-$ than with the less chaotropic, Cl$^-$. The same trend is obtained if we consider the polarizability of the ions.[33]

At the isoionic point (pH ~5.3), we still observe an anion specificity; indeed about 14 SCN$^-$ ions and 10 Cl$^-$ ions are bound, respectively. The fact that at the isoionic point there are more bound anions than cations agrees with the higher polarizability of the former with respect to the latter ions. A higher polarizability means a stronger dispersion interaction in addition to the unspecific coulombic force which would be the
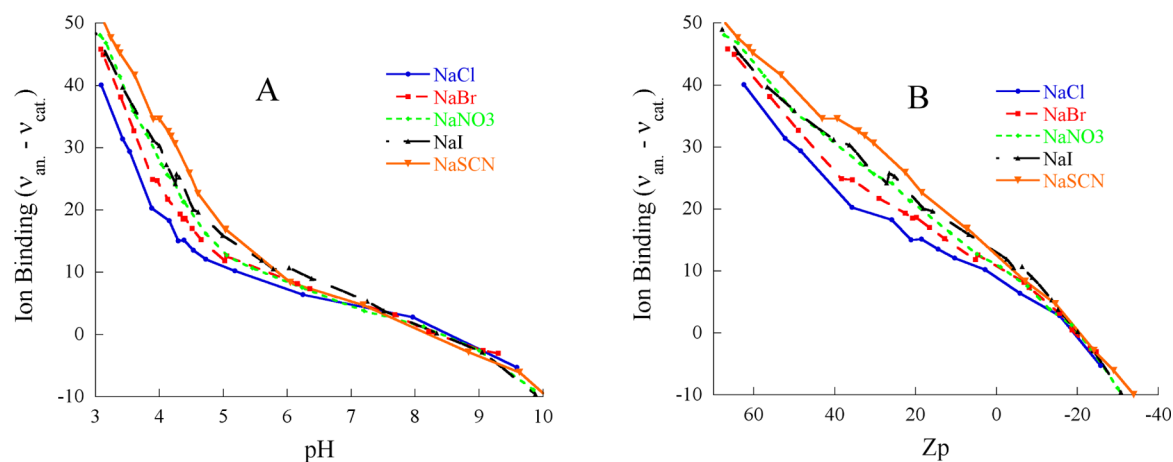
Figure 5. Specific-ion binding vs (A) pH and vs (B) Z_p.

same for both univalent anions and cations with the isoionic protein. At a basic pH, all the curves coincide and ion binding goes to zero at about pH 8.5. This does not mean that there are no bound ions, but that we have the same number of bound anions and cations. Indeed at pH > 8.5, the difference $\nu_{anion} - \nu_{cation}$ becomes negative, meaning that there are more bound cations than anions. In the pH range 7.5−10, where all the curves coincide, we can imagine that anion specificity is always present, but a higher number of bound SCN⁻ (compared with Cl⁻) produce a more negative surface potential which attracts more sodium anions close to the surface. The resulting effect is that the anion specificity, although present in the curves reported in Figures 3 and 4, is lost in the "ion binding" plot.

4. CONCLUSIONS

In conclusion, we have shown that BSA surface charge versus pH curves, obtained through potentiometric titrations, depend on anion-specific effects. The effect is appreciable at a physiological concentration of 0.1 M. Despite the fact that protein titrations were extensively studied by Tanford and co-workers, as well as by many authors before and after him, a study of specific-ion effects has, surprisingly, not been reported previously. But the result is per se not really surprising. Z_p/pH curves are ion specific both below and above the isoionic point according to a Hofmeister series: Cl⁻ < Br⁻ < NO₃⁻ < I⁻ < SCN⁻. At first sight, the ion-specific effects might be more easily rationalized only if the effect of salt concentration is better understood. The effect of different anions, at the same concentration (0.1 M), is to mimic the concentration effect. The more polarizable anions (SCN⁻) behave as do higher concentrations of less polarizable anions (Cl⁻). This explanation, anyway, would need a theoretical confirmation which is outside the scope of the present paper.

The combined use of PT and ELS allowed us to quantify ion binding, as the difference between bound anions and cations, in the range of pH investigated. We found that anions bind to the protein surface at an acidic pH ($Z_p > 0$) according to a Hofmeister series, as well as at the isoionic point ($Z_p = 0$). This appears to be consistent with the higher polarizability of anions compared with that of cations. Indeed, the number of bound cations exceeds that of anions (i.e., $\nu_{anion} - \nu_{cation} < 0$) only at pH > 8.5.

Our results agree with those found by Chen et al., resulting from an investigation of specific-ion effects on the interfacial water structure adjacent to a BSA monolayer at the air/water interface through vibrational sum frequency spectroscopy.[24]

The results, we have arrived at make reasonable sense. It would seem, however, that the complications of specific-ion effects demand a more sophisticated interpretation of ion binding than has been brought to bear previously.

But like the problem of pH, the interpretation of measurements performed depend on electrostatic theories that ignore the very specific effects they are supposed to reveal.[73] This conflation complicates the real situation enormously. It occurs universally. It seems that it can only be resolved once more advanced theories that include specific-ion effects via dispersion forces are incorporated into the basic theory that underlies such measurements.

■ AUTHOR INFORMATION

Corresponding Author
*E-mail: asalis@unica.it. Tel: +39 070 6754362. Fax: +39 070 6754388.

Notes
The authors declare no competing financial interest.

■ REFERENCES

(1) Ninham, B. W.; Lo Nostro, P. *Molecular Forces and Self Assembly: In Colloid, Nano Sciences and Biology*; Cambridge University Press: Cambridge, 2010.

(2) Poiseuille, J. M. L. Sur le mouvement des liquides de nature très différente dans les tubes de très petits diamètres. *Ann. Chim. Phys.* **1847**, *21*, 76−109.

(3) Kunz, W.; Henle, J.; Ninham, B. W. Zur Lehre von der Wirkung der Salze (about the science of the effect of salts): Franz Hofmeister's historical papers. *Curr. Opin. Colloid Interface Sci.* **2004**, *9*, 19−37.

(4) Lo Nostro, P.; Ninham, B. W. Hofmeister phenomena: An update on ion specificity in biology. *Chem. Rev.* **2012**, *112*, 2286−2322.

(5) Robertson, B. T. Contributions to the theory of the mode of action of inorganic salts upon proteins in solution. *J. Biol. Chem.* **1911**, *9*, 303.

(6) Lo Nostro, P.; Fratoni, L.; Ninham, B. W.; Baglioni, P. Water absorbency by wool fibers: Hofmeister effect. *Biomacromolecules* **2002**, *3*, 1217−1224.

(7) Dishon, M.; Zohar, O.; Sivan, U. From repulsion to attraction and back to repulsion: The effect of NaCl, KCl, and CsCl on the force between silica surfaces in aqueous solution. *Langmuir* **2009**, *25*, 2831−2836.

(8) Lo Nostro, P.; Ninham, B. W.; Lo Nostro, A.; Pesavento, G.; Fratoni, L.; Baglioni, P. Specific ion effects on the growth rates of *Staphylococcus aureus* and *Pseudomonas aeruginosa*. *Phys. Biol.* **2005**, *2*, 1−7.

(9) Bilaničová, D.; Salis, A.; Ninham, B. W.; Monduzzi, M. Specific anion effects on enzymatic activity in nonaqueous media. *J. Phys. Chem. B* **2008**, *112*, 12066−12072.

(10) Pinna, M. C.; Bauduin, P.; Tourand, D.; Monduzzi, M.; Ninham, B. W.; Kunz, W. Hofmeister effects in biology: Effect of choline addition on the salt-induced superactivity of HRP and its implication for salt resistance of plants. *J. Phys. Chem. B* **2005**, *109*, 16511−16514.

(11) Pinna, M. C.; Salis, A.; Monduzzi, M.; Ninham, B. W. Hofmeister series: the hydrolytic activity of *Aspergillus niger* lipase depends on specific anion effects. *J. Phys. Chem. B* **2005**, *109*, 5406−5408.

(12) Salis, A.; Bilanicova, D.; Ninham, B. W.; Monduzzi, M. Hofmeister effects in enzymatic activity: Weak and strong electrolyte influences on the activity of *Candida rugosa* lipase. *J. Phys. Chem. B* **2007**, *111*, 1149−1156.

(13) Varhac, R.; Tomásková, N.; Fabián, M.; Sedlák, E. Kinetics of cyanide binding as a probe of local stability/flexibility of cytochrome c. *Biophys. Chem.* **2009**, *144*, 21−26.

(14) Murgia, S.; Portesani, F.; Ninham, B. W.; Monduzzi, M. Interaction of sodium ions with cationic surfactant interfaces. *Chem.— Eur. J.* **2006**, *12*, 7689−7698.

(15) Gokarn, Y. R.; Fesinmeyer, R. M.; Saluja, A.; Razinkov, V.; Chase, S. F.; Laue, T. M.; Brems, D. N. Effective charge measurements reveal selective and preferential accumulation of anions, but not cations, at the protein surface in dilute salt solutions. *Protein Sci.* **2011**, *20*, 580−587.

(16) Salis, A.; Cugia, F.; Parsons, D. F.; Ninham, B. W.; Monduzzi, M. Hofmeister series reversal for lysozyme by change in pH and salt concentration: Insights from electrophoretic mobility measurements. *Phys. Chem. Chem. Phys.* **2012**, *14*, 4343−4346.

(17) Zhang, Y.; Cremer, P. S. The inverse and direct Hofmeister series for lysozyme. *Proc. Natl. Acad. Sci. U.S.A.* **2009**, *106*, 15249−15253.

(18) Lo Nostro, P.; Peruzzi, N.; Severi, M.; Ninham, B. W.; Baglioni, P. Asymmetric partitioning of anions in lysozyme dispersions. *J. Am. Chem. Soc.* **2010**, *132*, 6571−6577.

(19) Lagi, M.; Lo Nostro, P.; Fratini, E.; Ninham, B. W.; Baglioni, P. Insights into Hofmeister mechanisms: Anion and degassing effects on the cloud point of dioctanoylphosphatidylcholine/water systems. *J. Phys. Chem. B* **2007**, *111*, 589−597.

(20) Rossi, S.; Lo Nostro, P.; Lagi, M.; Ninham, B. W.; Baglioni, P. Specific anion effects on the optical rotation of α-amino acids. *J. Phys. Chem. B* **2007**, *111*, 10510−10519.

(21) Medda, L.; Salis, A.; Magner, E. Specific ion effects on the electrochemical properties of cytochrome c. *Phys. Chem. Chem. Phys.* **2012**, *14*, 2875−2883.

(22) Deyerle, B. A.; Zhang, Y. Effects of Hofmeister anions on the aggregation behavior of PEO-PPO-PEO triblock copolymers. *Langmuir* **2011**, *27*, 9203−9210.

(23) Gurau, M. C.; Lim, S.-M.; Castellana, E. T.; Albertorio, F.; Kataoka, S.; Cremer, P. S. On the mechanism of the Hofmeister effect. *J. Am. Chem. Soc.* **2004**, *126*, 10522−10523.

(24) Chen, X.; Flores, S. C.; Lim, S.-M.; Zhang, Y.; Yang, T.; Kherb, J.; Cremer, P. S. Specific anion effects on water structure adjacent to protein monolayers. *Langmuir* **2010**, *26*, 16447−16454.

(25) Kherb, J.; Flores, S. C.; Cremer, P. S. Role of carboxylate side chains in the cation Hofmeister series. *J. Phys. Chem. B* **2012**, *116*, 7389−7397.

(26) Salis, A.; Parsons, D. F.; Bostrom, M.; Medda, L.; Barse, B.; Ninham, B. W.; Monduzzi, M. Ion specific surface charge density of SBA-15 mesoporous silica. *Langmuir* **2010**, *26*, 2484−2490.

(27) Das, M. R.; Borah, J. M.; Kunz, W.; Ninham, B. W.; Mahiuddin, S. Ion specificity of the zeta potential of [alpha]-alumina, and of the adsorption of p-hydroxybenzoate at the [alpha]-alumina-water interface. *J. Colloid Interface Sci.* **2010**, *344*, 482−491.

(28) Salis, A.; Bhattacharyya, M. S.; Monduzzi, M. Specific ion effects on adsorption of lysozyme on functionalized SBA-15 mesoporous silica. *J. Phys. Chem. B* **2010**, *114*, 7996−8001.

(29) Zhang, Y.; Cremer, P. S. Chemistry of Hofmeister anions and osmolytes. *Annu. Rev. Phys. Chem.* **2010**, *61*, 63−83.

(30) Schwierz, N.; Horinek, D.; Netz, R. R. Reversed anionic Hofmeister series: The interplay of surface charge and surface polarity. *Langmuir* **2010**, *26*, 7370−7379.

(31) Kim, H.-K.; Tuite, E.; Nordén, B.; Ninham, B. W. Co-ion dependence of DNA nuclease activity suggests hydrophobic cavitation as a potential source of activation energy. *Eur. Phys. J. E: Soft Matter Biol. Phys.* **2001**, *4*, 411−417.

(32) Boström, M.; Tavares, F. W.; Finet, S.; Skouri-Panet, F.; Tardieu, A.; Ninham, B. W. Why forces between proteins follow different Hofmeister series for pH above and below pI. *Biophys. Chem.* **2005**, *117*, 217−224.

(33) Boström, M.; Parsons, D. F.; Salis, A.; Ninham, B. W.; Monduzzi, M. Possible origin of the inverse and direct Hofmeister series for lysozyme at low and high salt concentrations. *Langmuir* **2011**, *27*, 9504−9511.

(34) Salis, A.; Pinna, M. C.; Bilanicova, D.; Monduzzi, M.; Lo Nostro, P.; Ninham, B. W. Specific anion effects on glass electrode pH measurements of buffer solutions: Bulk and surface phenomena. *J. Phys. Chem. B* **2006**, *110*, 2949−2956.

(35) Flores, S. C.; Kherb, J.; Cremer, P. S. Direct and reverse Hofmeister effects on interfacial water structure. *J. Phys. Chem. C* **2012**, *116*, 14408−14413.

(36) Lund, M.; Jagoda-Cwiklik, B.; Woodward, C. E.; Vacha, R.; Jungwirth, P. Dielectric interpretation of specificity of ion pairing in water. *J. Phys. Chem. Lett.* **2010**, *1*, 300−303.

(37) Lund, M.; Jungwirth, P. Patchy proteins, anions and the Hofmeister series. *J. Phys.: Condens. Matter* **2008**, *20*, 4.

(38) Lund, M.; Vrbka, L.; Jungwirth, P. Specific ion binding to nonpolar surface patches of proteins. *J. Am. Chem. Soc.* **2008**, *130*, 11582−11583.

(39) dos Santos, A. P.; Levin, Y. Ion specificity and the theory of stability of colloidal suspensions. *Phys. Rev. Lett.* **2011**, *106*, 167801.

(40) Calero, C.; Faraudo, J.; Bastos-Gonzalez, D. Interaction of monovalent ions with hydrophobic and hydrophilic colloids: Charge inversion and ionic specificity. *J. Am. Chem. Soc.* **2011**, *133*, 15025−15035.

(41) Levin, Y.; dos Santos, A. P.; Diehl, A. Ions at the air-water interface: An end to a hundred-year-old mystery? *Phys. Rev. Lett.* **2009**, *103*, 257802.

(42) Lima, E. R. A.; Tavares, F. W.; Biscaia, E. C., Jr. Finite volume solution of the modified Poisson−Boltzmann equation for two colloidal particles. *Phys. Chem. Chem. Phys.* **2007**, *9*, 3174−3180.

(43) Tavares, F. W.; Bratko, D.; Blanch, H.; Prausnitz, J. M. Ion-specific effects in the colloid−colloid or protein−protein potential of mean force: Role of salt−macroion van der Waals interactions. *J. Phys. Chem. B* **2004**, *108*, 9228−9235.

(44) Collins, K. D. Ions from the Hofmeister series and osmolytes: Effects on proteins in solution and in the crystallization process. *Methods* **2004**, *34*, 300−311.

(45) Kunz, W. Specific ion effects in colloidal and biological systems. *Curr. Opin. Colloid Interface Sci.* **2010**, *15*, 34−39.

(46) Ninham, B. W.; Yaminsky, V. Ion binding and ion specificity: The Hofmeister effect and Osanger and Lifshits theories. *Langmuir* **1997**, *13*, 2097−2108.

(47) Parsons, D. F.; Bostrom, M.; Lo Nostro, P.; Ninham, B. W. Hofmeister effects: Interplay of hydration, nonelectrostatic potentials, and ion size. *Phys. Chem. Chem. Phys.* **2011**, *13*, 12352−12367.

(48) Ninham, B. W.; Duignan, T. T.; Parsons, D. F. Approaches to hydration, old and new: Insights through Hofmeister effects. *Curr. Opin. Colloid Interface Sci.* **2011**, *16*, 612−617.

(49) Craig, V. S. J. Bubble coalescence and specific-ion effects. *Curr. Opin. Colloid Interface Sci.* **2004**, *9*, 178−184.

(50) Loeb, J. The proteins and colloid chemistry. *Science* **1920**, *LII*, 449−456.

(51) Salis, A.; Cugia, F.; Parsons, D. F.; Ninham, B. W.; Monduzzi, M. Hofmeister Series Reversal for Lysozyme by change in pH and Salt Concentration: Insights from Electrophoretic Mobility Measurements. *Phys. Chem. Chem. Phys.* **2012**, *14*, 4343−4346.

(52) Boström, M.; Craig, V. S. J.; Albion, R.; Williams, D. R. M.; Ninham, B. W. Hofmeister effects in pH measurements: Role of added salt and co-ions. *J. Phys. Chem. B* **2003**, *107*, 2875−2878.

(53) Evens, T. J.; Niedz, R. P. Are Hofmeister Series Relevant to Modern Ion-Specific Effects Research?, 2008; Vol. *2008*.

(54) Buck, R. P.; Rondinini, S.; Covington, A. K.; Baucke, F. G. K.; Brett, C. M. A.; Camoes, M. F.; Milton, M. J. T.; Mussini, T.; Naumann, R.; Pratt, K. W.; Spitzer, P.; Wilson, G. S. Measurement of pH. Definition, standards, and procedures (IUPAC Recommendations 2002). *Pure Appl. Chem.* **2002**, *74*, 2169−2200.

(55) Nylander, T.; Kekicheff, P.; Ninham, B. W. The Effect of solution behavior of insulin on interactions between adsorbed layers of insulin. *J. Colloid Interface Sci.* **1994**, *164*, 136−150.

(56) Haynes, C. A.; Norde, W. Globular proteins at solid/liquid interfaces. *Colloids Surf., B* **1994**, *2*, 517−566.

(57) Finet, S.; Skouri-Panet, F.; Casselyn, M.; Bonneté, F.; Tardieu, A. The Hofmeister effect as seen by SAXS in protein solutions. *Curr. Opin. Colloid Interface Sci.* **2004**, *9*, 112−116.

(58) Kakizuka, A. Protein precipitation: A common etiology in neurodegenerative disorders? *Trends Genet.* **1998**, *14*, 396−402.

(59) Lee, E. B.; Lee, V. M. Y.; Trojanowski, J. Q. Gains or losses: Molecular mechanisms of TDP43-mediated neurodegeneration. *Nat. Rev. Neurosci.* **2012**, *13*, 38−50.

(60) Toth, K.; Sedlak, E.; Sprinzl, M.; Zoldak, G. Flexibility and enzyme activity of NADH oxidase from *Thermus thermophilus* in the presence of monovalent cations of Hofmeister series. *Biochim. Biophys. Acta, Proteins Proteomics* **2008**, *1784*, 789−795.

(61) Tanford, C.; Buzzell, J. G.; Rands, D. G.; Swanson, S. A. The reversible expansion of bovine serum albumin in acid solutions. *J. Am. Chem. Soc.* **1955**, *77*, 6421−6428.

(62) Tanford, C. The Interpretation of Hydrogen Ion Titration Curves of Proteins. In *Advances in Protein Chemistry*; Academic Press: San Diego, 1963; Vol. *17*, pp 69−165.

(63) Tanford, C.; Swanson, S. A.; Shore, W. S. Hydrogen ion equilibria of bovine serum albumin. *J. Am. Chem. Soc.* **1955**, *77*, 6414−6421.

(64) Scatchard, G.; Black, E. S. The Effect of salts on the isoionic and isoelectric points of proteins. *J. Phys. Colloid Chem.* **1949**, *53*, 88−100.

(65) Winzor, D. J.; Jones, S.; Harding, S. E. Determination of protein charge by capillary zone electrophoresis. *Anal. Biochem.* **2004**, *333*, 225−229.

(66) Salis, A.; Boström, M.; Medda, L.; Cugia, F.; Barse, B.; Parsons, D. F.; Ninham, B. W.; Monduzzi, M. Measurements and theoretical interpretation of points of zero charge/potential of BSA protein. *Langmuir* **2011**, *27*, 11597−11604.

(67) Mörnstam, B.; Wahlund, K.-G.; Jönsson, B. Potentiometric acid-base titration of a colloidal solution. *Anal. Chem.* **1997**, *69*, 5037−5044.

(68) Kuehner, D. E.; Engmann, J.; Fergg, F.; Wernick, M.; Blanch, H. W.; Prausnitz, J. M. Lysozyme net charge and ion binding in concentrated aqueous electrolyte solutions. *J. Phys. Chem. B* **1999**, *103*, 1368−1374.

(69) Fraaije, J. G. E. M.; Lyklema, J. Thermodynamics of ion binding by proteins phenomenological linkage relations for binding of electrolyte and interpretation by double layer theory. *Biophys. Chem.* **1991**, *39*, 31−44.

(70) Chen, X.; Yang, T.; Kataoka, S.; Cremer, P. S. Specific ion effects on interfacial water structure near macromolecules. *J. Am. Chem. Soc.* **2007**, *129*, 12272−12279.

(71) Smith, J. D.; Saykally, R. J.; Geissler, P. L. The effects of dissolved halide anions on hydrogen bonding in liquid water. *J. Am. Chem. Soc.* **2007**, *129*, 13847−13856.

(72) Pegram, L. M.; Record, M. T. Hofmeister salt effects on surface tension arise from partitioning of anions and cations between bulk water and the air/water interface. *J. Phys. Chem. B* **2007**, *111*, 5411−5417.

(73) Evans, D. F.; Mitchell, D. J.; Ninham, B. W. Ion binding and dressed micelles. *J. Phys. Chem.* **1984**, *88*, 6344−6348.

PAPER III

Langmuir

Article

Ion Specific Surface Charge Density of SBA-15 Mesoporous Silica

Andrea Salis,*,[†] Drew F. Parsons,[‡] Mathias Boström,[†,§] Luca Medda,[†] Brajesh Barse,[†,‖]
Barry W. Ninham,[‡] and Maura Monduzzi*,[†]

[†]*Department of Chemical Sciences, University of Cagliari-CNBS and CSGI, Cittadella Universitaria, S.S. 554
Bivio Sestu, 09042 Monserrato, Italy,* [‡]*Research School of Physical Sciences and Engineering, Australian
National University, Canberra (CA), 0200 Australia,* [§]*Division of Theory and Modeling, Department of Physics,
Chemistry and Biology, Linköping University, SE-581 83 Linköping, Sweden, and* [‖]*Department of
Pharmaceutical Technology* (*Biotechnology*), *National Institue of Pharmaceutical Education and Research*
(*NIPER*), *SAS Nagar, Punjab 160062, India*

Potentiometric titrations were used to estimate the surface charge density of SBA-15 mesoporous silica in different salt solutions. It was found that surface charge depends both on cation type, following a Hofmeister series (Cs^+ < Guanidinium$^+$ < K^+ < Na^+ < Li^+), and on salt concentration (in the range 0.05−1 M). The surface charge series is reproduced by theoretical calculations performed using a modified Poisson−Boltzmann equation that includes ionic dispersion forces with *ab initio* ion polarizabilities and hydrated ions. The hydration model assigns an explicit hydration shell to kosmotropic (strong hydrated) ions only. The Hofmeister series appears to be due to the combination of ion-surface dispersion interactions and ion hydration.

1. Introduction

Apparent surface charge and electrostatic double layer interactions at solid−liquid and liquid−liquid interfaces are ion specific.[1−9] Such effects, Hofmeister phenomena,[10] reflecting both co- and counterion specificity, are universal. They occur in situations as diverse as bacterial growth,[11] enzymatic activity,[12−14] pH of buffer solutions,[6] self-assembly of surfactants,[7−9] interfacial tensions,[15] hydrophobic chromatography,[16] binding with protein surface charges,[17] and water retention in wool fibers.[18]

Typical Hofmeister effects, such as the dependence of surface charge on the specific background salt solution, are not accounted for by classical theories of colloid chemistry. It has been shown[4] that a major source for this failure of theory is due to the omission of dispersion (nonelectrostatic (NES)) forces that act between ions, between ions and water molecules, and/or between an ion and a surface.[1−4] These forces are not included in standard theories. They are coupled to and can be larger than electrostatic effects.

One source for the origin of Hofmeister effects is now established to be due to ion polarizabilities and quantum mechanical forces that originate from these polarizabilities. Ion polarizabilities as a function of imaginary frequency have been recently calculated by *ab initio* quantum chemistry by Parsons and Ninham.[19]

Previous studies[20] used a single-mode model of the polarizability ($\alpha(i\omega)$) with characteristic frequency estimated from the ionization potential of the ion. It turns out that the single mode approximation is too crude, falling to zero at too low frequency and omitting the crucial contribution due to high frequencies at far UV, and thereby severely underestimates the nonelectrostatic potential acting between different ions and surfaces.

In the present work, a comparison is made between the experimental and theoretical surface charge density (σ) of mesoporous silica. Experimental σ values were obtained through potentiometric titration measurements, while theoretical σ were calculated via a modified Poisson−Boltzmann equation where dispersion potentials were estimated from quantum chemical *ab initio* calculations of ionic polarizabilities.

The mesoporous silica sample used for potentiometric titrations is called SBA-15.[21] It is an ordered mesoporous structure

*Corresponding author. E-mail: asalis@unica.it (A.S.); monduzzi@unica.it (M.M.).

(1) Boström, M.; Lima, E. R. A.; Tavares, F. W.; Ninham, B. W. *J. Chem. Phys.* **2008**, *128*, 135104.
(2) Boström, M.; Deniz, V.; Ninham, B. W.; Franks, G. *Adv. Colloid Interface Sci.* **2006**, *5*, 123.
(3) Boström, M.; Williams, D. R. M.; Ninham, B. W. *Phys. Rev. Lett.* **2001**, *87*, 168103.
(4) Ninham, B. W.; Yaminsky, V. *Langmuir* **1997**, *13*, 2097.
(5) Salis, A.; Monduzzi, M.; Ninham, B. W. Hofmeister Effects in Enzymatic Activity, Colloid Stability and pH Measurements: Ion-Dependent Specificity of Intermolecular Forces. In *Nanoparticles and Nanodevices in Biological Applications*; Bellucci, S., Ed.; Springer-Verlag: Berlin, Heidelberg, 2009; p 159.
(6) Salis, A.; Pinna, M. C.; Bilanicova, D.; Monduzzi, M.; Lo Nostro, P.; Ninham, B. W. *J. Phys. Chem. B* **2006**, *110*, 2949.
(7) Murgia, S.; Monduzzi, M.; Ninham, B. W. *Curr. Opin. Colloid Interface Sci.* **2004**, *9*, 102.
(8) Murgia, S.; Portesani, F.; Ninham, B. W.; Monduzzi, M. *Chem.—Eur. J.* **2006**, *12*, 7689.
(9) Caboi, F.; Chittofrati, A.; Lazzari, P.; Monduzzi, M. *Colloids Surf., A* **1999**, *160*, 47.
(10) Kunz, W.; Lo Nostro, P.; Ninham, B. W. *Curr. Opin. Colloid Interface Sci.* **2004**, *9*, 1.
(11) Lo Nostro, P.; Ninham, B. W.; Lo Nostro, A.; Pesavento, G.; Fratoni, L.; Baglioni, P. *Phys. Biol.* **2005**, *2*, 1.
(12) Pinna, M. C.; Salis, A.; Monduzzi, M.; Ninham, B. W. *J. Phys. Chem. B* **2005**, *109*, 5406.
(13) Salis, A.; Bilanicova, D.; Ninham, B. W.; Monduzzi, M. *J. Phys. Chem. B* **2007**, *111*, 1149.
(14) Bilanicova, D.; Salis, A.; Ninham, B. W.; Monduzzi, M. *J. Phys. Chem. B* **2008**, *112*, 12066.
(15) Boström, M.; Kunz, W.; Ninham, B. W. *Langmuir* **2005**, *21*, 2619.
(16) Collins, K. D. *Proc. Natl. Acad. Sci. U.S.A.* **1995**, *92*, 5553.
(17) Hess, B.; van der Vegt, N. F. A. *Proc. Natl. Acad. Sci. U.S.A.* **2009**, *106*, 13296.
(18) Lo Nostro, P.; Fratoni, L.; Ninham, B. W.; Baglioni, P. *Biomacromolecules* **2002**, *3*, 1217.

(19) Parsons, D. F.; Ninham, B. W. *Langmuir* **2009**, in press; DOI: 10.1021/la902533x.
(20) Tavares, F. W.; Bratko, D.; Blanch, H.; Prausnitz, J. M. *J. Phys. Chem. B* **2004**, *108*, 922.
(21) Zhao, D.; Feng, J.; Huo, Q.; Melosh, N.; Fredrickson, G. H.; Chmelka, B. F.; Stucky, G. D. *Science* **1998**, *279*, 548.

constituted by cylindrical channels organized in a hexagonal array that has a very high surface area (up to 1000 m²/g). It has a monomodal pore size distribution usually in the range 6−10 nm. Since its discovery, SBA-15 has been used for several applications such as catalysis and drug delivery.[22] Because its pore size is comparable to that of most proteins, SBA-15 can be used as a protein adsorbent. If the adsorbing protein is an enzyme, an immobilized biocatalyst is obtained.[23−26] It has been found that ionic strength affects the amount of protein that can be adsorbed by mesoporous silica.[27] That ion type can also be important in affecting protein adsorption is a matter not studied yet.

Here we show that the surface charge density of SBA-15 does indeed depend on specific ion effects. This is interesting. It suggests that other porous media with characteristics similar to those of SBA-15 might also depend on specific ion effects. This would be of some importance in understanding and exploiting the properties of such materials as adsorbents for drugs, proteins, or other macromolecules.

2. Materials and Methods

2.1. Experimental Methods. *Chemicals.* Tetraethoxysilane (TEOS, 98%) and Pluronic copolymer 123 ($EO_{20}PO_{70}EO_{20}$) were purchased from Aldrich. Salts, sodium chloride (>98%) sodium thiocyanate (98%), cesium chloride (> 98%), and guanidinium hydrochloride (99%); lithium chloride (98%); potassium chloride (> 98%) were from Sigma-Aldrich (Milan, Italy). Buffers (pH 1, 4, 7, 9, 10) were from Hanna Instruments (Szeged, Hungary). Salt solutions were prepared by using distilled water purified through a Millipore system (Simplicity 185) and with conductivity < 0.054 mS/cm.

Synthesis and Characterization of SBA-15 Mesoporous Silica. SBA-15 samples were prepared by dissolving 4 g of Pluronic copolymer 123 in 20 mL of 37 wt % HCl and 120 mL of distilled water. The resulting mixture was stirred at 35 °C for 16 h. Then 8.5 g of TEOS was added, and the final solution was stirred at this temperature for 24 h. Finally, the mixture was aged into a Teflon-lined autoclave at 100 °C for 24 h. After filtration and washing, the solid was dried at 40 °C and then calcined at 550 °C for 5 h.

X-ray scattering patterns were recorded with a S3-MICRO SWAXS camera system (HECUS X-ray Systems, Graz, Austria). Cu Kα radiation of wavelength 1.542 Å was provided by a GeniX X-ray generator, operating at 50 kV and 1 mA. A 1D-PSD-50 M system (HECUS X-ray Systems, Graz, Austria) containing 1024 channels of width 54.0 µm was used for detection of scattered X-rays in the small-angle region. The working q-range was 3 × 10^{-3} Å^{-1} ≤ q ≤ 0.6 Å^{-1}, where $q = 4\pi \sin(\theta)\lambda^{-1}$ is the modulus of the scattering wave vector. Calibration in the small-angle region was performed with a silver stearate standard. The distance between the sample and detector was 285 mm. The scattering patterns were recorded at 25 °C. A few milligrams of sample were put in a 2 mm (diameter) quartz capillary and inserted in a rotating sample holder. To minimize scattering from air, the camera volume was kept under vacuum during the measurements. Scattering patterns were recorded for 1000 s.

Textural analysis was carried out on a Thermoquest-Sorptomatic 1990 instrument, by determining the N₂ adsorption/desorption isotherms at 77 K. Before analysis, pure silica samples were heated up to 250 °C at a rate of 1 °C/min under vacuum. The specific surface area, the total pore volume, and the pore size distribution were assessed by the Brunauer−Emmett−Teller (BET)[28] and the Barret−Joyner−Halenda (BJH) methods,[29] respectively.

Determination of Surface Charge of SBA-15. Potentiometric titrations were performed using an automatic titrator, Titrando 836 from Metrohm (Herizau, Switzerland), connected to a PC (software: Tiamo 1.3). The pH electrode was standardized by buffers (pH = 1, 4, 7, 9, 10). An amount of 0.04 g of SBA-15 (dried overnight at 105 °C) was suspended in 20 mL of a HCl (0.01 M) and salt solution (LiCl, NaCl, KCl, CsCl, guanidiniumHCl) of a given ionic strength (0.05, 0.5, and 1 M). The suspension was first equilibrated for 15 h and then titrated with 0.1 M NaOH solution in a thermostated (T = 25 °C) double-walled water-jacketed vessel. The pH was recorded after each addition of titrant as a function of its volume. Blank titrations were carried out on a solution (20 mL) having the same composition of the sample (HCl 0.01 M) but without the SBA-15 in suspension. The rate at which the titrant is added to the suspension is an important parameter for acid−base titration experiments. Consequently, in order to minimize the effect of SBA-15 equilibration, the minimal delay separating two consecutive additions of titrant was 180 s with a maximal signal drift of 2 mV/min (measured during a time of 320 s).

The surface charge density (σ) of a material is calculated for each pH value using the potentiometric titration data according to the following equation:[30]

$$\sigma_{pH} = \frac{F\Delta n_{pH}}{S_{BET}m} \tag{1}$$

where σ_{pH} is the surface charge density (C/m²) at a given pH value, F is the Faraday constant (96 487 C/mol), S_{BET} is the surface area determined through the BET method, and m is the mass of the SBA-15 sample (g). Δn_{pH} is the difference between the moles of titrant used for the titration of the blank and those used for the titration of the SBA-15 sample at a same value of pH and is calculated according to the following equation:

$$\Delta n_{pH} = |V_b - V_s|_{pH} C_{OH^-} \tag{2}$$

where C_{OH^-} is the concentration of the titrant (NaOH) solution, V_b is the volume of titrant used to reach the desired pH in the blank, and V_s is the volume of titrant used to reach the desired pH in the sample.

2.2. Computational Methods. *Modified Poisson−Boltzmann Analysis for a Planar SBA-15-like Surface.* The theoretical surface charge is obtained from a Poisson−Boltzmann analysis, modified to include ionic dispersion interactions. The self-consistent electrostatic potential near a planar silica surface is found by solving the modified Poisson−Boltzmann equation,[2]

$$\frac{d^2\varphi}{dx^2} = -\frac{e}{\varepsilon_0 \varepsilon_w(0)} \sum_i z_i c_i(x) \tag{3a}$$

$$c_i(x) = c_{i,0} \exp[-(z_i e\varphi(x)) + U_i(x))/kT] \tag{3b}$$

where $c_{i,0}$, z_i, and $\varphi(x)$ denote, respectively, the bulk concentrations (of cations, anions, and hydronium ions), the valency of ionic species i, and the electrostatic self-consistent potential. $U_i(x)$ is the nonelectrostatic ion-surface dispersion interaction plus the hard sphere repulsion which is infinite when the ions are less than a distance of one hard sphere radius from the surface. The NES

(22) Hoffmann, F.; Cornelius, M.; Morell, J.; Fröba, M. *Angew. Chem., Int. Ed.* **2006**, *45*, 3216.

(23) Hartmann, M. *Chem. Mater.* **2005**, *17*, 4577.

(24) Salis, A.; Meloni, D.; Ligas, S.; Casula, M. F.; Monduzzi, M.; Solinas, V.; Dumitriu, E. *Langmuir* **2005**, *21*, 5511.

(25) Salis, A.; Bhattacharyya, M. S.; Monduzzi, M.; Solinas, V. *J. Mol. Catal. B: Enzym.* **2009**, *57*, 262.

(26) Salis, A.; Pisano, M.; Monduzzi, M.; Solinas, V.; Sanjust, E. *J. Mol. Catal. B: Enzym.* **2009**, *58*, 175.

(27) Essa, H.; Magner, E.; Cooney, J.; Hodnett, B. K. *J. Mol. Catal. B: Enzym.* **2007**, *49*, 61.

(28) Brumaner, S.; Emmet, P. H.; Teller, E. *J. Am. Chem. Soc.* **1938**, *60*, 309.

(29) Barret, E. P.; Joyner, L. G.; Halenda, P. P. *J. Am. Chem. Soc.* **1951**, *73*, 373.

(30) Gun'ko, V. M.; Seledets, O.; Skubiszewska-Zieba, J.; Zarko, V. I.; Leboda, R.; Janusz, W.; Chibowski, S. *Microporous Mesoporous Mater.* **2005**, *87*, 133.

Table 1. Theoretical Dispersion B Coefficients and Ion Radii a[a]

ion	ion radius (Å)	hard sphere ion radius (Å)	intrinsic α_1 (Å^3)	excess α_1^* (Å^3) (in water)	B (10^{-50} J m^3)
H_3O^+	0.97	1.07	0.963	0.205	−0.79
unhydrated Li^+	0.38	0.42	0.0285	0.000421	−0.041
hydrated Li^+	2.18	2.40	7.155	0.950	−4.32
unhydrated Na^+	0.61	0.67	0.139	0.0139	−0.18
hydrated Na^+	1.64	1.81	4.415	0.918	−3.01
K^+	0.96	1.06	0.814	0.159	−0.73
Cl^-	1.69	1.86	4.859	1.011	−1.70

[a] For reference, ionic polarizabilities are also given (at the lowest optical, that is, the first nonzero, frequency, $\omega_1 = 3.9 \times 10^{13}$ Hz, used in the calculation of B). B has been summed over all frequencies; see eq 8.
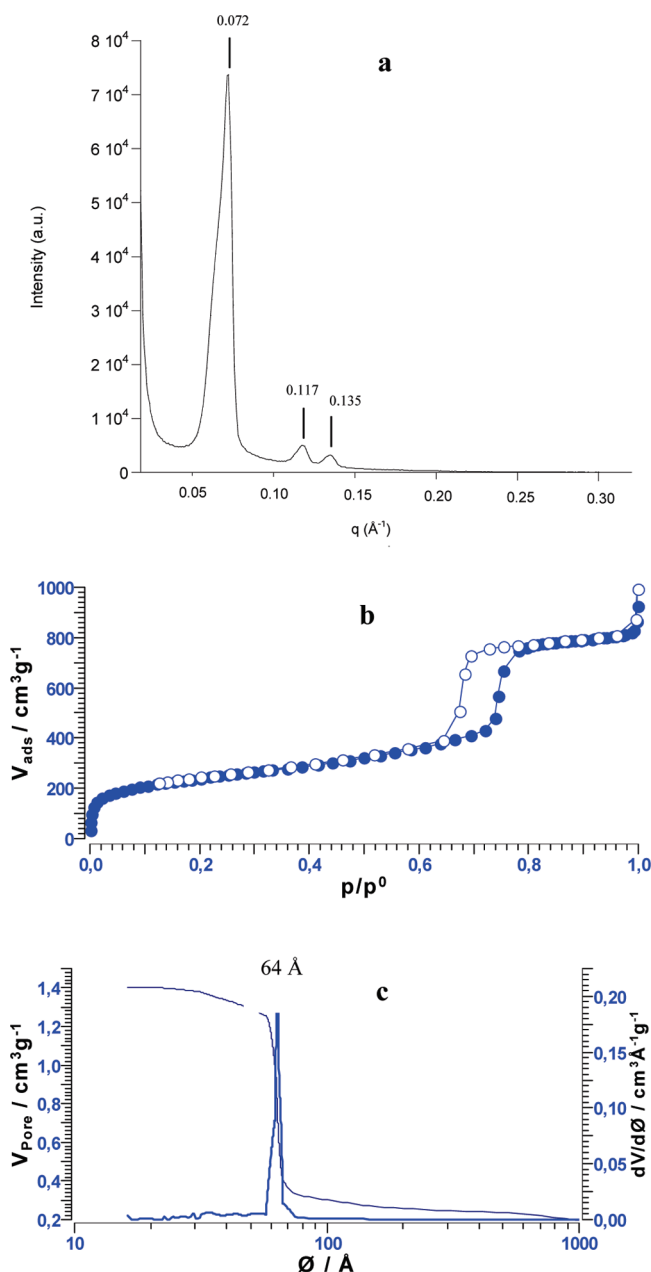
Figure 1. Characterization of SBA-15 mesoporous silica: (a) SAXS pattern, (b) N$_2$ adsorption/desorption isotherm, and (c) pore size distribution calculated by the desorption branch through the BJH method.[29]

potential is explained in more detail below. This equation can be solved numerically using appropriate boundary conditions. The first boundary condition is that the electric field goes to zero far

Table 2. Characterization Data of SBA-15 Mesoporous Silica Obtained by SAXS Analysis and N$_2$ Adsorption/Desorption Isotherms

sample	S_{BET} (m^2/g)	V_{BJH} (cm^3/g)	d_{BJH} (Å)	lattice spacing (Å)	phase
SBA-15	840	1.4	64	117.9	hexagonal

from the interface. We use a charge regulated boundary condition for the surface charge density,[2]

$$\frac{d\phi}{dx}\Big|_{x=0} = \frac{-\sigma_0}{\varepsilon_0\,\varepsilon_2(0)} \tag{4a}$$

$$\sigma_0 = eN_s \frac{[H_s^+]10^{pK_{a1}} - [H_s^+]^{-1}10^{-pK_{a2}}}{1 + [H_s^+]10^{pK_{a1}} + [H_s^+]^{-1}10^{-pK_{a2}}} \tag{4b}$$

$$[H_s^+] = 10^{-pH}\exp[-(e\phi(0) + U_{H_3O^+}(0))/kT] \tag{4c}$$

We take $pK_{a1} = 1.34$ and $pK_{a2} = 4.6$ from the literature, and the unknown site density ($N_s = 0.95$ sites/nm^2) of SBA-15 was fitted to the experimental surface charge density in the presence of 0.05 M LiCl.

Ion-Surface Dispersion Potential Plus an Ion-Surface Hard Sphere Potential. These potentials acting on each ion near the surface in a mesopore are[3]

$$U_i(x) = U_{disp}(x) + U_{HS}(x) \tag{5}$$

where

$$U_{HS}(x) = \begin{cases} \infty, & x < a_{HS} \\ 0, & x \geq a_{HS} \end{cases} \tag{6}$$

and

$$U_{disp}(x) = \frac{B_i f(x)}{x^3} \tag{7a}$$

taking

$$f(x) = 1 + \frac{2x}{\sqrt{\pi}a}\left[\frac{2x^2}{a^2} - 1\right]\exp\left(\frac{-x^2}{a^2}\right) - \left[1 + \frac{4x^4}{a^4}\right]\mathrm{erfc}\left(\frac{x}{a}\right) \tag{7b}$$

a is a Gaussian radius, describing the electron cloud of the ion as a Gaussian sphere,[31] and a_{HS} is the equivalent hard sphere radius.[31] At large distances (more than several ion radii), $f(x) = 1$, while as the ion approaches the surface at $x = 0$, $f(x)/x^3$ reaches a constant finite value, $16/(3\sqrt{\pi}a^3)$.[31] Dispersion B coefficients were calculated

(31) Mahanty, J.; Ninham, B. W. *Faraday Discuss. Chem. Soc.* **1975**, *59*, 13.
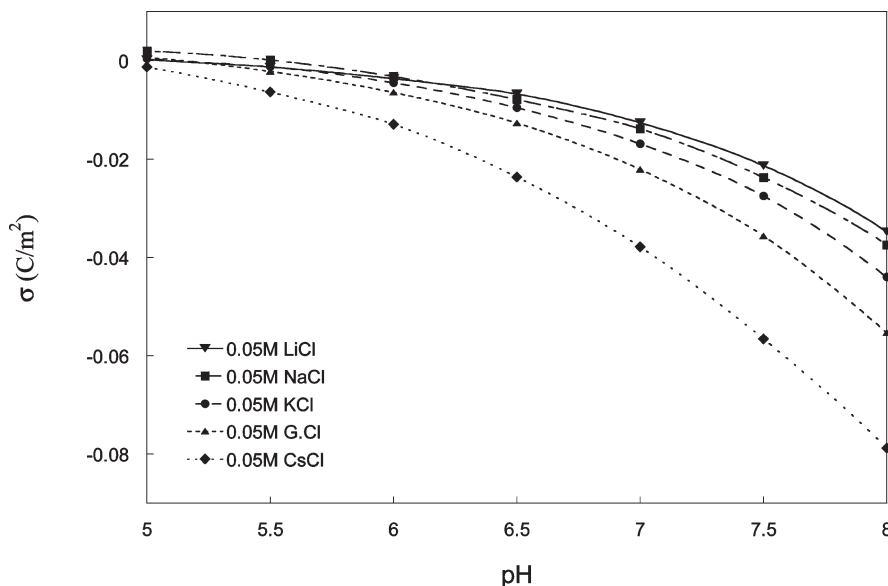
Figure 2. Cation specific effects on experimental surface charge density versus pH of a SBA-15 mesoporous silica sample (salt concentration = 0.05 M; $T = 25$ °C).
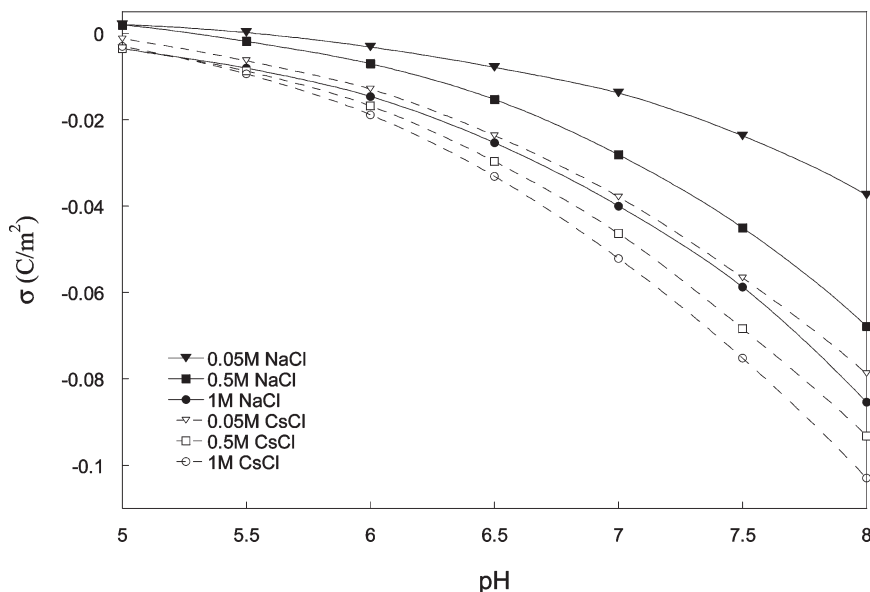
Figure 3. Experimental surface charge density versus pH of a SBA-15 mesoporous silica sample in different salt solutions ($T = 25$ °C).

at $T = 25$ °C by summing over temperature-dependent imaginary frequencies $\omega_n = 2\pi kTn/\hbar$,

$$B_i = \frac{kT}{4} \sum_{n=0}^{\infty} (2 - \delta_{0,n}) \frac{\alpha_i^*(i\omega_n)}{\varepsilon_w(i\omega_n)} \left(\frac{\varepsilon_w(i\omega_n) - \varepsilon_c(i\omega_n)}{\varepsilon_w(i\omega_n) + \varepsilon_c(i\omega_n)} \right) \quad (8)$$

where $\varepsilon_w(i\omega)$ and $\varepsilon_c(i\omega)$ are the dielectric permittivity spectra for water[31] and silica,[32] respectively. α_i^* in eq 8 refers to the excess polarizability of the cation or anion, after subtracting out the depolarization response of the solvent surrounding the ion from the intrinsic *ab initio* polarizability of the ions.[32]

Excess polarizabilities describe the difference between the polarization response of water and the intrinsic polarizability of the ion. The intrinsic polarizabilities of the ions and the neutral water

molecule (in vacuum) were calculated by *ab initio* quantum chemical methods using Molpro.[33] Electron correlation provides a substantial contribution to electronic polarizabilities and was included by calculating under the couple-cluster singles and doubles (CCSD) level of theory.[34] The aug-cc-pV5Z basis set[35,36] was used for all atoms, with $x = Q$ (Li, Na), $x = 5$ (H_2O, H_3O^+), or $x = 6$ (Cl), except potassium, for which the ECP10MDF basis set[37] with pseudopotentials was used.

The ionic dispersion B coefficients for lithium, sodium, potassium, and chloride are given in Table 1, together with their Gaussian radii (a).[38] We have omitted CsCl from calculations, since the analysis of the quantum dispersion forces of Cs^+ is

(32) Netz, R. R. *Curr. Opin. Colloid Interface Sci.* **2004**, *9*, 192.
(33) Werner, H.-J. e. a. *MOLPRO, a package of ab initio programs*, version 2008.1; **2008**; see http://www.molpro.net.

(34) Hampel, C.; Peterson, K. A.; Werner, H.-J. *Chem. Phys. Lett.* **1992**, *190*, 1.
(35) Woon, D. E.; Thom, H.; Dunning, J. *J. Chem. Phys.* **1993**, *98*, 1358–1371.
(36) Peterson, K. A.; Thom, H.; Dunning, J. *J. Chem. Phys.* **2002**, *117*, 10548–10560.
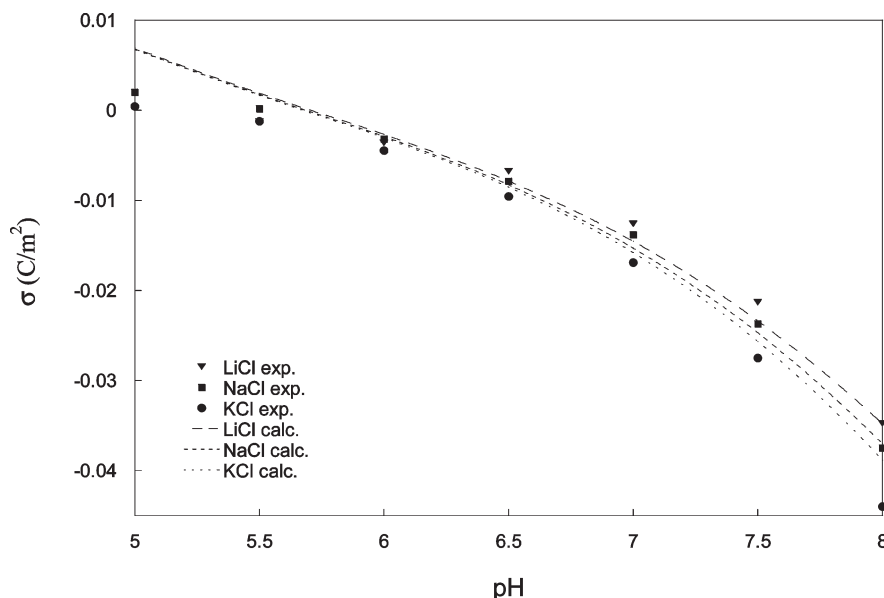(37) Lim, I. S.; Schwerdtfeger, P.; Metz, B.; Stoll, H. *J. Chem. Phys.* **2005**, *122*, 104103.
(38) Parsons, D. F.; Ninham, B. W. *J. Phys. Chem. A* **2009**, *113*, 1141.

Figure 4. Comparison between experimental and theoretically deduced surface charge density versus pH of a silica surface with a bulk salt concentration of 0.05 M. Kosmotropic ions (Li$^+$, Na$^+$) are hydrated, whereas chaotropic K$^+$ is unhydrated.

complicated by the presence of *f*-orbitals,[39] which are not accounted for in the model used to derive $U_i(x)$. We also omit guanidinium, since *ab initio* polarizability data for this ion is not yet available.

To give an indication of the relationship between ion polarizabilities and the *B* coefficients, we have listed single frequency polarizabilities α_1 in Table 1, giving both the intrinsic ion polarizability and the excess polarizability in water. These polarizabilities correspond to the static polarizability, but are given for the lowest nonzero frequency in the sum of eq 6, $\omega_1 = 3.9 \times 10^{13}$ Hz, rather than zero frequency, in order to avoid misrepresenting the relationship between polarizability and dispersion coefficient. The dynamic polarizability decreases smoothly from α_1 down to 0 at very high frequencies, such that the relative magnitudes of the *B* values tend to match the magnitudes of α_1. The true static (zero frequency) excess polarizabilities α_0^*, on the other hand, tend to jump sharply away from the value of α_1 because of the sharp jump in the dielectric function of water at zero frequency ($\varepsilon_w = 78.36$ at zero frequency, but only 1.99 at ω_1). Hence, α_1^* is a more representative indicator of the magnitude of *B* than α_0^*. Thus, we observe as a general rule that *B* values are large where α_1 values are large, but the correlation is not exact, as seen when α_1 values are close (e.g., Cl$^-$ and hydrated Li$^+$ and Na$^+$). That is, the single frequency α_1 values do not give a complete prediction of *B* values. Each frequency contribution to *B* in eq 8 may be positive or negative depending on the relationship between the dielectric functions of the surface and solvent at each frequency (similarly for the excess polarizability itself[34]). In other words, the surface dispersion *B* coefficient truly is a dynamic quantity depending on the behavior of the ion, surface, and solvent at all frequencies, as indicated in eq 8. It cannot be fully reduced to the ion polarizability at any one given frequency, except for the purpose of indicating general relative magnitudes. The *B* coefficients shown in Table 1 have been calculated by summation over all frequencies (up to $n = 2100$, corresponding to soft X-rays at 8×10^{16} Hz), following eq 8.

The kosmotropic (strongly hydrated) ions Li$^+$ and Na$^+$ are treated as hydrated while the remaining chaotropic (weakly hydrated) ions are treated as unhydrated, in line with Collins' concept of matching water affinity.[40] The hydrated ions have their

ion radius increased by the width of the hydration shell, and their ion polarizability is enhanced by adding the *ab initio* polarizability of the hydration water molecules. The hydration number and width of the hydration shell are taken from Marcus,[41] with the hydration numbers of Li$^+$ and Na$^+$ being 5 and 3, respectively. The hydration of kosmotropic ions has been demonstrated to be crucial, for instance, in obtaining correct Hofmeister series for the activity coefficients[39] and osmotic coefficients[42] of ions in solution.

3. Results and Discussion

3.1. Experimental Results. A sample of SBA-15 was synthesized and characterized as described in the previous section. Results are reported in Figure 1 and Table 2. Small angle X-ray scattering (SAXS) analysis of the SBA-15 sample gave the typical pattern of a hexagonal phase (Figure 1a) with lattice spacing of 117.9 Å (Table 2).

Lattice spacing is the sum of pore diameter and wall thickness. The pore diameter was obtained by the desorption branch of the N$_2$ isotherm (Figure 1b and c), with the maximum of the monomodal pore size distribution being around 64 Å.

The surface area (S_{BET}) determined by the BET method was 840 m^2/g, and the total pore volume was 1.4 cm^3/g. S_{BET} is a key parameter used for the calculation of surface charge density according to eq 1.

The surface charge density of SBA-15 was determined through potentiometric titration according to the procedure reported in the previous section. The aqueous suspensions containing the SBA-15 sample powder in the presence of the different chlorides were titrated with a NaOH standard solution. Potential (pH) was measured through a glass electrode. As we reported in a previous work, pH measurements through a glass electrode are affected by salt type and concentration.[10] Here such ion specific effects are counterbalanced through the difference reported in eq 2, that is, the results of the titration of both the solid suspension and the blank. Thus, Δn_{pH} is not affected by deviations due to different ion specific adsorption at the glass electrode.
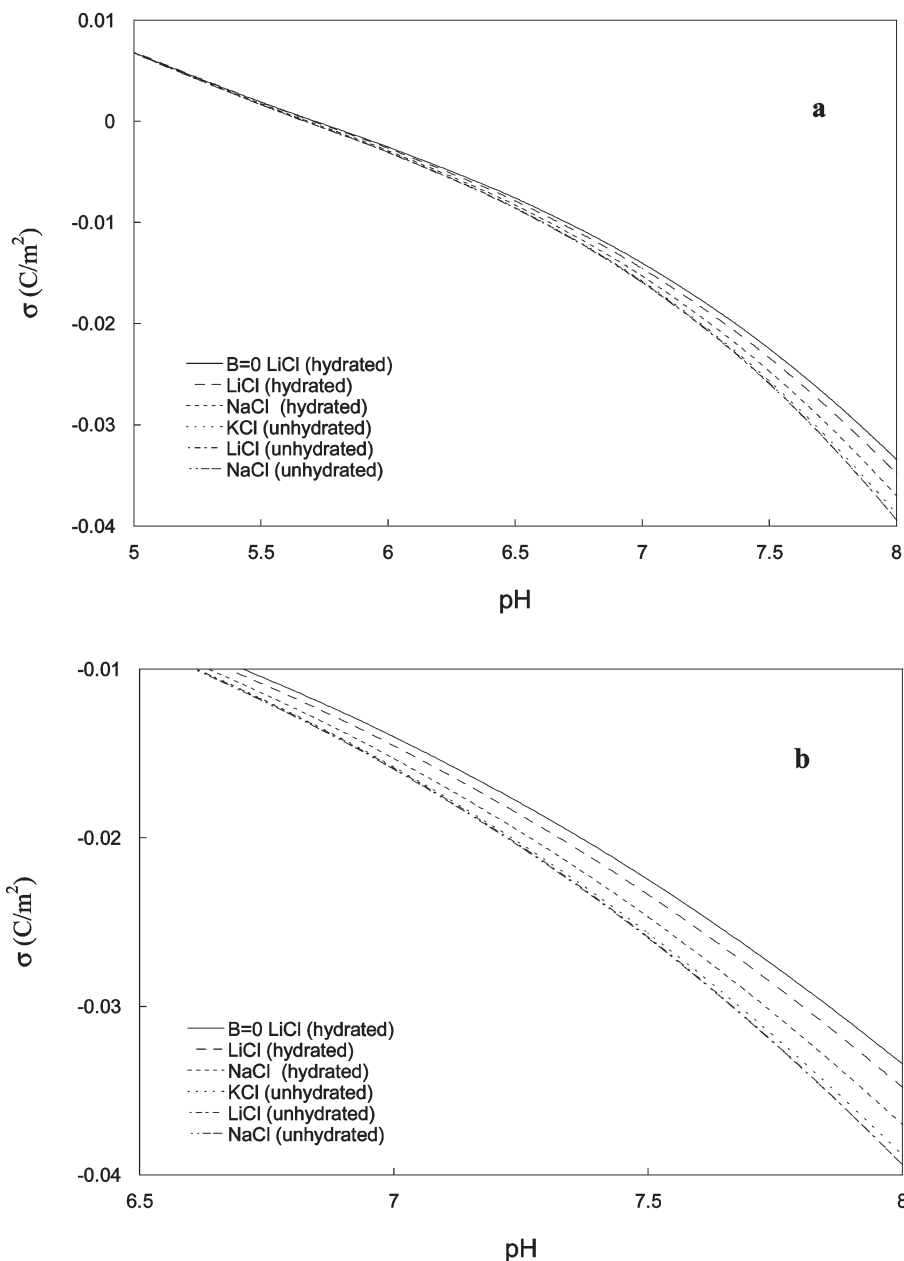
Figure 2 shows the effect of cations on surface charge density of SBA-15 mesoporous silica as a function of pH. It was found that

(39) Parsons, D. F.; Deniz, V.; Ninham, B. W. *Colloids Surf., A* **2009**, *343*, 57.
(40) Collins, K. *Biophys. Chem.* **2006**, *119*, 271.
(41) Marcus, Y. *Pure Appl. Chem.* **1987**, *59*, 1093.
(42) Parsons, D. F.; Vrbka, L. Personal communication.

Figure 5. (a) Theoretical surface charge density versus pH, comparing hydrated against unhydrated kosmotropic cations (Li$^+$, Na$^+$). Surface charge density is for a silica surface; bulk chloride concentration is 0.05 M. Chaotropic KCl is also shown. (b) Expansion of (a).

surface charge density σ depends on cation type following a Hofmeister series Cs$^+$ < G (guanidinium$^+$) < K$^+$ < Na$^+$ < Li$^+$ at a salt concentration equal to 0.05 M.

Figure 3 shows the effect of salt concentration on the surface charge density of the SBA-15 sample as a function of pH. In particular, we investigated the effect of increasing the concentration of Na$^+$ and Cs$^+$ up to 1 M. At pH 5, the curves are very close each other, whereas as pH increases σ becomes negative but to a different extent depending on salt type and concentration. In particular, for a given pH value, the higher the salt concentration, the more negative the value of σ for the SBA-15 mesoporous silica. CsCl and KCl give rise to more negative σ compared with the same concentration of NaCl. Moreover, the distance between different curves, obtained with the same salt, decreases as concentration increases. We performed the experiments for the highly negatively charged silica surfaces using different co-ions (NaSCN and NaCl) and got virtually the same result. As opposed to what is

more usually observed in other systems,[6,12,13] in this case, anions do not appear to show a marked effect.

3.2. Theoretical Results. The experimental charge of the mesoporous silica surface depends on ion specific interactions between salt ions and surfaces as well as those acting on the hydronium and hydroxide ions.

The existence of theoretical Hofmeister series appears to be mainly due to the nonelectrostatic (NES) potentials. There is also an additional effect of hard sphere repulsion when the ions are one hard sphere radius from the surface or less. Without these two effects, all cations show the same behavior (producing identical σ versus pH curves). The question arises if one should use hydrated or unhydrated NES potentials, and hydrated or unhydrated ion radii. It turns out that for the surface charge density considered in the present work hydration of Li$^+$ and Na$^+$ ions must be included to obtain the correct Hofmeister series. Some further insights can be gained by considering the experimental pressure between two

silica surfaces in different salt solutions. Dishon et al.[43] recently used atomic force microscopy measurements to demonstrate that the force between two silica surfaces is ion specific. Preliminary calculations (unpublished data) have clearly demonstrated that hydration should be included to get the correct Hofmeister series for pressures between two silica surfaces in salt solutions. So we henceforth take the ions that are hydrated in bulk solution to remain hydrated near the silica surface.

The surface charges were calculated using eqs 4b and 4c where the results of the ion dispersion potential (eqs 7a and 8) were introduced. The ion dispersion potentials, in turn, were obtained using the surface dispersion B coefficients reported in Table 1.

The charge density curves with hydrated kosmotropes are shown in Figure 4. The agreement between experimental and theoretical is good in the pH range 6−8. Magnitudes also match reasonably well, even though experimental curves display a higher degree of ion specificity. Ions with smaller size and therefore larger surface NES potentials, $U_i(0) = 16B_i/(3\sqrt{\pi}a^3)$, interact stronger with the silica surface. K^+ accumulates at higher concentrations near the silica surface than the hydrated Li^+ ion. This gives rise to less H_3O^+ ions near the surface with K^+ ions present in the system and thus to a more negatively charged surface.

The correct series $K^+ < Na^+ < Li^+$, seen in Figure 4, was obtained by hydrating the kosmotropic ions Na^+ and Li^+. It is worth exploring the significance of ion hydration more closely. In Figure 5, we show calculated surface charge densities by comparing curves made for chlorides of both hydrated and unhydrated Li^+ and Na^+. The case of chaotropic KCl is also shown. When hydration of the kosmotropic ions is not taken into account, then the wrong series is obtained: $Li^+ \simeq Na^+ < K^+$. The effect of ion hydration is an interesting and subtle one which is surface specific. The results reported here indicate that hydrated ions retain

their hydration shell at the silica surface, which is corroborated by other studies.[44] Other surfaces, for instance, mica[19] or alumina,[44,45] appear to be able to strip the hydration shell off ions as they approach the surface.[46−49]

4. Conclusions

As more precise theoretical modeling is now in sight due to the recent availability of *ab initio* dynamic polarizabilities,[19] it is possible to make quantitative comparison with different experiments. This should provide better insights into the correctness and usefulness of the theoretical modeling. We have here presented experimental results for the ion specific hydronium ion titration of silica surfaces. These experimental results have been analyzed in terms of a model that accounts for effects of hard sphere repulsion, hydration, and ionic specific nonelectrostatic dispersion potentials. The discovery that the charging of mesoporous silica surfaces is ion specific has huge impact for applications such as catalysis and drug delivery. It is now clear that, for example, protein adsorption in SBA-15 and other mesoporous structures could be effectively manipulated by the choice of background salt solution.

(43) Dishon, M.; Zohar, O.; Sivan, U. *Langmuir* **2009**, *25*, 2831.
(44) Parsons, D. F.; Boström, M.; Maceina, T. J.; Salis, A.; Ninham, B. W. Submitted for publication, 2009.
(45) Colic, M.; Franks, G. V.; Fisher, M. L.; Lange, F. F. *Langmuir* **1997**, *13*, 3129.

(46) Lyons, J. S.; Furlong, D. N.; Healy, T. W. *Aust. J. Chem.* **1981**, *34*, 1177.
(47) Brady, P. V.; Krumhansl, J. L.; Papenguth, H. W. *Geochim. Cosmochim. Acta* **1996**, *60*, 727.
(48) Pandit, S. A.; Bostick, D.; Berkowitz, M. L. *Biophys. J.* **2003**, *84*, 3743.
(49) Draper, D. E. *RNA* **2004**, *10*, 335.

PAPER IV

Specific ion effects on the electrochemical properties of cytochrome c†

Luca Medda,[ab] Andrea Salis*[b] and Edmond Magner*[a]

The range of salts used as supporting electrolytes in electrochemical studies of redox proteins and enzymes varies widely, with the choice of an electrolyte relying on the assumption that the electrolyte used does not affect the electrochemical properties of the proteins and enzymes under investigation. Examination of the electrochemical properties of the redox protein cytochrome c (cyt c) at a 4,4′-bipyridyl modified gold electrode demonstrates that both the redox potential ($E^{o\prime}$) and the faradaic current are influenced by the nature of the electrolyte used, in a manner explained primarily by Hofmeister effects. The faradaic peak currents display an atypical trend on switching from kosmotropic to chaotropic anions, with a maximum current observed in the presence of Cl^-. For a series of cations, the peak current increased in the sequence: Li^+ (0.34 μA) < guanidinium$^+$ (0.36 μA) < Na^+ (0.37 μA) < K^+ (0.38 μA) < Cs^+ (0.40 μA) and for anions it decreased in the sequence: Cl^- (0.37 μA) > Br^- (0.35 μA) > ClO_4^- (0.35 μA) > SCN^- (0.31 μA) > F^- (0.30 μA). $E^{o\prime}$ decreased by a total of 24 mV across the series $F^- > Cl^- > Br^- > ClO_4^- > SCN^-$ whereas no specific ion effect on $E^{o\prime}$ was observed for cations. Factorisation of $E^{o\prime}$ into its enthalpic and entropic components showed that while no specific trends were observed, large changes in $\Delta H^{o\prime}$ and $\Delta S^{o\prime}$ occurred with individual ions. The effect of anions on the faradaic peak current can be qualitatively explained by considering Collins' empirical rule of 'matching water affinities'. The effect of cations cannot be explained by this rule. However, both anion and cation effects can be understood by taking into account the cooperative action of electrostatic and ion dispersion forces. The results demonstrate that the choice of a supporting electrolyte in electrochemical investigations of redox proteins is important and emphasize that care needs to be taken in the determination and comparison of $E^{o\prime}$, $\Delta H^{o\prime}$ and $\Delta S^{o\prime}$ in different solutions.

1. Introduction

Understanding of the electrochemical properties of redox enzymes is intrinsic to their successful utilization as biocatalysts, biofuel cells or biosensors.[1–3] Cytochrome c (cyt c) is an electron transport protein comprised of a heme group and a 104 amino acid residue organized into a series of five α-helices and six β-turns.[4] It is one of the most extensively studied redox proteins and has been widely used as a model to study electron transfer in proteins.[4] The protein contains a number of lysine residues clustered around its heme edge which allow the protein to dock with the negatively charged groups of its

redox partners such as cytochrome c oxidase and cytochrome c peroxidase, a feature that has been exploited to probe the electrochemical properties of cyt c.

The charge distribution on the protein is heterogeneous, resulting in dipole moments of 308 and 325 D for the reduced and oxidized protein, respectively, at neutral pH.[4] The relatively high value of $E^{o\prime}$ (258 mV vs. SHE (standard hydrogen electrode)) arises in part from the π-electron-acceptor character of the thioether sulfur atom of the axially bound methionine to iron, which preferentially stabilizes the ferrous state (Fig. 1). This selective stabilization is further enhanced by the poor accessibility of the heme to solvent and burial of the heme within a hydrophobic pocket.[4] Binding of the protein to the surface of an electrode prior to electron transfer can be promoted by a range of modifiers.[5–8] A detailed investigation of the mechanism of reduction of cyt c at a 4,4′-bipyridyl modified gold electrode demonstrated that the binding step provides approximately half of the activation free energy for electron transfer and is a crucial factor in the enhancement of the rate of electron transfer.[5] The use of self-assembled monolayers on electrodes to promote electron transfer between the

*[a] Department of Chemical and Environmental Sciences & Materials and Surface Science Institute, SFI-SRC in Solar Energy Conversion, University of Limerick, Limerick, Ireland. E-mail: edmond.magner@ul.ie*

[b] Department of Chemical Sciences, University of Cagliari-CSGI and CNBS, Cittadella Universitaria, S.S. 554 bivio Sestu, 09042-Monserrato (CA), Italy. E-mail: asalis@unica.it; Fax: +39 070 6754388; Tel: +39 070 6754362
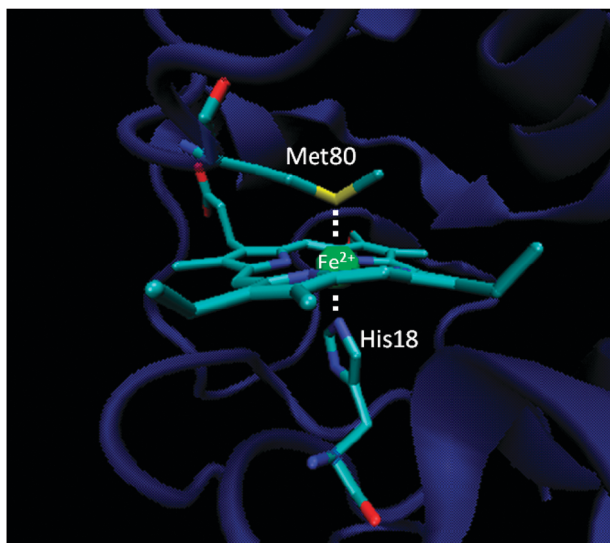
Fig. 1 Representation of the Fe^{2+} in the heme group of *cyt c* (PDB code: 1HRC).

redox protein of interest and the electrode has been widely studied.[5–11]

Insight into the correlation between $E^{o'}$ and structural properties of redox proteins can be obtained from the factorization of the enthalpic ($\Delta H_{rc}^{o'}$) and entropic ($\Delta S_{rc}^{o'}$) components (eqn (1)). Ligand–heme interactions dominate the enthalpic term, with the methionine ligand stabilizing the ferroheme.[4] Solvent reorganization effects and the more compact structure of the ferroheme form contribute to the entropic term.[10,12]

$$E^{o'} = \frac{-\Delta H_{rc}^{o'}}{nF} + \frac{T\Delta S_{rc}^{o'}}{nF} \qquad (1)$$

Electrochemical measurements require the presence of an electrolyte whose sole function is ideally that of charge transport. Typical supporting electrolytes for *cyt c* electrochemical measurements are $NaClO_4$,[5] KNO_3,[8] or mixtures of salts (*i.e.* Na_2SO_4, $KClO_4$ and KCl).[13] However, the nature of the ions present in a solution can affect the properties of an enzyme, including properties such as protein folding and enzymatic activity.[14] The effect of the ions can follow the Hofmeister series which lists the ions in order of their relative effects on the properties of the protein. Such effects were first described by Hofmeister who observed that the nature of the salt used affected the solubility of egg-white proteins in aqueous solutions.[15] The efficiency of salts in promoting protein precipitation was found to be:

Anions: $SO_4^{2-} > F^- > Cl^- > NO_3^- > Br^- > I^- > ClO_4^- > SCN^-$.

Cations: $Cs^+ > NH_4^+ > K^+ > Na^+ > Li^+ > Mg^{2+}$.

Hofmeister 'specific ion effects' are ubiquitous in biology, chemistry and physics.[16,17] In addition to protein precipitation,[18] properties such as enzymatic activities,[19–21] aggregation behavior of triblock copolymers,[22] neutral lipid membrane interactions,[23] anion affinities at the air–water interface,[24] asymmetric partitioning of anions in lysozyme dispersions,[25] protein adsorption on mesoporous materials,[26] pH of buffers[27] are all ion specific.[28–30]

It has been proposed that the ordering of the ions arises from changes in the hydrogen-bonding network of water in bulk solution as a result of electrostatic effects which depend on the charged nature of the ions. In this approach, ion specificity is associated with electrolyte induced changes in water structure that depend on the capacity of ions to form (kosmotropic ions), or to break (chaotropic ions) hydrogen bonds. Such correlations arise from a theoretical framework that includes only electrostatic and hydration forces between ions and water.[31,32] However this theory cannot satisfactorily explain the range of effects that have been observed and recent data indicate that hydrogen-bonding networks in aqueous solutions are unaffected by the addition of different anions.[33]

In more recent approaches,[34] it has been shown that standard theories are deficient in that they omit non-electrostatic, ion specific electrodynamic fluctuation (dispersion) forces. The DLVO description of forces between colloidal particles can be separated into two types; an electrostatic, double layer component due to an inhomogeneous profile of ions at the interface and opposing attractive quantum mechanical forces which are described by van der Waals–Hamaker interactions. The latter ignores the ion profiles and the specific dispersion forces acting on ions.[34] The ion specific dispersion potentials acting on ions can be included at the same level as electrostatic forces within a Poisson–Boltzmann description. Within this approach electrostatic and dispersion forces combine to induce structuring of the local water molecules around ions (kosmotropy, chaotropy). The interactions, long and short range, between such "modified" ions are reflected in bulk properties such as activity. The key parameter of this approach is the ion polarizability, α, which is usually large for ions with a large radius (*i.e.* I^-, SCN^-, Cs^+) and small for ions with a small radius and high electrical charge (*i.e.* F^-, Li^+, Mg^{2+}). The common observation that ion specific effects are usually stronger for anions is due to the fact that they are more polarizable than cations, however a full description of Hofmeister effects also requires the inclusion of hydration effects and ionic size.[35]

In this paper we report measurements of the faradaic peak currents and the $E^{o'}$ of cytochrome *c* in the presence of a range of cations and anions and demonstrate that the nature of the ion influences both these parameters in a manner which can be ascribed to the Hofmeister effect. While the peak current is influenced by both anions and cations, $E^{o'}$ is affected only by anions. Specific ion effects on the peak current can be understood by considering the polarizability of the ions, which affects the interaction between *cyt c* and the modified-gold electrode. Elucidation of the enthalpic and entropic components of $E^{o'}$ demonstrates that the overall changes in $E^{o'}$ are masked by significant, opposing changes in $\Delta H^{o'}$ and $\Delta S^{o'}$. These changes are analyzed and compared to ion-specific effects observed for other systems.

2. Experimental

2.1 Materials

Horse heart cytochrome *c* (type VI) was purchased from Sigma-Aldrich and used without further purification. Potassium hydrogen phosphate, potassium di-hydrogen phosphate,

2876 | *Phys. Chem. Chem. Phys.*, 2012, **14**, 2875–2883

This journal is © the Owner Societies 2012

sodium fluoride, sodium chloride, sodium bromide, sodium perchlorate, sodium thiocyanate, lithium chloride, potassium chloride, caesium chloride, guanidine in chloridric acid, 4,4′-bipyridyl, sulfuric acid and hydrogen peroxide were obtained from Sigma-Aldrich. Agar was obtained from BDH. Deionised water was obtained from an Elga Maxima water purification system and had a resistivity of 18.2 MΩ cm on delivery.

2.2 Methods

A 2 mm-diameter gold work electrode (CH Instruments) was used for all experiments. The electrode was cleaned by immersion in piranha solution ($7H_2SO_4 : 3H_2O_2$) for 10 min, mechanically polished with alumina slurry (1.0, 0.3, and 0.05 μm) and sonicated for 5 minutes prior to use. A stock solution of cytochrome c was prepared in 4.4 mM potassium phosphate buffer (pH 7.0) and frozen in aliquots of 1 mL. Salts were dried in an oven at 110 °C for 24 h prior to use. A stock solution of 4,4′-bipyridyl was prepared in potassium phosphate buffer (4.4 mM, pH 7.0). Electrochemical measurements were performed using solutions containing $cyt\ c$, the appropriate salt (200 mM), and 4,4′-bipyridyl (10 mM) made up to a total volume of 5 mL. The pH of the solutions was measured with an Orion 420A pH meter, calibrated with Thermo scientific buffers at pH 4.01, 7.00, 10.01. The average pH was 7.15 ± 0.15. Cytochrome c concentrations were determined spectrophotometrically (Shimadzu UV-11800) using an extinction coefficient of 106 100 M^{-1} cm^{-1} at 410 nm.[4] The concentration of cytochrome c in solution was 99 ± 5 μM.

Differential pulse voltammetry was performed on a CHI630A potentiostat (CH Instruments), using an increment of 0.001 V, an amplitude of 0.05 V, a pulse width of 0.06 s and a quiet time of 10 sec. A two-compartment, "nonisothermal" cell was employed in which the reference electrode was isolated from the working electrode compartment. Electrical contact between the compartments was maintained via a 1 M KCl/agar salt bridge. The reference (Ag|AgCl||KCl sat) and counter electrodes (platinum wire) were placed in a solution of 1 M KCl maintained at 20 ± 1 °C using a water bath (Clifton Bennet). Unless otherwise stated, all potentials reported here are referenced to the SHE ($E^{o'}_{SHE} = E^{o'}_{Ag/AgCl} + 0.204$ V at 20 °C). The working electrode was placed in the second compartment, which was comprised of a 10 mL cell with a heating jacket connected to a water bath (Lauda ecoline003). Each value of $E^{o'}$ represents an average of 3 ± 1 data points. The electrostatic surface potential of $cyt\ c$ was calculated using APBS,[36] PDB2PQR,[37] which employs PROPKA,[38] was used to calculate the partial charges on the protein residues. PRODRG[39] was used to generate the parameters for the heme.

3. Results and discussion

3.1 Effect of ionic strength on E'_0 and peak current

Differential pulse voltammograms of cytochrome c at a 4,4′-bipyridyl modified electrode (Fig. 2) show reversible behavior with a peak width at half maximum of 92 mV. The response obtained displayed excellent reproducibility (Fig. S1 in the ESI†). The peak current increased slightly on increasing the ionic strength from 0.02 to 0.1 M (Fig. 3A), after which it
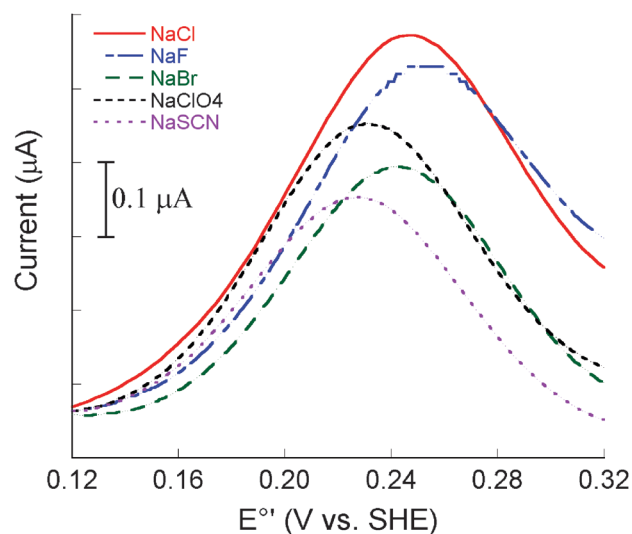
Fig. 2 Differential pulse voltammograms of $cyt\ c$ in a solution of potassium phosphate buffer (4.4 mM, pH 7.15) at 298 K in the presence of a range of anions.

decreased linearly with increasing ionic strength. This decrease indicates that the specific binding interaction between cytochrome c and the 4,4′-bipyridyl modified electrode surface is, at least at lower I values, electrostatic in nature. The formal reduction potential of $cyt\ c$ decreased as the ionic strength increased (Fig. 3B). Previous work has shown that at low ionic strength (0.04 to 0.06 M) the $E^{o'}$ of $cyt\ c$ follows the Debye–Hückel equation.[40] Using a Debye–Hückel model of $cyt\ c$ as a low dielectric constant spherical cavity with a spherical surface charge distribution in a solvent of a continuum dielectric gives:[8]

$$E^{o'} = E^o - 0.059A\ (Z^2_{ox} - Z^2_{red})f(I) \qquad (2)$$

where

$$f(I) = \frac{\sqrt{I}}{1 + Ba_1\sqrt{I}} \qquad (3)$$

I is the ionic strength, $B = 0.329$ and $a_1 = 18$. The formal potential shows a dependence on $f(I)$ (Fig. 3C), though the response is not linear across the range examined, with deviations from linearity at high ionic strength which may arise from non-electrostatic effects.[41]

3.2 Specific ion effects on peak current of $cyt\ c$

As the faradaic current is proportional to the amount of protein interacting with the electrode, specific ion–protein interactions may alter the measured current. Specific ion effects were examined at an ionic concentration of 200 mM, a concentration reasonably close to that where specific ion effects are observed but sufficiently low to provide an observable faradaic response. Plots of peak current for a range of anions (Fig. 4A) and cations (Fig. 4B) display atypical trends when compared with the monotonic trends that are usually observed. The highest current for the anion series was obtained with Cl$^-$, while in the cation series, the highest current was obtained with Cs$^+$. A similar trend has been observed recently for $cyt\ c$.[42]
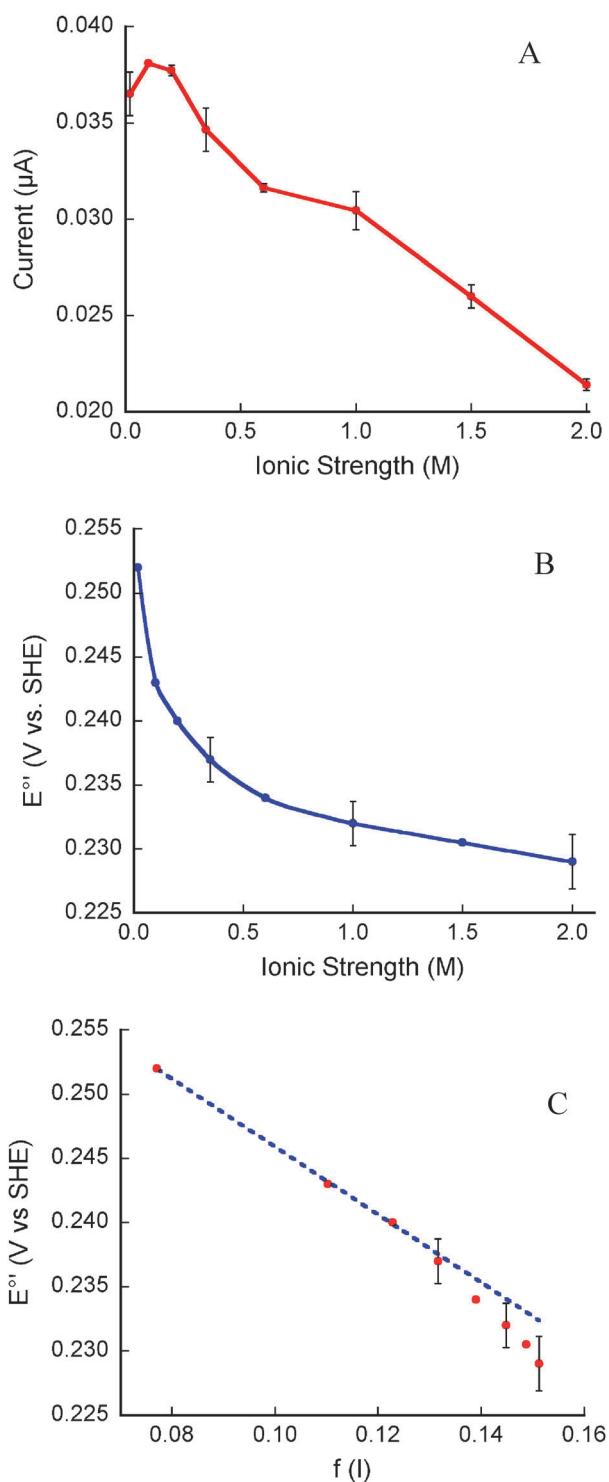
Fig. 3 Plot of (A) peak current, (B) $E^{o\prime}$ of *cyt c* as a function of ionic strength at 298 K and (C) $E^{o\prime}$ of *cyt c* as a function of $f(I)$ in the presence of NaCl. The dashed line represents a plot of eqn (3).

Apart from the unexpected behavior of F^-, the observed results can be explained by Collins' empirical rule of 'matching water affinities'.[31] Chaotropic anions can bind to chaotropic charged residues such as lysine on the surface of *cyt c*. In contrast to pure electrostatic effects, this approach considers the effect of the surface charge density of the ion on ion–water interactions.[31] Small ions, such as Li^+, Na^+ and F^-, have a high surface charge density (they are "hard" or "kosmotropic") and bind water molecules strongly, whereas large ions, *i.e.* Cs^+, ClO_4^-, SCN^-, have a low charge density (they are "soft" or "chaotropic") and bind water molecules weakly. This rule states that ions prefer to pair with counterions or ionic groups which have comparable hydration enthalpies, *i.e.* similar water affinities. In this classification, the charged groups on a protein surface, *i.e.* carboxylates and alkyl ammonium, are kosmotropic and chaotropic, respectively. At a pH of 7.1, *cyt c* has a net positive charge (Fig. 5). The chaotropic ammonium groups of lysine residues can form strong ion pairs with chaotropic anions, with the strength of interactions increasing in the order: $Cl^- < Br^- < ClO_4^- < SCN^-$. These ion pairs can have a detrimental effect on the binding between *cyt c* and the 4,4'-bipyridyl modified gold electrode, thus leading to a decrease in the peak current (Fig. 5A). Fluoride does not follow this trend, possibly because its strongly kosmotropic nature does not permit the formation of ion pairs with chaotropic cationic groups at the surface of *cyt c*. The effect of F^- on the peak current is similar to that produced by a chaotropic anion, producing the observed atypical curve. A similar trend was previously observed by Sedlak *et al.*[42] where the effect of a series of ions on the rate constant for cyanide association with the heme iron of *cyt c* was a result of modulation of the Met80–heme iron bond strength and/or conformational flexibility of the heme region. Such atypical behaviour has been frequently observed. As recently reported by Schwiertz *et al.*,[43] a partial or total reversal in the series can be ascribed to changes in the polarity or charge of the surface. A reversal of the order of the series was observed for lysozyme on changing from low to high salt concentrations,[18] arising from change in the surface charge due to ion specific adsorption.[44] A transition region has usually been observed where the order of ions can be partially or fully re-arranged. It is feasible that the ion concentrations of 0.2 M used here are in this transition region, accounting for the observed position of F^-.

The cation effects on the peak current (Fig. 4B) display a monotonic increase from Li^+ to Cs^+ followed by a decrease for guanidinium. Guanidinium is usually considered to be a strongly denaturing (chaotropic and poorly hydrated) ion. On the basis of this classification it should be placed close to either ammonium or caesium in the conventional Hofmeister series (as is shown here). For example, the surface charge density of a silica based porous material followed the series: $Li^+ > Na^+ > K^+ >$ guanidinium$^+ > Cs^+$.[45] In this study, the effect of guanidinium lies between that of Li^+ and Na^+. Using the conventional classification of guanidinium as a strong chaotrope its atypical position in the series can be explained in the same manner as for F^-, *i.e.* the effects of the ion are observed in the transition region between the direct and the reversed Hofmeister series. It is clear that the behavior of guanidinium cannot be classified in the context of the conventional Hofmeister series.[46]

The overall cation effects (Fig. 4B) cannot be rationalized using the approach described for anions. While *cyt c* has a net positive charge at pH 7.1, it also has a significant number of
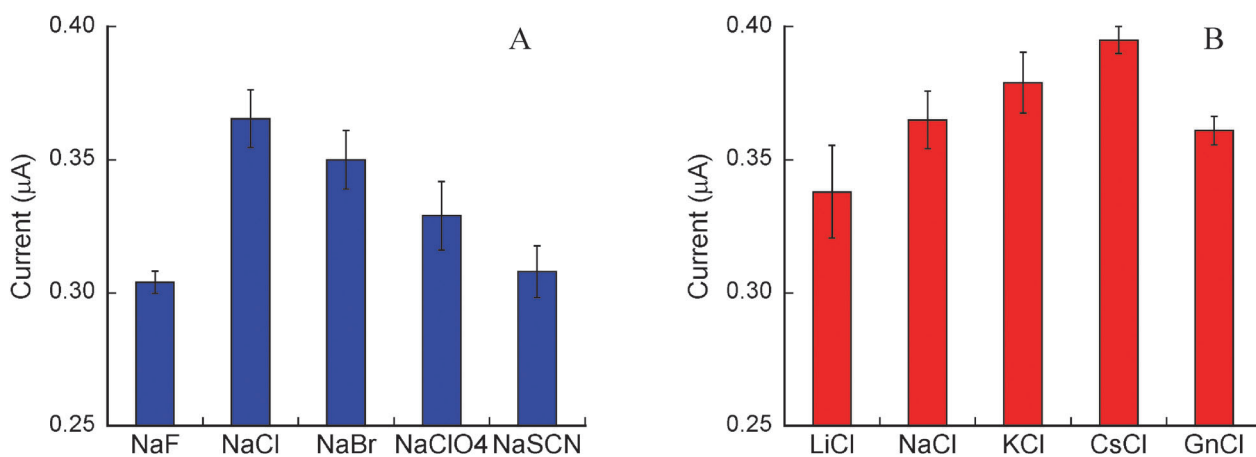
Fig. 4 Plot of peak current of *cyt c* at 298 K in the presence of a range of (A) anions (200 mM) and (B) cations (200 mM).
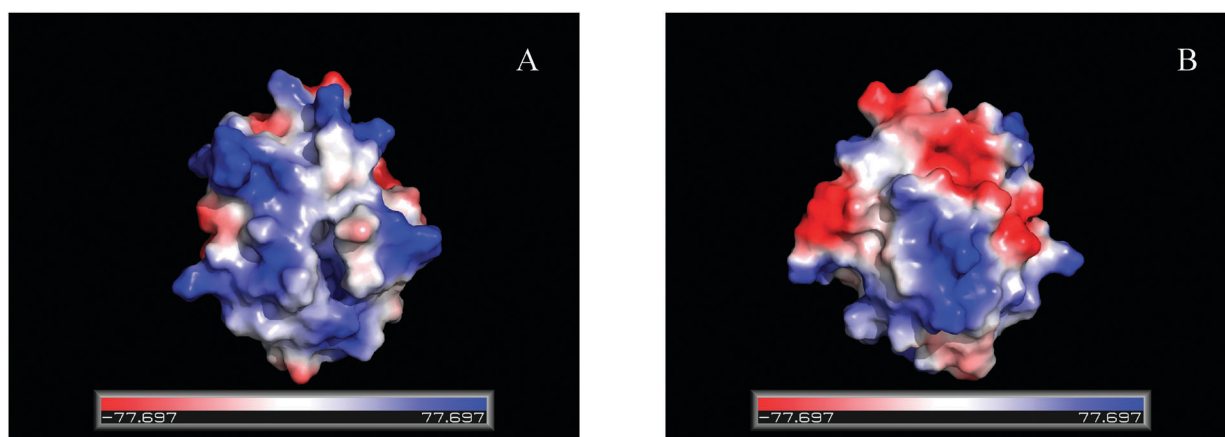

Fig. 5 Electrostatic surface potential (red negative, blue positive) calculations using APBS[36] of cytochrome *c* (PDB code: 1HRC) visualized from (A) the heme edge and (B) on rotation of (A) by 180°.

negatively charged residues which can act as adsorption sites for cations (Fig. 5B). These residues are clustered at the distal side of the protein, away from the heme edge. The order of binding of cations to kosmotropic carboxylate groups would, according to Collins,[31] follow the trend: $Li^+ > Na^+ > K^+ > Cs^+$. However, binding of cations to the negatively charged residues would not be expected to affect the binding of *cyt c* to the modified gold electrode surface as electron transfer occurs through the heme edge of the protein. The effect of cations is significant, with the peak current following the trend: $Cs^+ > K^+ > Na^+ > Gn^+ > Li^+$. The increase in the peak current, from 0.34 to 0.39 μA, in the presence of Li^+ and Cs^+, respectively, indicates that more subtle cation effects are occurring.[29]

From the theory of the double layer, a charged colloidal particle will establish an inhomogeneous concentration profile of cations and anions, $\rho_i(x)$.[47] The ionic distribution follows from the equation:

$$\nabla^2 \phi(x) = 4\pi \frac{\sum_i \rho_i(x)}{\varepsilon} \qquad (4)$$

where ϕ is the electrostatic potential and ε the dielectric constant. For a simple 1 : 1 electrolyte, such as the salts used in the present work, and for a positively charged surface, such as

the heme edge of *cyt c* at pH 7.1, the ionic concentration profile ($\rho_-(x)$ and $\rho_+(x)$ for anions and cations respectively) can be described by the Boltzmann distribution:

$$\rho_-(x) = \rho_0 \exp\left(\frac{e\phi}{kT}\right) \qquad (5A)$$

$$\rho_+(x) = \rho_0 \exp\left(-\frac{e\phi}{kT}\right) \qquad (5B)$$

where e is the unit charge and ρ_0 the bulk salt concentration. Under suitable boundary conditions the resulting

Table 1 List of ionic sizes (hard sphere radius), a,[48] static ionic polarizabilities, α_0,[48] and dispersion coefficients (water–protein), B[44]

Ion	$a/\text{Å}$	$\alpha_0/\text{Å}^3$	B (10^{-50} J m^3)
F^-	1.12	1.218	n.a.
Cl^-	1.86	4.220	−1.26
Br^-	2.16	6.028	−1.70
ClO_4^-	2.35	5.488	−1.53
SCN^-	2.39	7.428	−2.27
Li^+	0.42	0.028	n.a.
Na^+	0.67	0.131	−0.20
K^+	1.06	0.795	n.a.
Cs^+	1.62	2.354	n.a.

This journal is © the Owner Societies 2012

Phys. Chem. Chem. Phys., 2012, **14**, 2875–2883 | 2879

Poisson–Boltzmann equation can be solved to show that a positively charged protein surface would adsorb counterions (anions) and repel cations. Conventional double-layer theory yields the same result, irrespective of which 1 : 1 electrolyte used, *i.e.* no specific ion effects should occur.

A qualitative rationalization of both anion and cation effects can be made by considering ion dispersion forces, as described in detail by Ninham and Lo Nostro.[29] Ionic dispersion forces operate together with electrostatic forces to modulate ion binding at colloidal surfaces,[34] introducing an additional term, $U_i^{dispersion}(z)$ (eqn (6) and (7)) to the electrostatic potential, ϕ (eqn (5)).

$$U_i^{dispersion}(x) = \frac{B_i}{x^3} f(x) \qquad (6)$$

$$\rho_i(x) = \rho_0 \exp\left(-\frac{\pm e\phi + U_i^{disp.}(x)}{kT}\right) \qquad (7)$$

where B_i is the dispersion coefficient, x is the distance of the ion from the protein surface, and $f(x)$[49] is the function of the reciprocal of the size of the ion (a). B_i depends on the ion

dynamic polarizability ($\alpha^*(i\omega)$) and the dielectric properties of both the surface and the solvent. Hofmeister effects are the result of a delicate interplay between hydration, non-electrostatic potentials and ionic size effects.[35] B_i is affected by all three parameters, whereas $f(x)$[49] depends only on ionic size. The size of the ion has two contrasting effects; polarizability increases with size, and so does B_i, whereas $f(x)$ decreases. The resulting value of U_i is a subtle balance between these effects.[35] Experimental verification of this theory has been hindered by the lack of accurate values of ion polarizabilities. Recently, progress in calculating B_i coefficients *ab initio* from ion polarizabilities for some surfaces (*i.e.* air–water,[50] water–silica,[45] water–alumina,[49] and water–protein[44]) has been made. While B_i values for a range of anions at the water–protein interface have been reported,[44] similar values for all cations are not yet available. The ionic sizes, static ion polarizabilities and dispersion coefficients for some ions used in the present work are listed in Table 1.

Ion dispersion forces combine with electrostatic forces to modulate the ionic distribution profile at the surface of *cyt c*. Anions can be adsorbed on the positively charged surface of
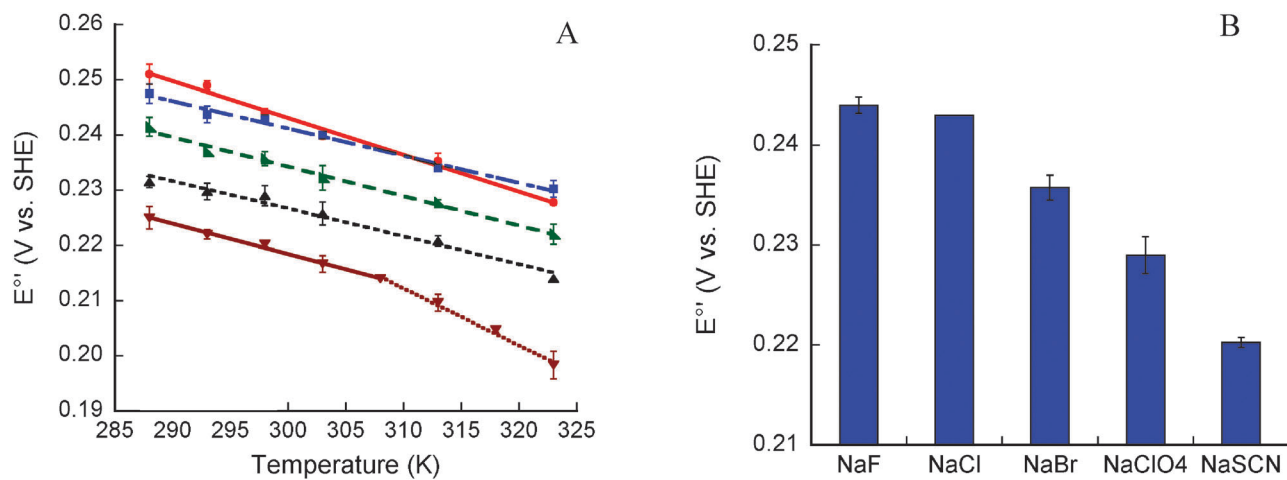
Fig. 6 Plot of (A) $E^{o\prime}$ of *cyt c vs. T* in the presence of 200 mM F⁻ (●), Cl⁻ (■), Br⁻ (▶), ClO₄⁻ (▲), SCN⁻ (▼), and (B) $E^{o\prime}$ of *cyt c* for a range of anions at 298 K.
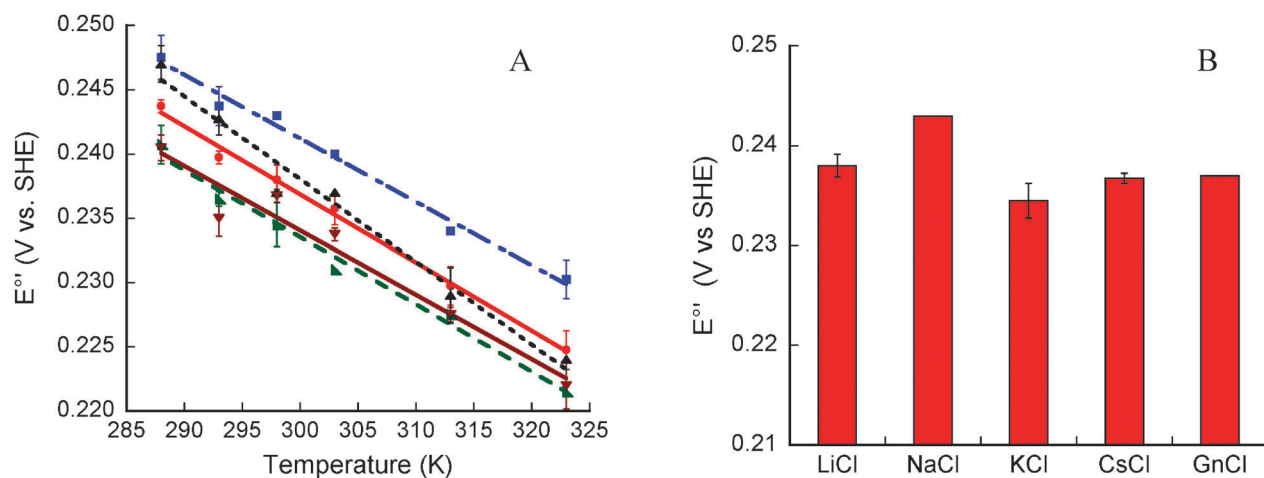

Fig. 7 Plot of (A) $E^{o\prime}$ of *cyt c vs. T* in the presence of 200 mM Li⁺ (●), Na⁺ (■), K⁺ (▶), Gn⁺ (▲), Cs⁺ (▼), and (B) $E^{o\prime}$ of *cyt c* for a range of cations at 298 K.

cyt c but to different extents according to the dispersion potential, $U_i^{\text{dispersion}}$, calculated from eqn (6). A higher value of polarizability and, consequently, a more negative value of B will result in a more attractive dispersion force (Table 1), according to the series $SCN^- > Br^- > ClO_4^- > Cl^-$. With the exception of the relative positions of Br^- and ClO_4^-, this series follows the experimental results (Fig. 4A). The relative ordering of Br^- and ClO_4^- is likely to arise from the fact that polyatomic ions, such as ClO_4^-, have a significant quadrupole moment that is not considered in the calculations only including induced dipole interactions.[44] Cations will be repelled from the surface of the protein but, similarly to anions, the more polarizable Cs^+ will be able to approach closer to the surface than the less polarizable Li^+. Strong anion binding, as for SCN^-, would reduce the positive surface potential of *cyt c* thus resulting in a decrease of the peak current (Fig. 4A). In contrast, cation adsorption, as for Cs^+, would increase the surface potential of *cyt c*, thus favoring electrostatic binding to the modified gold electrode and increasing the peak current. The observed ion specific effects can be rationalized in this manner. While the effect of specific adsorption of the ions on the 4,4′-bipyridyl modified gold electrode surface cannot be excluded, it is not likely that such an effect is significant as disruption of the 4,4′-bipyridyl layer would be expected to affect the peak currents, but not $E^{o\prime}$, $\Delta H^{o\prime}$ and $\Delta S^{o\prime}$. Specific ion effects on $E^{o\prime}$, $\Delta H^{o\prime}$ and $\Delta S^{o\prime}$ will be discussed in the next section.

3.3 Specific ion effects on $E^{o\prime}$ of *cyt c*

Plots of $E^{o\prime}$ of *cyt c* as a function of temperature (Fig. 6A and 7A) are in agreement with previously published data with $E^{o\prime}$ decreasing with increasing temperature. However, the temperature dependence of $E^{o\prime}$ is also dependent on the nature of the anion present in the solution. While *cyt c* displays essentially the same value of $E^{o\prime}$ in solutions containing fluoride and chloride, in the presence of Br^-, ClO_4^- and SCN^-, $E^{o\prime}$ undergoes a progressive decrease. An exception to the linear dependence of $E^{o\prime}$ on temperature was observed for thiocyanate which showed a biphasic response with a break point at 308 K. This behavior may arise from a change in the conformation of the protein from a low to high-temperature conformer and has been observed previously in mixtures of solvents.[10,12] The values of $E^{o\prime}$ as a function of different salts are shown in Fig. 6B. $E^{o\prime}$ decreases according to the Hofmeister series, ranging from a higher redox potential for lower polarizable (kosmotropic) ions to a lower redox potential for highly polarizable (chaotropic). A difference of 22 ± 2 mV was observed between the two limits, with $E^{o\prime}$ of 244 and 222 mV for NaF and NaSCN, respectively. Fig. 7A shows $E^{o\prime}$ as a function of temperature for a series of cations. Unlike the anion series, no clear trend could be ascribed to ion specific effects. For example, no significant difference was observed in $E^{o\prime}$ in LiCl and CsCl (Fig. 7B).

Analysis of the temperature dependence of $E^{o\prime}$ indicates that the enthalpy and entropy changes are compensative with the enthalpy term being the dominant component in all solutions examined (Fig. 8 and Table 2). The observed changes in $E^{o\prime}$ mask significant changes in $\Delta S^{o\prime}$ and $\Delta H^{o\prime}$. Upon changing the
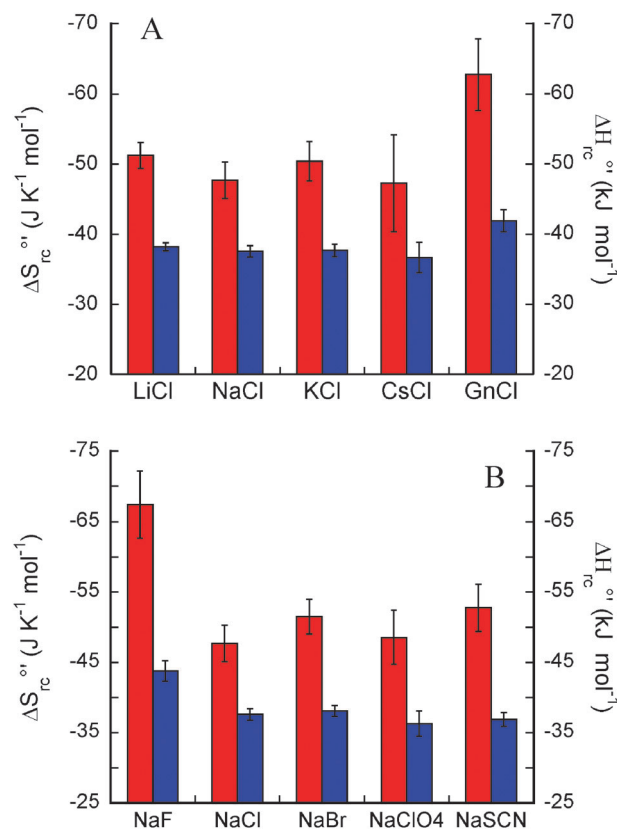
Fig. 8 $\Delta S_{rc}^{o\prime}$ (■) and $\Delta H_{rc}^{o\prime}$ (■) for the reduction of *cyt c* in the presence of a range of (A) anions and (B) cations at concentrations of 200 mM.

anion from F^- to ClO_4^-, $\Delta H^{o\prime}$ decreased significantly by 78 mV while $\Delta S^{o\prime}$ increased by 49 mV. In contrast, little change was observed in the cation series with the exception of guanidinium.

This trend is not so surprising as cations are less polarizable than anions and their lower ionic dispersion forces can account for the small changes observed for the cation series. The enthalpy of reduction is a function of a range of effects including the nature of the axial ligand(s), the net charge (of both the heme and the peptide), the extent of the hydrogen bond network, and the degree of solvent exposure. Reduction entropies of redox proteins are considered to be due to solvent induced reorganization effects, alteration of solvent dielectric about the metal redox centers, and the influence of ligation. It is not possible to identify a general trend in $\Delta H^{o\prime}$ and $\Delta S^{o\prime}$ for either the cation or the anion series. For example, in the case of NaCl the entropic contribution ($T\Delta S_{rc}^{o\prime}/nF$) is -0.147 V while the enthalpic term ($-\Delta H_{rc}^{o\prime}/nF$) is 0.390 V. The entropic term in the presence of Cl^-, while being less negative and indicative of preferential stabilization of the reduced form of *cyt c*, is similar to that of ClO_4^-. The values for Br^- and SCN^- are lower and similar in magnitude. In contrast, the enthalpic term for Cl^- is similar to those of Br^-, ClO_4^- and SCN^-, indicative of no specific ion effects. For the cation series, Na^+, K^+ and Cs^+ display similar values of ($-\Delta H_{rc}^{o\prime}/nF$) which are slightly larger than that of Li^+, while the entropic contributions for all four cations are broadly similar.

This journal is © the Owner Societies 2012

Phys. Chem. Chem. Phys., 2012, **14**, 2875–2883 | 2881

Table 2 Thermodynamic parameters for the reduction of *cyt c* in the presence of a range of ions

Salt	$E^o_{298 K}$ (mV *vs.* SHE)	$\Delta S^{o\prime}_{rc}$/JK^{-1}mol^{-1}	$\Delta H^{o\prime}_{rc}$/kJ^{-1}mol^{-1}	$-\Delta H^{o\prime}_{rc}/nF$(V)	$T\Delta S^{o\prime}_{rc}/nF$(V)
NaF	0.244 ± 0.001	−67.4 ± 4.8	−43.8 ± 1.5	0.454	−0.208
NaCl	0.243 ± 0.001	−47.7 ± 2.6	−37.6 ± 0.8	0.390	−0.147
NaBr	0.234 ± 0.001	−51.5 ± 2.5	−38.1 ± 0.8	0.394	−0.159
NaClO$_4$	0.229 ± 0.002	−48.5 ± 3.8	−36.3 ± 1.8	0.376	−0.149
NaSCN	0.222 ± 0.002	−52.7 ± 3.3	−36.9 ± 1.0	0.382	−0.163
LiCl	0.238 ± 0.001	−51.2 ± 1.8	−38.2 ± 0.6	0.396	−0.158
KCl	0.234 ± 0.002	−50.4 ± 2.8	−37.7 ± 0.9	0.390	−0.155
CsCl	0.237 ± 0.001	−47.3 ± 6.9	−36.7 ± 2.2	0.380	−0.146
GuanidiniumCl	0.237 ± 0.001	−62.7 ± 5.0	−41.9 ± 1.6	0.434	−0.129

4. Conclusions

The specific effects of both anions and cations on the $E^{o\prime}$ and the peak current of *cyt c* have been probed using differential pulse voltammetry at 4,4′-bipyridyl modified gold electrodes. The anions examined have a more pronounced effect than cations on the $E^{o\prime}$ of *cyt c*, with $E^{o\prime}$ decreasing in the sequence: F$^-$ > Cl$^-$ > Br$^-$ > ClO$_4^-$ > SCN$^-$. This effect can be explained by the tendency of kosmotropic anions to stabilize the reduced state of the iron in the heme, increasing $E^{o\prime}$. The peak currents showed an atypical trend in the presence of anions, with a maximum value obtained with Cl$^-$ instead of the conventional monotonic series. Anion–protein interactions affect the peak current, since the latter is proportional to the amount of protein interacting with 4,4′-bipyridyl adsorbed on the electrode surface. Apart from the unexpected behaviour of F$^-$, chaotropic anions can bind to the chaotropic, charged lysine residues on the surface of *cyt c*, weakening the electrostatic interactions between the charged lysine residues of *cyt c* and the modified gold electrode. The presence of cations can also affect the response, with the peak current decreasing in the sequence: Cs$^+$ > K$^+$ > Na$^+$ > Gn$^+$ > Li$^+$. This trend can be explained by the existence of attractive dispersion forces between the ions and the protein, providing experimental corroboration to Ninham's theory of ionic dispersion forces.[34] The results obtained here demonstrate the importance of the choice of the electrolyte in examining the electrochemical properties of redox proteins. In addition to the effects established here, the nature of the ion may affect the kinetics of the reaction. While this study has described the response of the model redox protein *cyt c*, it is feasible that similar changes can arise with other redox proteins and enzymes, which may ultimately be displayed as changes in sensitivity or response for such enzymes when utilized in applications such as biosensors and biofuel cells.

References

1 A. Heller, *Acc. Chem. Res.*, 2010, **43**, 963.
2 A. Schmid, J. S. Dordick, B. Hauer, A. Kiener, M. Wubbolts and B. Witholt, *Nature*, 2001, **409**, 258.
3 A. Heller, *Phys. Chem. Chem. Phys.*, 2004, **6**, 209.
4 R. A. Scott and A. G. Mauk, *Cytochrome c, A Multidisciplinary Approach*, University Science Books, Sausalito, California, 1996.
5 W. J. Albery, M. J. Eddowes, H. A. O. Hill and A. R. Hillman, *J. Am. Chem. Soc.*, 1981, **103**, 3904.
6 S. Casalini, G. Battistuzzi, M. Borsari, C. A. Bortolotti, A. Ranieri and M. Sola, *J. Phys. Chem. B*, 2008, **112**, 1555.
7 C. M. DiCarlo and D. L. Compton, *Chem. Commun.*, 2005, 218.
8 J. Petrović, R. A. Clark, H. Yue, D. H. Waldeck and E. F. Bowden, *Langmuir*, 2005, **21**, 6308.
9 F. Armstrong, H. Heering and J. Hirst, *Chem. Soc. Rev.*, 1997, **26**, 169.
10 G. Battistuzzi, M. Borsari, G. Rossi and M. Sola, *Inorg. Chim. Acta*, 1998, **272**, 168.
11 A. Kranich, H. K. Ly, P. Hildebrandt and D. H. Murgida, *J. Am. Chem. Soc.*, 2008, **130**, 9844.
12 N. J. O'Reilly and E. Magner, *Langmuir*, 2005, **21**, 1009.
13 A. Szucs and M. Novák, *J. Electroanal. Chem.*, 1995, **384**, 47.
14 M. C. Pinna, P. Bauduin, D. Tourand, M. Monduzzi, B. W. Ninaham and W. Kunz, *J. Phys. Chem. B*, 2005, **109**, 16511.
15 F. Hofmeister, *Arch. Exp. Pathol. Pharmakol.*, 1888, **24**, 247.
16 W. Kunz, P. Lo Nostro and B. W. Ninham, *Curr. Opin. Colloid Interface Sci.*, 2004, **9**, 1.
17 Y. Zhang and P. S. Cremer, *Curr. Opin. Chem. Biol.*, 2006, **10**, 658.
18 Y. Zhang and P. S. Cremer, *Proc. Natl. Acad. Sci. U. S. A.*, 2009, **106**, 15249.
19 M. C. Pinna, A. Salis, M. Monduzzi and B. W. Ninham, *J. Phys. Chem. B*, 2005, **109**, 5406.
20 A. Salis, D. Bilanicova, B. W. Ninham and M. Monduzzi, *J. Phys. Chem. B*, 2007, **111**, 1149.
21 D. Bilanicova, A. Salis, B. W. Ninham and M. Monduzzi, *J. Phys. Chem. B*, 2008, **112**, 12066.
22 B. A. Deyerle and Y. Zhang, *Langmuir*, 2011, **27**, 9203.
23 H. I. Petrache, T. Zemb, L. Belloni and V. A. Parsegian, *Proc. Natl. Acad. Sci. U. S. A.*, 2006, **103**, 7982.
24 J. Cheng, C. D. Vecitis, M. R. Hoffman and A. J. Colussi, *J. Phys. Chem. B*, 2006, **110**, 25598.
25 P. Lo Nostro, N. Peruzzi, M. Severi, B. W. Ninham and P. Baglioni, *J. Am. Chem. Soc.*, 2010, **132**, 6571.
26 A. Salis, M. S. Bhattacharyya and M. Monduzzi, *J. Phys. Chem. B*, 2010, **114**, 7996.
27 A. Salis, M. C. Pinna, D. Bilanicova, M. Monduzzi, P. Lo Nostro and B. W. Ninham, *J. Phys. Chem. B*, 2006, **110**, 2949.
28 Y. Zhang and P. S. Cremer, *Annu. Rev. Phys. Chem.*, 2010, **61**, 63.
29 B. W. Ninham and P. Lo Nostro, *Molecular Forces and Self Assembly—In Colloid, Nano Sciences and Biology*, Cambridge University Press, Cambridge, 2010.
30 W. Kunz, *Specific Ion Effects*, World Scientific Publishing, Singapore, 2010.
31 K. D. Collins, *Methods*, 2004, **34**, 300.
32 K. D. Collins, G. W. Neilson and J. E. Enderby, *Biophys. Chem.*, 2007, **128**, 95.
33 A. W. Omta, M. F. Kropman, S. Woutersen and H. J. Bakker, *Science*, 2004, **301**, 347.
34 B. W. Ninham and V. Yaminsky, *Langmuir*, 1997, **13**, 2097.
35 D. F. Parsons, M. Bostrom, P. L. Nostro and B. W. Ninham, *Phys. Chem. Chem. Phys.*, 2011, **13**, 12352.
36 N. A. Baker, D. Sept, S. Joseph, t. M. J. Hols and J. A. McCammon, *Proc. Natl. Acad. Sci. U. S. A.*, 2001, **98**, 10037.

2882 | *Phys. Chem. Chem. Phys.*, 2012, **14**, 2875–2883

This journal is © the Owner Societies 2012

37 T. J. Dolinsky, J. E. Nielsen, J. A. McCammon and N. A. Baker, *Nucleic Acids Res.*, 2004, **32**, 665.

38 H. Li, A. D. Robertson and J. H. Jensen, *Proteins*, 2005, **61**, 704.

39 A. W. Schuettelkopf and D. M. F. van Aalten, *Acta Crystallogr., Sect. D: Biol. Crystallogr.*, 2004, **60**, 1355.

40 R. Margalit and A. Schejter, *Eur. J. Biochem.*, 1974, **46**, 387.

41 S. Wherland and H. B. Gray, *Proc. Natl. Acad. Sci. U. S. A.*, 1976, **73**, 2950.

42 R. Varhac, N. Tomásková, M. Fabián and E. Sedlák, *Biophys. Chem.*, 2009, **144**, 21.

43 N. Schwiertz, D. Horinek and R. R. Netz, *Langmuir*, 2010, **26**, 7370.

44 M. Boström, D. F. Parsons, A. Salis, B. W. Ninham and M. Monduzzi, *Langmuir*, 2011, **27**, 9504.

45 A. Salis, D. F. Parsons, M. Bostrom, L. Medda, B. Barse, B. W. Ninham and M. Monduzzi, *Langmuir*, 2010, **26**, 2484.

46 W. Kunz, *Curr. Op. Colloid Int. Sci.*, 2010, **15**, 34.

47 J. Israelachvili, *Intermolecular & Surface Forces*, Academic Press, London, 1992.

48 D. F. Parsons and B. W. Ninham, *J. Phys. Chem. A*, 2009, **113**, 1141.

49 D. F. Parsons, M. Boström, T. J. Maceina, A. Salis and B. W. Ninham, *Langmuir*, 2010, **26**, 3323.

50 D. F. Parsons, V. Deniz and B. W. Ninham, *Colloids Surf., A*, 2009, **343**, 57.

This journal is © the Owner Societies 2012

Phys. Chem. Chem. Phys., 2012, **14**, 2875–2883 | 2883

PAPER V

Lysozyme Adsorption and Release from Ordered Mesoporous Materials

Mani S. Bhattacharyya,[†,§] **Pradip Hiwale,**[†,§] **Monica Piras,**[‡] **Luca Medda,**[†] **Daniela Steri,**[†] **Marco Piludu,**[‡] **Andrea Salis,*,**[†] **and Maura Monduzzi*,**[†]

Dipartimento di Scienze Chimiche, Università di Cagliari-CSGI and CNBS, Cittadella Universitaria, S.S. 554 bivio Sestu, 09042-Monserrato (CA), Italy, and Dipartimento di Citomorfologia, Università di Cagliari, Cittadella Universitaria, S.S. 554 bivio Sestu, 09042-Monserrato (CA), Italy

Received: August 18, 2010; Revised Manuscript Received: October 12, 2010

Ordered mesoporous materials (OMMs) are interesting matrixes for nanomedicine applications such as innovative drug delivery systems. Here, we compare the behavior of the widely studied SBA-15 mesoporous silica with that of the less investigated MSE (a periodic mesoporous organosilica whose silicon atoms are alternatively connected by means of $-Si-O-Si-$ and $-Si-CH_2-CH_2-Si-$ groups) toward the adsorption (pH 7.0 and 9.6) and in vitro release (pH 7.4; $T = 37$ °C) of an antimicrobial protein (hen egg white lysozyme). Both OMMs have a hexagonal ordered mesoporous structure and texture, as confirmed by SAXS, TEM, and N_2 adsorption isotherms, but differ for the chemical composition and surface charge density, as determined by ATR-FTIR spectroscopy and potentiometric titrations, respectively. Rather than the structural and textural features, the different chemical composition of SBA-15 and MSE seems to be responsible for the different lysozyme loading and release and for the different stability toward the lixiviating action of the physiological medium (pH 7.4; $T = 37$ °C).

1. Introduction

Ordered mesoporous materials (OMMs) have outstanding textural and structural features[1] that make them suitable hosts for bioactive molecules.[2] They have high surface area (about 1000 m^2/g) and a highly ordered, and hence a highly reproducible structure, with uniform pore size (2−50 nm) which is comparable with the diameter of many biomacromolecules. Most previous work concerning the use of OMMs as sorbents for biomacromolecules was aimed to stably immobilize an enzyme into the pores to obtain a stable and active biocatalyst[3,4] for potential industrial,[5,6] environmental,[7] or biosensing applications.[8]

Innovative emerging applications are the use of OMMs in different nanomedicine topics, namely, carriers for the release of drugs and bioactive agents[9] and tissue engineering.[10] The use of OMMs for biocatalysis or release depends on the fact that the interaction between the macromolecule and the sorbent surface is strong or weak, respectively. Consequently, given a bioactive agent, the chemical surface of the sorbent material has an important effect on the strength of the interaction and hence on the possible application.[5] In addition, it is relevant that the OMM's surface can be easily modified by a wide number of suitable functionalizing agents[11,12] that allow for tailoring of the sorbent surface to get the desired, weak or strong, interaction with the adsorbing molecule.[13] Moreover, the surface interaction can be modulated by the suitable choice of the pH,[4,14] the ionic strength,[14] and also the type of salt[15,16] of the adsorbing solution.

SBA-15 and similar materials have been studied as delivery systems for different locations. Most researchers focused attention on oral therapy, studying the controlled release of ibuprofen,[17] nimodipine,[18] itraconazole,[19] and many poorly soluble drugs.[20] Vallet-Regì and co-workers, taking advantage of the bioactive behavior of mesoporous silica, which can be covered by a layer of hydroxyapatite[21,22] and thus used as bioceramics for bone tissue regeneration,[10] deeply studied the local release of drugs for bone disease.[12,23−26] Lopez et al. used ordered mesoporous silica for the storage and release of valproic acid and sodic phenytoin in the brain of rats.[27]

An important issue for the use of OMMs as drug delivery systems concerns their toxicity and biocompatibility. Hudson et al. found that subcutaneous injection of some OMMs in rats resulted in a general good biocompatibility as determined through histological investigations. In contrast, intraperitoneal and intravenous injections in mice produced fatal events.[28]

Another key point for the application of OMMs in drug delivery systems is the stability of the matrix in the releasing medium. Very recently, Izquierdo-Barba et al. investigated the stability of SBA-15 like materials in selected aqueous media mimicking body fluids. They found that, although the mesoporous structure of SBA-15 was partially lost after 60 days in all tested media, organically modified SBA-15 samples exhibited a higher resistance to lixiviation.[29]

Here, we report the characterization through TEM, SAXS, N_2 adsorption/desorption isotherms, ATR-FTIR, and potentiometric titrations of two different OMMs, namely, SBA-15 and MSE, and their use for the adsorption and the in vitro release of an antimicrobial protein, hen egg white lysozyme (Lyz), in physiological conditions (pH = 7.4, $T = 37$ °C). The effect of the different chemical surface and the adsorbing pH is investigated. Besides the structural features, it will be shown that the different material surfaces can affect both the loading amount and the kinetics of the release. Finally, a comparison of the stability of the two matrixes toward the lixiviation effect of the release medium is presented.

* To whom correspondence should be addressed. Tel.:+39 070 6754362. Fax: +39 070 6754388. E-mail: asalis@unica.it (A.S.); monduzzi@unica.it (M.M.).
† Università di Cagliari-CSGI and CNBS.
‡ Università di Cagliari.
§ Both authors contributed equally to this paper.

Lysozyme Adsorption and Release from OMMs

J. Phys. Chem. C, Vol. 114, No. 47, 2010 **19929**

2. Experimental Details

2.1. Chemicals. Chemicals for the synthesis and modification of OMMs, tetraethylorthosilicate (TEOS, 98%), pluronic copolymer 123 ($EO_{20}PO_{70}EO_{20}$), 1,2-bis(trimethoxysilyl)ethane (BTMSE) (96%) and buffer components, sodium hydrogencarbonate (99%), Na_2HPO_4 (99%), and NaH_2PO_4 (99%), were purchased from Sigma−Aldrich. Lysozyme from hen egg white (92717 U/mg) was purchased from Fluka.

2.2. Characterization of OMMs and Lysozyme. SBA-15 mesoporous silica and MSE mesoporous organosilica were synthesized according to the methods reported in refs 30 and 31, respectively. SBA-15 and MSE were characterized with the following techniques. SAXS patterns were recorded (2400 s) with a S3-MICRO SWAXS camera system (HECUS X-ray Systems, Graz, Austria). Cu Kα radiation of wavelength 1.542 Å was provided by a GeniX X-ray generator, operating at 50 kV and 1 mA. A 1D-PSD-50 M system (HECUS X-ray Systems, Graz, Austria) containing 1024 channels of width 54.0 μm was used for the detection of scattered X-rays in the small-angle region. Transmission electron microscopy (TEM) images were obtained on a JEOL 100S microscope. Finely ground samples were placed directly onto Formvar-coated electron microscopy nichel grids. Textural analysis was carried out on a Thermoquest-Sorptomatic 1990 by determining the N_2 adsorption/desorption isotherms at 77 K. Before analysis, the sample was outgassed overnight at 40 °C. The specific surface area, the total pore volume, and the pore size distribution were assessed by the BET[32] and BJH[33] (calculated from both adsorption and desorption branches) methods. ATR-FTIR studies were conducted with a Bruker Tensor 27 spectrophotometer equipped with a diamond-ATR accessory and DTGS detector. A number of 128 scans at a resolution of 4 cm^{-1} were averaged from wavenumber 4000 to 400 cm^{-1}. The Opus spectroscopic software was used for data handling. Surface charge densities of SBA-15 and MSE were determined through potentiometric titrations according to the procedure reported in ref 15. The theoretical titration curve of lysozyme and the corresponding theoretical pI were obtained through PROPKA 2.0 software.[34,35] Lysozyme images in Figure 5a−d were made with VMD software support. VMD is developed with NIH support by the Theoretical and Computational Biophysics group at the Beckman Institute, University of Illinois at Urbana−Champaign.

2.3. Loading of Lysozyme. To load lysozyme on SBA-15 and MSE, 0.2 g of the mesoporous sample was suspended in 10 mL of an aqueous solution of lysozyme (10 mg/mL) prepared in 10 mM phosphate buffer (pH 7.0) or 10 mM sodium hydrogencarbonate buffer at pH 9.6 and soaked for 96 h with shaking at 100 rpm and 37 °C. The concentration of lysozyme was measured by an UV spectrophotometer at a wavelength of 280 nm. The amount of lysozyme loaded onto the samples was determined according to the change of concentration before and after soaking. After loading, the powders were quickly and thoroughly washed with water and dried under vacuum. The loading of lysozyme, L_{Lyz} (mg/g), on mesoporous material was calculated according the following formula

$$L_{Lyz} = \frac{[Lyz_i]V - [Lyz_r]V - [Lyz_w]V_w}{m_s} \qquad (1)$$

where [Lyz_i] is the protein concentration in the initial solution (mg$_{Lyz}$/mL$_{solution}$), [Lyz_r] is the residual concentration of protein in solution (mg$_{Lyz}$/mL$_{solution}$), [Lyz_w] is the protein concentration determined in the washing solution (mg$_{Lyz}$/mL$_{solution}$), V is the
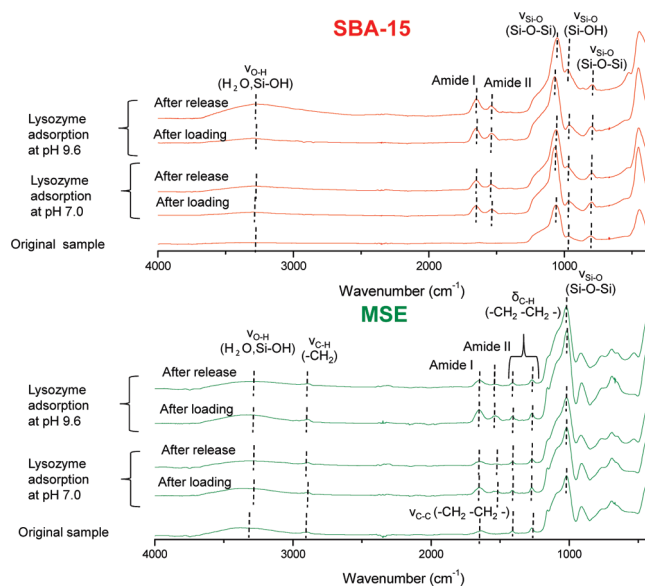
Figure 1. ATR-FTIR spectra of original OMMs after lysozyme loading (pH 7 and 9.6) and release (T = 37 °C and pH 7.4).

volume of the lysozyme solution (mL), V_w is the washings volume (mL), and m_s is the mass of the support (g).

2.4. In Vitro Lysozyme Release Studies. The in vitro lysozyme release from the loaded materials was studied in phosphate buffer solution (PBS) (pH 7.4, 50 mM) by suspending 50 mg of lysozyme-loaded SBA-15 (or MSE) in 100 mL of PBS and maintaining it at 37 °C in an orbital shaker (100 rpm). These experimental conditions were chosen according to what was previously reported.[36] At fixed time intervals, 5 mL of the release medium was withdrawn, and an identical volume of a fresh PBS solution was added to maintain sink conditions. The lysozyme concentration in each of the collected samples was measured at 280 nm using a Cary UV−Vis spectrophotometer. The amount of lysozyme released at time t, M_t, was determined from the appropriate calibration line (with an absorption coefficient ε_{280} = 2.803 mL mg^{-1} cm^{-1}). The total amount of lysozyme incorporated in the material was taken as M_0; thus, the percentage of the lysozyme released was expressed as M_t/M_0 (%). An exponential decay model was used for the fitting of the experimental data according to ref 13.

$$\frac{M_t}{M_0} (\%) = A(1 - e^{-k_1 t}) \qquad (2)$$

where A is the maximal mass percentage released and k_1 is the release rate constant. The correlation coefficient (r) was calculated to evaluate the accuracy of the fitting procedure.

3. Results and Discussion

3.1. OMMs and Protein Characterization. *3.1.1. OMM Characterization.* The two investigated OMMs present a different surface from the chemical point of view. SBA-15 is a silica-based mesoporous structure; hence, its surface is constructed of silanols. MSE is a periodic mesoporous organosilica, whose synthesis consists of silicon atoms alternatively connected through −Si−O−Si− and −Si−CH$_2$−CH$_2$−Si− groups. The presence of the methylene groups confers a higher hydrophobic character to the MSE material compared to that of SBA-15. The different chemical composition of OMMs was qualitatively confirmed by ATR-FTIR spectroscopy (Figure 1). Both materi-

Figure 2. TEM images of OMMs. (a,b) Original SBA-15; (c) SBA-15 sample after Lyz release; (d,e) orginal MSE; (f) MSE sample after Lyz release.

Figure 3. SAXS pattern of original OMMs after lysozyme loading (at pH 7.0 and 9.6) and after in vitro release (pH 7.4, $t = 37$ °C).

TABLE 1: Characterization of OMMs Obtained Through N_2 Adsorption/Desorption Isotherms and SAXS

	$S_{BET}{}^a$ (m²/g)	$V_p{}^b$ (cm³/g)	$d_{BJH}{}^c$ (Å)	$d_{BJH}{}^d$ (Å)	a^e (Å)
SBA-15	718	1.2	86	65	112
MSE	1752	2.2	76	58	119

[a] Specific surface area calculated by the BET method. [b] Cumulative pore volume. [c] Pore diameter calculated by applying the BJH method to the data of the adsorption branch. [d] Pore diameter calculated by applying the BJH method to the data of the desorption branch. [e] Lattice parameter calculated by the equation $a = 2d_{100}/\sqrt{3}$, where d_{100} is the spacing of the (100) plane of the hexagonal (p6mm) array of pores.

with a steep increase typical of mesoporous solids at a relative pressure around 0.70−0.75 (Figure 4a). The presence of a hysteresis cycle, defined by IUPAC as H1, is closely associated with channel-like mesopores.[37] Table 1 reports the specific surface area (S_{BET}) and the total pore volume (V_p), calculated by the BET method.[32] SBA-15 has $S_{BET} = 718$ m²/g and $V_p = 2.1$ cm³/g; a very high value of the surface area, $S_{BET} = 1752$ m²/g, and $V_p = 2.2$ cm³/g are obtained for MSE. The pore size distribution (d_{BJH}) of the materials was calculated from both adsorption and desorption branches of the isotherms through the BJH model. A $d_{BJH} = 86$ Å (adsorption branch) and $d_{BJH} = 65$ Å were obtained for SBA-15, whereas a $d_{BJH} = 76$ Å and $d_{BJH} = 58$ Å were obtained for MSE. Although the BJH model is known to underestimate the diameter of the mesopores, it is still the most used calculation method because software using more accurate models (i.e., NLDFT)[38] is not easily available.

The last characterization of the OMMs was the determination of surface charge density as a function of pH, which was carried out through potentiometric titration; the results are displayed in Figure 4b. The SBA-15 surface is practically neutral from pH 3 to pH 5−6, whereas at higher pH, it becomes negatively charged due to the acidic behavior of surface silanols. According to its hydrophobic nature, the surface charge density of MSE is practically zero up to pH 7; then, it becomes only slightly negatively charged at basic pH (>8) values.

3.1.2. Protein Characterization. The protein used for this work was hen egg white lysozyme (E.C.3.1.1.17). Lysozyme

als present an intense band at 1070 cm⁻¹ due to Si−O stretching, one less intense at 450 cm⁻¹ due to Si−O−Si bending, and also a band at 950 cm⁻¹ due to silanols. In addition, MSE shows bands due to stretching vibrations at 2916 (ν_{C-H}) and 1645 cm⁻¹ (ν_{C-C}) and to bending vibrations (δ_{C-H}) at 1412 and 1271 cm⁻¹.

Figure 2 shows the TEM micrographs of the two materials. For SBA-15, the side view (Figure 2a) shows that the material is constructed of cylindrical channels, and the top view (Figure 2b) shows the ordered hexagonal array of the pores. MSE particles (Figure 2d and e) were less regular than those of SBA-15, but the ordered hexagonal structure can clearly be seen also in this case.

SAXS analysis carried out on OMMs shows the typical pattern of a hexagonal phase where a strong peak due to the (100) plane and other two weak peaks due to the (110) and (200) planes occur (Figure 3). From SAXS measurements, the lattice spacing (a) of the two structures was determined; this was 112 Å for SBA-15 and 119 Å for MSE (Table 1).

The OMMs were then characterized through N_2 adsorption/desorption isotherms. Both samples show a type IV isotherm,

Lysozyme Adsorption and Release from OMMs

J. Phys. Chem. C, Vol. 114, No. 47, 2010 **19931**

Figure 4. Characterization of SBA-15 and MSE. (a) N_2 adsorption/desorption isotherms; (b) surface charge density versus pH.

belongs to the family of hydrolases that, thanks to its biological function (the hydrolysis of polysaccharides constituting the bacterial cell wall), can be used as an antimicrobial agent. It is a globular protein consisting of 129 residues (MW = 14.3 kDa) in the form of five α-helices, three antiparallel β-sheets, and a large number of random coils and β-turns. Four disulfide bridges are responsible for the stabilization of the structure of the protein that displays an ellipsoidal shape with a large cleft acting as the active site. Its dimensions (19 × 25 × 43 Å) allow for the adsorption into the pores of both investigated materials.

As shown below, the adsorption and the release processes of Lyz are strongly dependent on the intermolecular interactions between the protein and OMM surfaces. Hence, the composition and disposition of amino acid residues of Lyz, shown in Figure 5, play a fundamental role. Charged amino acids are mainly located on the protein surface, the basic amino acids being more abundant (Figure 5a) than the acidic ones (Figure 5b). Uncharged amino acids are more abundant than those with charge; clearly, nonpolar residues are less exposed at the hydrophilic external surface with respect to polar amino acids, as illustrated in Figure 5c and d. Figure 5e reports the number of different types of amino acids (basic, acidic, polar, and nonpolar). The presence of a higher number of basic residues with respect to acidic residues is reflected in the high isoelectric point of the protein ($pI \approx 11$) and by the theoretical protein charge as a function of pH reported in Figure 5f.

3.2. Adsorption of Lysozyme on OMMs. The adsorption of Lyz on the two OMMs matrixes was carried out by suspending a weighed amount of the material in a Lyz solution at 37 °C. The effect of pH was also investigated by dissolving lysozyme powder in two different buffer solutions at pH 7.0 and 9.6. The higher pH was chosen because the maximal loading is usually obtained in proximity of the protein isoelectric point.[4,39] Unfortunately we could not use pH 11 because, at a so high pH, silica becomes soluble in the solution. Hence, pH 9.6 was chosen as the best compromise between these two exigencies.[40] Lyz adsorption was determined through UV spectroscopy (λ = 280 nm), and loading was calculated, according to eq 1, as the difference between the protein concentration in the buffer solution at the beginning and at the end of the adsorption process.
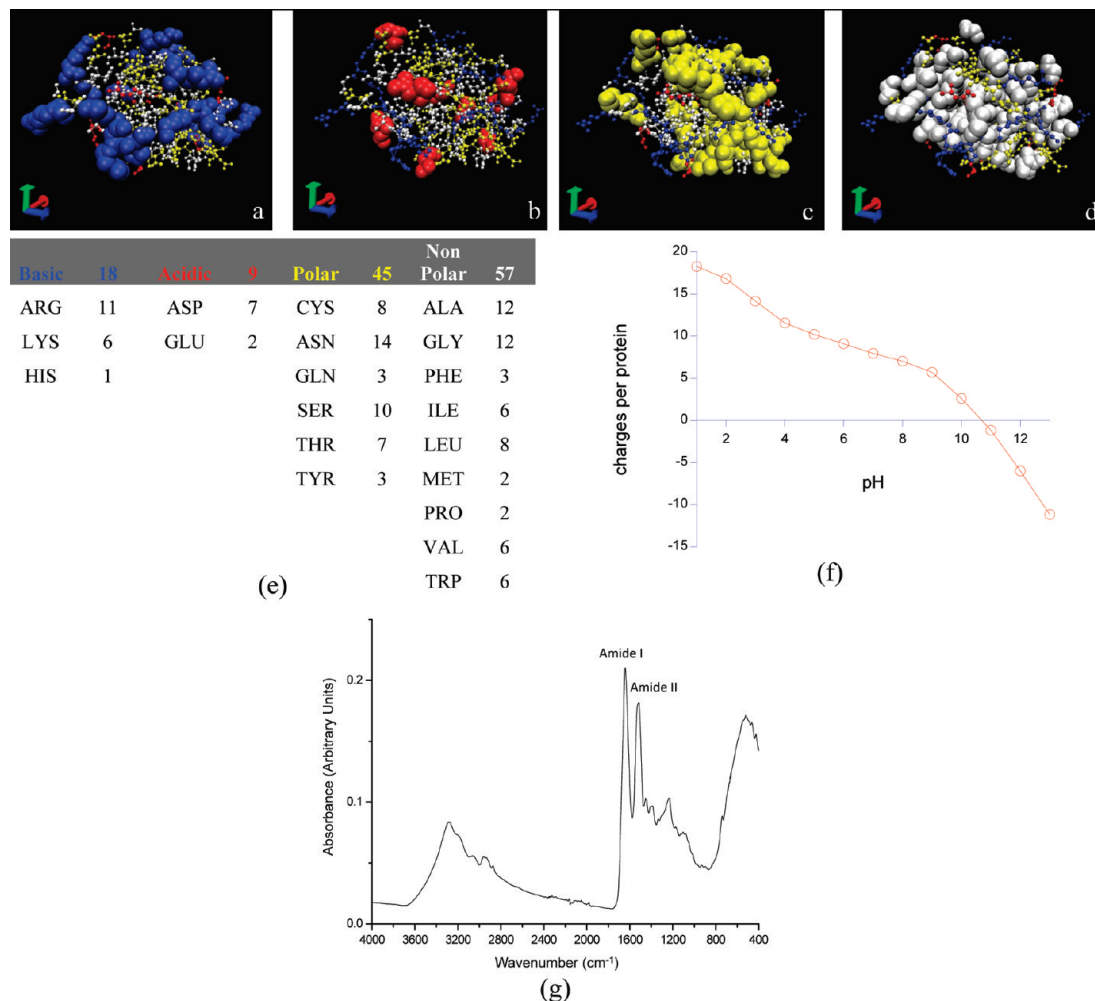
The adsorption of lysozyme on the OMMs was also qualitatively demonstrated by means of ATR-FTIR spectroscopy. FTIR spectrum of free lysozyme shows the two typical bands of proteins, namely, amide I at 1643 cm^{-1}, and amide II at 1522 cm^{-1} (cf. Figure 5g). The same bands, although a bit shifted in frequency (amide I: 1653 cm^{-1}; amide II: 1537 cm^{-1}), occur in the spectra of the Lyz-loaded OMMs, as shown in Figure 1.

The experimental results for Lyz loading on the OMMs at pH 7.0 and 9.6 are reported in Table 2. Lyz loading at pH 7.0 was 587 mg/g for SBA-15 and 450 mg/g for MSE, whereas at pH 9.6, it was 646 mg/g for SBA-15 and 500 mg/g for MSE. These results deserve some comments. The physicochemical properties of the adsorbing material, both electrochemical (surface charge density and hydrophilic/hydrophobic character) and textural (pore size, pore volume, and surface area) properties should be considered to explain the obtained results.

Let us consider the experimental surface charge densities (σ) of OMMs at pH 7.0 and 9.6 (see Table 2) and the lysozyme theoretical charge (+8.0 at pH 7.0, and +3.7 at pH 9.6) taken by the graph shown in Figure 5f. Electrostatic forces seem to be the leading interactions in the adsorption of positively charged Lyz on negatively charged SBA-15. At pH 9.6, a higher loading is obtained due to the lower electrostatic repulsion among lysozyme molecules.[4] If electrostatics was the only type of intermolecular interaction involved, the low charge carried by MSE at both pH values, due to its hydrophobic character, would lead to a very low loading of lysozyme. Nevertheless, although lower than that of SBA-15, MSE reached a quite high loading likely due to the establishment and the action of nonelectrostatic forces (i.e., van der Waals and, particularly, London forces) between hydrophobic groups at MSE and lysozyme surfaces.

Besides, the ionic strength of the adsorbing solution and of the release medium can have important effects. Hudson et al. showed that increasing the ionic strength disfavored the adsorption of cytochrome c and xylanase on SBA-15, whereas an initial decrease followed by an increase was observed for the same enzyme on MSE.[14] Essa et al. showed that the effect of ionic strength is not univocal for a protein/adsorbent pair (i.e., myoglobin/SBA-15), but different results are obtained at different adsorbing pHs.[39] Very recently, we found that lysozyme adsorption on functionalized SBA-15 depends not only on the ionic strength of the solution but also on the type of salt. We could order the effectiveness of anions and cations on promoting protein adsorption according to the Hofmeister series.[16] The involved phenomena are complicated but can be easily explained invoking Collins' empirical law of matching water affinities.[41] Briefly, ionic strength can either promote or disfavor adsorption, depending on the nature (dispersion and/or electrostatic) of protein−adsorbent interactions.

Concerning the textural properties, pore size is an important parameter that can affect protein adsorption. Serra et al. investigated the immobilization of *Candida antarctica* lipase B on OMMs having different pore sizes.[37] They found that, during the adsorption process, diffusion limitations occurred when the pore size was similar to the enzyme size, but these

Basic	18	Acidic	9	Polar	45	Non Polar	57
ARG	11	ASP	7	CYS	8	ALA	12
LYS	6	GLU	2	ASN	14	GLY	12
HIS	1			GLN	3	PHE	3
				SER	10	ILE	6
				THR	7	LEU	8
				TYR	3	MET	2
						PRO	2
						VAL	6
						TRP	6

(e)

(f)

(g)

Figure 5. Hen egg whyte lysozyme characterization by taking the amino acid composition available at the protein data bank (1LYZ.pdb). Structural representation of the amino acid residues by using VMD (video molecular dynamics) of (a) basic amino acids, (b) acidic amino acids, (c) polar (uncharged) amino acids, (d) nonpolar amino acids. (e) Number of amino acids of different classes. (f) Theoretical titration curve of lysozyme obtained through the PROPKA 2.0 software. (g) ATR-FTIR spectrum.

TABLE 2: Lysozyme Loading and Release Parameters on OMMs and Their Surface Charge Densities (σ) at the Adsorption pH

OMM	adsorption pH	σ (charges/nm^2)	$L_{Lyz}{}^a$ (mg/g)	A^b(%)	$k_1{}^c$ ($\times 10^{-6}$ s^{-1})	r^d	$a_{ads}{}^e$ (Å)	$a_{ref}{}^f$ (Å)
SBA-15	7	−1.6	587 ± 63	43 ± 2	5 ± 0.8	0.986	116	121
SBA-15	9.6	−12.0	646 ± 34	46 ± 2	14 ± 3	0.958	117	119
MSE	7	−0.2	450 ± 48	17.2 ± 0.3	139 ± 28	0.990	119	119
MSE	9.6	−0.7	500 ± 50	28.6 ± 0.5	81 ± 8	0.989	119	119

^{a} Loading of adsorbed lysozyme. ^{b} Maximal amount of released lysozyme. ^{c} Release rate constant. ^{d} Correlation coefficient. ^{e} Lattice parameter after lysozyme adsorption. ^{f} Lattice parameter after lysozyme release.

disappeared when the pore diameter was around twice the largest enzyme dimension. On the basis of these findings and OMM's pore size (Table 1), we would expect an easier adsorption due to faster mass diffusion of lysozyme (dimensions: 19 × 25 × 43 Å) in SBA-15 compared to that in MSE. In any case, because we carried out the adsorption process for a long time (96 h), even a very slow diffusion should take place. Concerning the other textural properties, the surface area and the pore volume are higher for MSE than that for SBA-15 and should lead to a higher loading for the former compared to the latter. Exactly the opposite occurs (see Table 2), likely because enzyme molecules occupy a small fraction of the total volume and surface.[37]

It can be substantially concluded that the obtained loadings are mainly due to surface properties (charges and hydrophobic/hydrophilic character) rather than to textural properties.

3.3. Release of Lysozyme. In vitro release of Lyz from OMMs was carried out, for about 30 days, in a phosphate buffer solution at physiological pH (7.4) and 37 °C.[36] Samples were withdrawn at fixed times and analyzed by UV spectroscopy. Experimental results of release, shown in Figure 6, were fitted by means of eq 2, which allowed determination of the maximal mass percentage released A and the release rate constant k_1. These data are listed in Table 2. A very different behavior between MSE and SBA-15, also modulated by the adsorption pH, was observed. SBA-15 is the material that releases the highest percentage of Lyz ($A_{pH\,9.6} = 46\%$; $A_{pH\,7.0} = 43\%$) followed by MSE ($A_{pH\,9.6} = 28.6\%$; $A_{pH\,7.0} = 17.2\%$). The maximal amount of release is higher for samples where Lyz was adsorbed at pH 9.6 both for SBA-15 and MSE.

Table 2 reports also the kinetic release constants k_1 as determined by the fitting procedure of the experimental data.

Lysozyme Adsorption and Release from OMMs

J. Phys. Chem. C, Vol. 114, No. 47, 2010 **19933**
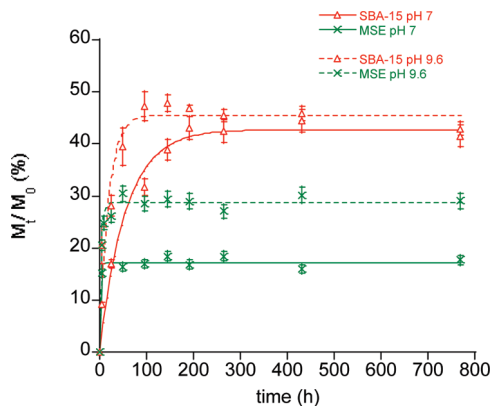
Figure 6. Release of lysozyme from OMMs (pH 7.4, $T = 37$ °C).

Lyz molecules adsorbed on MSE were released faster ($k_1 = 139 \, \mu s^{-1}$ at pH 7.0; $k_1 = 81 \, \mu s^{-1}$ at pH 9.6) than those adsorbed on SBA-15 ($k_1 = 5 \, \mu s^{-1}$ at pH 7.0; $k_1 = 14 \, \mu s^{-1}$ at pH 9.6).

The fact that more than 50% of adsorbed lysozyme was not released is not surprising. The reason is evidently due to the strength of the interactions between the surfaces of the protein and the hosting material. Indeed, there are several works in which enzymes are immobilized by physical adsorption for biocatalytic purposes.[3,8,14,42,43] In those works, desorption is an unwanted effect that is different than what is needed for release studies. The amount of lysozyme released depends on the choice of the protein−adsorbent pair. Very recently, Nieto et al. found that the amount of released BSA was strongly dependent on the chemical groups present on the SBA-15 surface.[13]

Here, although electrostatic interactions lead to a higher Lyz loading with SBA-15, this kind of interaction is not able to retain the protein when in contact with the releasing medium. A rather burst release occurs. On the other hand, nonelectrostatic forces, responsible for lysozyme adsorption on the more hydrophobic MSE, are likely to adsorb more strongly than protein molecules that, hence, are less available for release. There is also a modulation effect due to the adsorption pH that increases both the loading and release as it approaches the isoelectric point of the protein. The higher release rates observed for MSE matrixes at both pHs, compared to SBA-15, are likely to be due to the high burst release of Lyz adsorbed on the outer surface of the MSE particles. Nevertheless, it can be remarked that burst release from MSE occurs at a much lower extent (and for a much shorter time) than that from SBA-15.

Another effect, not investigated here, might be obtained with other release medium. In the literature, different media having the same pH but higher ionic strength (i.e., 0.9% NaCl)[13] or SBF (simulated body fluid) have been used.[44] We may expect that a change in the ionic strength, and also the ionic composition, of the release medium would strongly affect both the release trends and the material stability.[29] For example, if the lysozyme−SBA-15 interaction is mainly based on electrostatics, we might expect an increased release at higher ionic strength due to salt adsorption at the protein and adsorbent charged groups. The opposite effect would be expected for MSE due to the hydrophobic interaction with lysozyme. In any case, the effects observed here, due to different chemical composition of the adsorbent and a different pH of adsorption, are quite remarkable since they affect the amount and the rate of lysozyme release.

3.4. OMM Stability in the Release Medium. The stability of OMM samples after 32 days of in vitro release in the release medium (pH 7.4 and 37 °C) was studied through FTIR, SAXS,

and TEM. FTIR analysis (Figure 1) shows that there is no appreciable change in the OMM spectra after release with respect to those after lysozyme loading at the two pH values (7.0 and 9.6). The amide I and amide II bands are still present according to the fact that a substantial amount of lysozyme molecules is still adsorbed in the matrixes.

In fact, looking at TEM micrographs (Figure 2c and f), it appears that the ordered structure of SBA-15 is partially destroyed due to the lixiviation action of the physiological medium. Effects at much lower extent are observed for MSE, which seems to be more resistant toward lixiviation. A similar result was found by Izquierdo-Barba et al., who focused on the in vitro stability of SBA-15 in different physiological media.[29]

Matrix lixiviation observed by TEM was furthermore confirmed by SAXS measurements. Figure 3 shows that a significant decrease of the intensity of the second- and third-order diffraction peaks occurs after Lyz release experiments. This could be due to the partial loss of the ordered hexagonal structure. This intensity loss was less important for MSE, in agreement with the lower degree of dissolution of the matrix observed in TEM pictures. Moreover, the comparison between the lattice parameters, obtained from SAXS analysis, reported in Tables 1 and 2, points out an interesting result; the original SBA-15 has a lattice parameter of 112 Å that increases to 116 Å after Lyz adsorption at pH 7 (117 Å at pH 9.6) and to 121 Å after Lyz release (119 Å at pH 9.6). On the contrary, MSE retains a constant lattice parameter of 119 Å during all steps of the study, thus confirming its higher resistance to the lixiviating action of both the adsorption and the release media.

From these results, besides the initial burst release due to Lyz adsorbed on the outer surface of both OMMs, a different mechanism of lysozyme release from the two matrixes can be suggested. Indeed, in the case of SBA-15, Lyz release is enhanced by the swelling of the channels due to the nucleophilic attack of water to siloxane groups, whereas for MSE, release is mainly due to the diffusion of Lyz molecules outside of the pores.

As a matter of fact, Izquierdo-Barba et al. found that the functionalization of the SBA-15 surface was a good procedure to enhance the structural stability.[29] Here, the use of a more hydrophobic structure, without the need of any post synthesis functionalization, allowed a similar result to be reached.

4. Conclusions

The present work focuses on two OMMs having similar structure and texture but different chemical composition and surface properties. These OMMs can be used for the adsorption and the release of lysozyme, a therapeutic protein. Among others, a peculiar advantage of these OMMs is the narrow range of pore sizes that constitutes the crucial size-selective parameter to address guest molecules adsorption. The use of BTMSE as the organosilica precursor produces the MSE OMM that shows a hexagonal matrix as well as SBA-15, but with a slightly smaller pore size and larger surface area. It should be remarked that the small reduction of the pore size does not prevent the adsorption of protein molecules whose maximal dimension is 43 Å. Indeed, this fact does not modify Lyz loading significantly, although the very different nature of the surface, in terms of surface charge, also implies different types of host−guest (surface−protein) interactions. The van der Waals interactions, mainly involved in the adsorption/release process at the Lyz/MSE interface, seem to produce stronger protein binding than the electrostatic forces that dominate the Lyz/SBA-15 interface. As a matter of fact, this strong protein binding in the Lyz-loaded

MSE matrix decreases both the time over which burst release occurs and the released amount of protein significantly. It is remarkable that a short burst release, in all cases, suggests that only a small amount of adsorbed protein is located on the outer surface of the OMM particle. Another very significant parameter that affects both adsorption and release is the pH of the adsorbing solution. This allows for a potential modulation of the global performance, in terms of the loaded amount of protein, and the rate of release. In other words, a personalized sustained release may be produced. Another important consideration concerns the longer shelf life in the physiological medium observed for MSE compared to that for SBA-15. Silica materials tend to dissolve in biological fluids, and this can develop toxicity when accumulation above certain concentrations occurs.[28] Hence, if a silica-based drug delivery system has to be projected in view of possible innovative applications (cf. protein drug delivery) and performances (cf. sustained release), it is relevant to introduce structural features that can prolong the shelf life and attenuate dangerous, though not fatal, side effects.

Finally, the last comment in favor of the MSE OMM being used as a sustained drug release carrier is given by the relatively easy and reproducible synthesis; this is a peculiar feature of all OMMs that does not involve any postsynthesis functionalization step.

References and Notes

(1) Davis, M. E. *Nature* **2002**, *417*, 813.
(2) Hudson, S.; Cooney, J.; Magner, E. *Angew. Chem., Int. Ed.* **2008**, *47*, 8582.
(3) Hartmann, M.; Jung, D. *J. Mater. Chem.* **2009**, *20*, 844.
(4) Salis, A.; Meloni, D.; Ligas, S.; Casula, M. F.; Monduzzi, M.; Solinas, V.; Dumitriu, E. *Langmuir* **2005**, *21*, 5511.
(5) Salis, A.; Bhattacharyya, M. S.; Monduzzi, M.; Solinas, V. *J. Mol. Catal. B: Enzym.* **2009**, *57*, 262.
(6) Salis, A.; Casula, M. F.; Bhattacharyya, M. S.; Pinna, M.; Solinas, V.; Monduzzi, M. *ChemCatChem* **2010**, *2*, 322.
(7) Salis, A.; Pisano, M.; Monduzzi, M.; Solinas, V.; Sanjust, E. *J. Mol. Catal. B: Enzym.* **2009**, *58*, 175.
(8) Hartmann, M. *Chem. Mater.* **2005**, *17*, 4577.
(9) Wang, S. *Microporous Mesoporous Mater.* **2009**, *117*, 1.
(10) Vallet-Regí, M. *J. Intern. Med.* **2009**, *267*, 22.
(11) Rosenholm, J. M.; Lindén, M. *Chem. Mater.* **2007**, *19*, 5023.
(12) Nieto, A.; Balas, F.; Colilla, M.; Manzano, M.; Vallet-Regí, M. *Microporous Mesoporous Mater.* **2008**, *116*, 4.
(13) Nieto, A.; Colilla, M.; Balas, F.; Vallet-Regi, M. a. *Langmuir* **2010**, *26*, 5038.
(14) Hudson, S.; Magner, E.; Cooney, J.; Hodnett, B. K. *J. Phys. Chem. B* **2005**, *109*, 19496.
(15) Salis, A.; Parsons, D. F.; Bostrom, M.; Medda, L.; Barse, B.; Ninham, B. W.; Monduzzi, M. *Langmuir* **2010**, *26*, 2484.
(16) Salis, A.; Bhattacharyya, M. S.; Monduzzi, M. *J. Phys. Chem. B* 2010.
(17) Song, S. W.; Hidajat, K.; Kawi, S. *Langmuir* **2005**, *21*, 9568.
(18) Yu, H.; Zhai, Q.-Z. *Microporous Mesoporous Mater.* **2009**, *123*, 298.
(19) Mellaerts, R.; Houthoofd, K.; Elen, K.; Chen, H.; Van Speybroeck, M.; Van Humbeeck, J.; Augustijns, P.; Mullens, J.; Van den Mooter, G.; Martens, J. A. *Microporous Mesoporous Mater.* **2010**, *130*, 154.
(20) Van Speybroeck, M.; Barillaro, V.; Thi, T. D.; Mellaerts, R.; Martens, J.; Van Humbeeck, J.; Vermant, J.; Annaert, P.; Van den Mooter, G.; Augustijns, P. *J. Pharm. Sci.* **2009**, *98*, 2648.
(21) Díaz, A.; López, T.; Manjarrez, J.; Basaldella, E.; Martínez-Blanes, J. M.; Odriozola, J. A. *Acta Biomater.* **2006**, *2*, 173.
(22) Andersson, J.; Areva, S.; Spliethoff, B.; Lindén, M. *Biomaterials* **2005**, *26*, 6827.
(23) Vallet-Regi, M.; Ràmila, A.; del Real, R. P.; Pérez-Pariente, J. *Chem. Mater.* **2001**, *13*, 308.
(24) Doadrio, A. L.; Doadrio, J. C.; Sánchez-Montero, J. M.; Salinas, A. J.; Vallet-Regí, M. *Microporous Mesoporous Mater.* **2010**, *132*, 559.
(25) Doadrio, A. L.; Sousa, E. M. B.; Doadrio, J. C.; Pérez Pariente, J.; Izquierdo-Barba, I.; Vallet-RegI, M. *J. Controlled Release* **2004**, *97*, 125.
(26) Colilla, M.; Manzano, M.; Vallet-Regí, M. *Int. J. Nanomed.* **2008**, *4*, 403.
(27) López, T.; Basaldella, E. I.; Ojeda, M. L.; Manjarrez, J.; Alexander-Katz, R. *Opt. Mater.* **2006**, *29*, 75.
(28) Hudson, S. P.; Padera, R. F.; Langer, R.; Kohane, D. S. *Biomaterials* **2008**, *29*, 4045.
(29) Izquierdo-Barba, I.; Colilla, M.; Manzano, M.; Vallet-Regí, M. *Microporous Mesoporous Mater.* **2010**, *132*, 442.
(30) Zhao, D.; Feng, J.; Huo, Q.; Melosh, N.; Fredrickson, G. H.; Chmelka, B. F.; Stucky, G. D. *Science* **1998**, *279*, 548.
(31) Bao, X. Y.; Zhao, X. S.; Li, X.; Chia, P. A.; Li, J. *J. Phys. Chem. B* **2004**, *108*, 4684.
(32) Brumaner, S.; Emmet, P. H.; Teller, E. *J. Am. Chem. Soc.* **1938**, *60*, 309.
(33) Barret, E. P.; Joyner, L. G.; Halenda, P. P. *J. Am. Chem. Soc.* **1951**, *73*, 373.
(34) Li, H.; Robertson, A. D.; Jensen, J. H. *Proteins* **2005**, *61*, 704.
(35) Bas, D. C.; Rogers, D. M.; Jensen, J. H. *Proteins* **2008**, *73*, 765.
(36) Izquierdo-Barba, I.; Vallet-Regí, M.; Kupferschmidt, N.; Terasaki, O.; Schmidtchen, A.; Malmsten, M. *Biomaterials* **2009**, *30*, 5729.
(37) Serra, E.; Mayoral, Á.; Sakamoto, Y.; Blanco, R. M.; Díaz, I. *Microporous Mesoporous Mater.* **2008**, *114*, 201.
(38) Ravikovitch, P. I.; Wei, D.; Chueh, W. T.; Haller, G. L.; Neimark, A. V. *J. Phys. Chem. B* **1997**, *101*, 3671.
(39) Essa, H.; Magner, E.; Cooney, J.; Hodnett, B. K. *J. Mol. Catal. B: Enzym.* **2007**, *49*, 61.
(40) Qiao, S. Z.; Djojoputro, H.; Hu, Q.; Lu, G. Q. *Prog. Solid State Chem.* **2006**, *34*, 249.
(41) Collins, K. D.; Neilson, G. W.; Enderby, J. E. *Biophys. Chem.* **2007**, *128*, 95.
(42) He, J.; Xu, Y.; Ma, H.; Evans, D. G.; Wang, Z. Q.; Duan, X. *Microporous Mesoporous Mater.* **2006**, *94*, 29.
(43) Hudson, S.; Cooney, J.; Hodnett, B. K.; Magner, E. *Chem. Mater.* **2007**, *19*, 2049.
(44) Lin, C. X.; Qiao, S. Z.; Yu, C. Z.; Ismadji, S.; Lu, G. Q. *Microporous Mesoporous Mater.* **2009**, *117*, 213.